Phenotyping of the Visceral and Subcutaneous Adipose Tissue in Pigs using Magnetic Resonance Imaging (MRI) and Dual Energy X-ray Absorptiometry (DXA)

Victoria Marisa Schneider

Inaugural-Dissertation
zur Erlangung der Doktorwürde
der Tierärztlichen Fakultät der Ludwig-Maximilians-Universität München

Phenotyping of the Visceral and Subcutaneous Adipose Tissue in Pigs using Magnetic Resonance Imaging (MRI) and Dual Energy X-ray Absorptiometry (DXA)

von Victoria Marisa Schneider
aus Nürtingen

München 2025

Aus dem Lehr- und Versuchsgut der Tierärztlichen
Fakultät
der Ludwig-Maximilians-Universität München

Arbeit angefertigt unter der Leitung von
Prof. Dr. Armin M. Scholz

Gedruckt mit Genehmigung der Tierärztlichen Fakultät

der Ludwig-Maximilians-Universität München

Dekan:	Univ.-Prof. Dr. Reinhard K. Straubinger, Ph.D.
Berichterstatter:	Prof. Dr. Armin M. Scholz
Korreferent:	Univ.-Prof. Dr. Mathias Ritzmann

Tag der Promotion: 26. Juli 2025

dedicated to my loved ones

TABLE OF CONTENTS

LIST OF ABBREVIATIONS

3D	Three-dimensional
ADG	Average daily gain
BFT	Back fat thickness
BFT A	Back fat thickness in point A
BFT B	Back fat thickness in point B
BFT C	Back fat thickness in point C
BFT1	Skin + first subcutaneous fat layer
BFT2	Skin + second subcutaneous fat layer
BFT3	Skin + all fat layers + lumbodorsal fascia
BMI	Body mass index
C18:2	Linoleic acid
CT	Computed tomography
DE	Large White
DL	German Landrace
DSAT	Deep subcutaneous adipose tissue
Du	Duroc
DXA	Dual energy X-ray absorptiometry
F	Filial generation
FCR	Feed conversion rate
FI_avg	Average daily feed intake
FI_d	Daily feed intake
GWAS	Genome wide association study
LSM	Least square means
MHF2	Mulit-hybrid F2
MHO	Metabolically healthy obesity
MId	musculus longissimus dorsi
MRI	Magnetic resonance imaging
MUFA	Monounsaturated fatty acid

NEFA	non-esterified fatty acids
NFE	Nitrogen-free extract
p	p-value
PCG	Protein coding gene
Pi	Piètrain
PSE	pale, soft, exudative
PUFA	Polyunsaturated fatty acid
QTL	Quantitative trait loci
R^2	Coefficient of determination
RMSE	Root mean square error
S	Class S (highest class in SEUROP classification system)
SAT	Subcutaneous adipose tissue
SD	Standard deviation
SEE	Standard error of estimation
SEM	Standard error of the mean
SEUROP	European pig carcass classification system
SFA	Saturated fatty acid
SSAT	Superficial subcutaneous adipose tissue
TAT	Total abdominal adipose tissue
TE	Time to echo
TR	Time to repeat
UCP1	Uncoupling Protein 1
US	Ultrasound
VAT	Visceral adipose tissue
VOC	Volatile organic compound
WHO	World Health Organisation

Units

%	Percent
°C	Degree celsius
cm	Centimeter
cm^3	Cubic centimeters
g	Gram
h	Hour
IU	International Unit
keV	Kiloelectronvolt
kg	Kilogram
kV	Kilovolt
mg	Milligram
min	Minute
MJ	Megajoule
ml	Milliliter
mm	Millimeter
mm^3	Cubic millimeter
ms	Millisecond
NE	Net energy
T	Tesla
U	Unit
µGy	Microgray
µm	Micrometer

LIST OF FIGURES

LIST OF TABLES

I. INTRODUCTION

The “global obesity epidemic” refers to the worldwide rapidly increasing prevalence of obesity rates over the past three decades, with the number of obese adults more than doubling between 1990 and 2022. According to the World Health Organisation (WHO), in 2022, approximately 890 million adults and 160 million children and adolescents were classified as obese (World Health Organization, 2024 *https://www.who.int/news-room/fact-sheets/detail/obesity-and-overweight*, last accessed 22.09.2024). WHO defines obesity as having a body mass index (BMI) of 30 or higher, resulting from a chronic imbalance between energy intake and energy expenditure. While excessive nutritional intake is a key contributor, the development of obesity is complex, involving various factors such as genetics, gender, age, lifestyle, and diet (Pant et al., 2015). Obesity is closely associated with an increased risk of multiple chronic diseases (Sørensen et al., 2022), such as diabetes type 2 (Neeland et al., 2019), cardiovascular diseases (Powell-Wiley et al., 2021), and musculoskeletal conditions like osteoporosis (Lin et al., 2023; Perna et al., 2023), raising significant concerns about its national and global economic impact on healthcare systems (Okunogbe et al., 2022). Especially the form of visceral obesity, characterised by a high accumulation of visceral adipose tissue (VAT), situated around internal organs, is particularly implicated in the pathogenesis of metabolic disorders and connected health issues (Després and Lemieux, 2006; Fox et al., 2007). In contrast, subcutaneous adipose tissue (SAT), located beneath the skin, has different metabolic properties and may have distinct health implications (Tchkonia et al., 2013). The distribution of adipose tissue varies between genders, ethnicities and ages (Machann et al., 2005; Lim et al., 2019; Streicher et al., 2023). Examining this heterogeneity is essential for gaining a comprehensive understanding of obesity, both for health monitoring and research purposes.

Pigs are recognised as a valuable model for human research due to their anatomical and metabolic similarities to humans, as well as their shared genetic variants (Spurlock and Gabler, 2008; Kogelman et al., 2013). With the sequencing of the pig genome, the genetic proximity of pigs to humans has

drawn attention, particularly regarding obesity research and related diseases (Pant et al., 2015). In addition to its relevance for human obesity research, understanding adipose tissue development and distribution in pigs is a crucial aspect of livestock production. Adipose tissue accumulation is closely related to growth rate, feed conversion efficiency, and lean tissue development, all of which have significant economic impacts. Moreover, the quantity and quality of adipose tissue influence meat palatability, processing potential, and overall consumer acceptance (Fontanesi et al., 2012). As consumer demand for improved animal welfare continues to rise, particularly in alternative housing systems, conditions such as outside-climate stables, as demonstrated in our study, can help to address the influence of additional extrinsic factors on pig phenotypes (Millet et al., 2005; Juska et al., 2013).

Magnetic resonance imaging (MRI) has emerged as a non-invasive tool for the assessment and quantification of visceral and subcutaneous adipose tissue in both humans and pigs. Offering high spatial resolution and the ability to differentiate between various (soft) tissues, MRI is recognised as the gold standard method (Streicher et al., 2023). Originally developed for bone mineral density assessment in humans, dual energy X-ray absorptiometry (DXA) has evolved to provide detailed information on fat and lean tissue distribution within the body, providing a quick and non-invasive method (Kracht et al., 2021).

This thesis aims to evaluate the GE Lunar *i*DXA CoreScan™ software in comparison to the gold standard method MRI for quantifying visceral and subcutaneous adipose tissue in the abdominal region of pigs. Additionally, the use of ultrasonography to measure back fat thickness will be assessed as a further non-invasive and accessible tool for adipose tissue evaluation.

By creating a porcine population with a wide range of phenotypes, this evaluation of body composition traits, with the focus on visceral and subcutaneous adipose tissue, will help to understand how intrinsic factors such as sex and genotype, as well as extrinsic factors like season and feed intake, influence fat distribution and overall body composition. These insights can contribute to improving pig breeding programs and assessing the impact of alternative housing conditions while also providing a foundation for

genome-wide association studies (GWAS) to identify quantitative trait loci (QTLs) and candidate genes related to adipose tissue accumulation and distribution, relevant to both animal and human research (Duarte et al., 2016).

II. LITERATURE REVIEW

1. Visceral and subcutaneous adipose tissue

1.1. Humans

Adipose tissue in humans is understood as a distinct organ, playing crucial roles in metabolism, thermoregulation, and overall health (Cinti, 2000; Poulos et al., 2010). It is mainly divided into two types: subcutaneous adipose tissue (SAT) and visceral adipose tissue (VAT). SAT is primarily found in the abdominal region and femoro-gluteal region, just beneath the skin, while VAT consists of fat depots around the abdominal organs (Mittal, 2019). It is important to distinguish adipose tissue from fat itself; adipose tissue refers to soft connective tissue composed of adipocytes, while fat refers to the lipid molecules stored within adipocytes. In humans, three types of adipocytes are known – white, brown, and beige adipocytes, each playing a distinct role in the lipid metabolism (Zhao et al., 2021). White adipocytes primarily function as energy reservoirs, storing triglycerides and releasing them as fatty acids when needed, while brown adipocytes can convert energy derived from fatty acids and glucose into heat through the action of Uncoupling Protein 1 (UCP1). Although developing in white adipose tissue, beige adipocytes exhibit functional similarities to brown adipocytes, contribution to heat production (Wu et al., 2012).

VAT, in particular, has gained attention for its specific role in the development of metabolic syndrome and cardiovascular diseases due to its endocrine activity (Després and Lemieux, 2006; Fox et al., 2007). In contrast, SAT is less hormonally active, serving a more protective function while acting as a storage site for excessive fat, where redundant free fatty acids and glycerol are accumulated as triglycerides within adipocytes (Tchkonia et al., 2013). SAT itself is further subdivided into two layers: the superficial and deep layer. Research indicates that the superficial subcutaneous adipose tissue (SSAT) layer is more metabolically active, characterised by adipocyte hypertrophy and fewer inflammatory cells, whereas the deeper SAT (DSAT) layer is associated with higher inflammatory cell infiltration, suggesting different roles for each

layer (Cancello et al., 2013; Kim et al., 2016). The varying degrees of adipose tissue accumulation and its distribution in different locations throughout the body impact health outcomes. For instance, individuals with metabolically healthy obesity (MHO) tend to have a greater capacity for SAT expansion, which may protect against fat deposition in visceral regions and mitigate associated metabolic risks (Blüher, 2014). Factors such as gender, age, ethnicity, and diet also affect adipose tissue distribution (Neeland et al., 2016). Furthermore, increasing obesity is associated with changes in the musculoskeletal system affecting muscle mass and bone density, particularly in older adults (Alalwan, 2020; Perna et al., 2023). Given these complexities, the study of adipose tissue and obesity remains a key area of scientific research.

1.2. Pigs

The domestic pig *sus domesticus* is widely used as an animal model in scientific research related to humans due to its similarities in terms of anatomy, physiology, pathology and metabolic characteristics. Its omnivorous dietary habits, similar lipoprotein profile and analogous patterns of anatomically distinct adipose tissue depots, such as visceral and subcutaneous adipose tissue, make the pig an ideal large animal model for obesity research (Bellinger et al., 2006; Aigner et al., 2010; Jin et al., 2023).

The accumulation and distribution of adipose tissue, along with the resulting overall body composition, play a significant role not only in the use of pigs as a model for translational research in human medicine but also in their role as meat-producing animals (Hinrichs et al., 2018; Renner et al., 2018).

Over the past few decades, pig breeding has continuously responded to consumer demand for lean pork, leading to the optimisation of pig carcasses for increased lean muscle content and reduced fat content. Reduced back fat thickness is associated with a greater amount of lean muscle, especially in the loin area (Gispert et al., 2007). As subcutaneous adipose tissue has a high degree of heritability, selective breeding has focused on reducing back fat thickness, making it a prime target (Lee et al., 2011; Ding et al., 2022; Oliveira et al., 2022).

Body composition, therefore, plays a crucial role, as the “SEUROP” grading model remains in use across Europe, with yields calculated accordingly. Carcass revenue is determined based on achieving a certain carcass weight and the highest possible lean tissue percentage, with a target of over 60 % lean tissue, which is rewarded with the highest grade, ‘S’. To predict the lean tissue percentage, the back fat thickness and the muscle depth of the longissimus dorsi muscle are measured 7 cm to the side of the dividing cut line between the second and third last rib, and a pre-developed prediction equation is then applied (*Schweineschlachtkörper-Handelsklassen-verordnung in der Fassung der Bekanntmachung vom 16. August 1990, (BGBl. I S. 1809), die zuletzt durch Artikel 5 der Verordnung vom 10. März 2022 (BGBl. I S. 428) geändert worden ist*, last assessed 18.08.2024). The aim of this standardised grading procedure is to establish fair and transparent

pricing for all farmers. However, some experts in the industry have raised concerns about this system, as it focuses solely on body composition when assessing pork production and quality, overlooking other important product- and process-related factors, such as nutritional value, sensory characteristics, food safety, and origin (Čandek-Potokar et al., 2024).

However, the selection pressure for lean pork can also have a negative impact on consumer satisfaction. This is because subcutaneous, intermuscular and intramuscular fat are important flavour carriers and are crucial for nutritional value and the further processing of certain products. Lipolysis, followed by fat oxidation, result in the formation of volatile organic compounds (VOCs), which are essential for the flavour development in dry-cured ham products (Pinna et al., 2012). Additionally, the subcutaneous fat layer plays a critical role in limiting water and flavour loss while preventing excessive salt absorption. The latter is particularly disadvantageous in lean ham concerning nutritional value (Candek-Potokar et al., 2002).

The quality of the meat is also influenced by the fatty acid composition of the adipose tissue. There is an antagonistic relationship between unsaturated and saturated fatty acids, which is dependent on the carcass's fat content (Zappaterra et al., 2022). The proportion of saturated fatty acids (SFAs) and monounsaturated fatty acids (MUFAs) is directly related to the degree of fat deposition in the carcass, as fat depots primarily accumulate as triacylglycerols composed of SFAs and MUFAs (van den Broeke et al., 2022). This higher proportion of SFAs and MUFAs, present along with increased fat deposition, results in greater tissue firmness and extended shelf life, as the fat is more resistant to oxidation. This is advantageous in the production of high-quality dried ham (Škrlep et al., 2020b). However, SFAs and MUFAs have a less favourable impact on human health compared to polyunsaturated fatty acids (PUFAs), which are present in higher proportions in lean meat. While PUFAs are beneficial for health, they are more susceptible to lipolytic and oxidative degradation, leading to faster rancidity and softening of fat, which can negatively alter flavour characteristics (Wood et al., 2004).

In pigs, fat is stored primarily in the form of triglycerides, which consist of a glycerol backbone and three long-chain fatty acids. Glucose, derived from a

diet rich in carbohydrates, plays a central role in the synthesis of these fatty acids through a process known as *de novo* lipogenesis. In this process, glucose is metabolised to pyruvate via glycolysis, which then enters the mitochondria and is converted into citrate. Citrate exits the mitochondria and is subsequently broken down into acetyl-CoA, which serves as the essential molecule for fatty acids through carboxylation and polymerisation. These newly synthesised fatty acids are incorporated into triglycerides, which are stored in white adipocytes (Figure 1). In addition to *de novo* synthesis, fatty acids can also be derived from dietary fat or from the breakdown of circulating triglycerides. The balance between fat synthesis (lipogenesis) and fat breakdown (lipolysis) in pigs is largely determined by their energy balance, which is influenced by their diet (reviewed by Dunshea, 2003). Notably, unlike humans and other mammals, pigs do not possess brown adipocytes due to a genetic defect in the expression of UCP1 (Zhao et al., 2021).

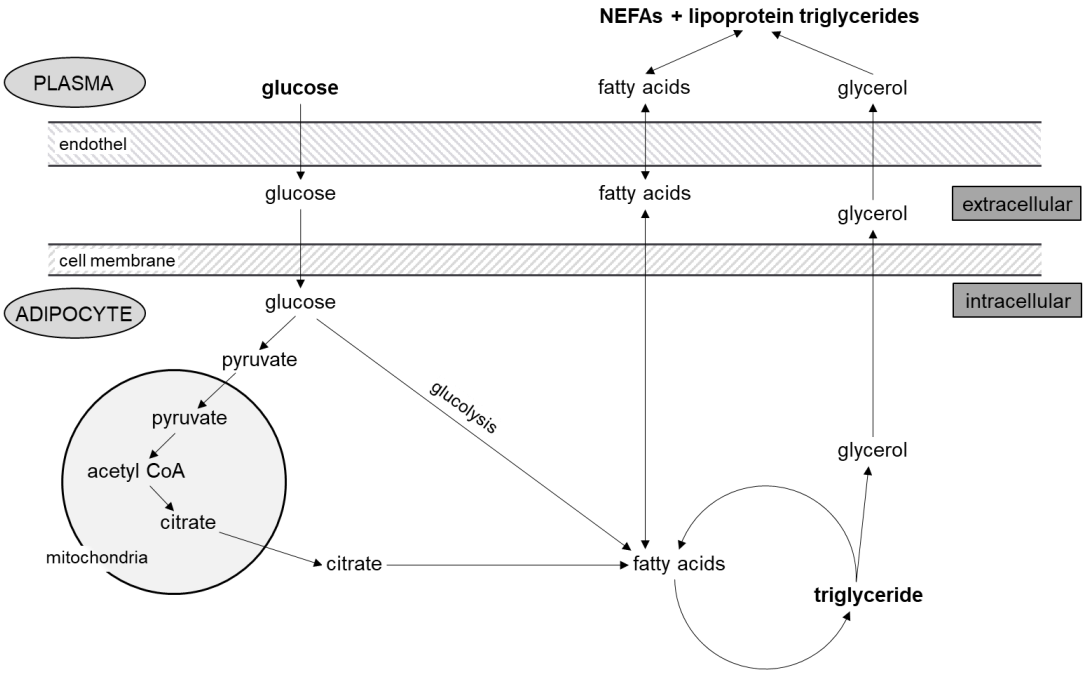

Figure 1: Lipogenesis and lipolysis pathways, simplified and modified according to Dunshea (2003)

In the neonatal pig, fat accumulation is initially minimal but quickly increases during the suckling period, likely because of the high fat content in the sow's milk. After weaning, when pigs transition to a solid high-carbohydrate diet, glucose becomes the primary source of energy and the main substrate for fatty acid synthesis (Dunshea, 2003; Soladoye et al., 2015).

According to Anderson and Kauffman (1973), adipose tissue growth in pigs is initially driven by an increase in number of fat cells, so called cellular hyperplasia, up until around 20 kg of body weight. The early stages are characterised by small but highly active cells that are efficient at synthesising lipids. As pigs grow from around 20 to 70 kg, both the number and size of fat cells increase. Beyond a body weight of around 70 kg, adipose tissue development transitions predominantly to hypertrophy, meaning the enlargement of existing fat cells. Despite a decline in lipid synthesis capacity as the cells mature and store more fat, adipose tissue accumulation continues to increase in later growth stages, primarily due to the expansion in size (Anderson and Kauffman, 1973).

The intricate balance between diet, metabolic processes, and growth stages determines the final composition of fat in pigs at the time of slaughter.

1.2.1. Subcutaneous adipose tissue

Adipose tissue development in pigs occurs in distinct stages, with subcutaneous back fat depots forming first, followed by visceral adipose tissue, intermuscular fat deposits, and lastly, intramuscular adipose tissue (Mourot et al., 1995).

Significant differences exist in the lipid content and fatty acid composition between subcutaneous adipose tissue and other fat tissues, as well as among the different layers within subcutaneous fat itself. Monziols et al. (2007) investigated the differences in lipid content between subcutaneous and intermuscular fat in pigs, finding that subcutaneous adipose tissue generally contains a higher total lipid content, ranging from 63.1 % to 67.8 %, compared to intermuscular fat with a lipid content of 57.5 % to 61.5 %, respectively. This suggests that intermuscular fat matures later and accumulates lipids more slowly than subcutaneous fat. Kouba and Bonneau (2009) confirmed these findings, showing that subcutaneous fat typically grows faster than intermuscular fat across most body regions, except for in the belly, where the growth rates are reversed. These findings support the idea that intermuscular fat matures later, accumulating lipids more slowly than subcutaneous adipose tissue.

Subcutaneous adipose tissue consists of two to three layers, with a third layer

typically present over the loin area. These layers develop unevenly across different anatomical sites and growth stages, with each exhibiting unique growth patterns that warrant consideration as separate tissues (Allen, 1976; Fortin, 1986; McEvoy et al., 2007). In general, the outer layer has been found to be the most prominent at birth, but as the pig matures, the middle layer thickens more rapidly, especially towards the end of the growth period. The inner layer develops later, contributing to the overall back fat thickness demonstrating an intermediate growth rate between the outer and middle layer (Fortin, 1986; Koch et al., 2011; González et al., 2017). Conversely, the middle layer was found to be most dependent on body weight changes and decreases more quickly under food restriction conditions (Leymaster and Mersmann, 1991).

Monziols et al. (2007) found no significant differences in lipid content between the outer and inner layers of subcutaneous fat, with values reported as 66.8 % and 67.8 %, respectively. However, they observed that the outer layer has a higher degree of unsaturation and a greater deposition of linoleic acid (C18:2), an essential fatty acid sourced directly from feed, compared to the inner layer. Supporting studies by Bee et al. (2002) indicate that lipid metabolism is less active in the outer layer than in the inner layer, where more endogenous fatty acids are synthesised through de novo lipogenesis. This leads to a lower concentration of polyunsaturated fatty acids (PUFAs), especially C18:2, in the inner layer relative to the outer layer. Additionally, Monziols et al. (2007) identified a gradient in monounsaturated fatty acid (MUFA) content across different adipose tissues, with the highest levels in the outer layer of subcutaneous fat, followed by the inner layer, intermuscular fat, and flare fat.

These findings underscore the intricate distribution of fatty acid within pigs' subcutaneous adipose tissues, a complexity further explored by researchers, which reveal that the composition of subcutaneous back fat and its fatty acids is significantly influenced by diet and environmental conditions during the finishing period, which begins when pigs reach 110-120 kg and continues until slaughter (Zappaterra et al., 2022). The fatty acid composition in tissues is shaped by a complex interplay of metabolic processes, including de novo fatty acid biosynthesis, lipolysis, and fatty acid deposition. Zappaterra et al. (2022)

emphasises that changes in fatty acid composition in back fat occur gradually over time. Consequently, the diet and environmental conditions during the finishing phase are critical factors influencing the fatty acid profile of the subcutaneous back fat layers at the time of slaughter.

Subcutaneous adipose tissue differs markedly from visceral adipose tissue at both metabolic and genomic levels. This reflects their distinct functional roles and potential health impacts. Differences in gene expression suggest that SAT and VAT may originate from different progenitor cells during development, contributing to their functional divergence (Chau et al., 2014). Given these disparities, SAT and VAT are often treated as separate organs, each with unique metabolic and inflammatory characteristics (Tchkonia et al., 2013).

SAT is generally associated with a metabolically protective role, characterised by the upregulation of protein-coding genes (PCGs) related to the structural components of the extracellular matrix (Jin et al., 2021). A flexible extracellular matrix in SAT allows to store excess nutrients in adipocytes, thereby preventing pathological consequences like inflammation and ectopic lipid deposition in other tissues.

Compared to VAT, SAT contains a higher proportion of smaller, more insulin-sensitive adipocytes, which are more efficient at storing free fatty acids and triglycerides compared to larger, more insulin-resistant adipocytes in VAT. Although SAT adipocytes initially offer metabolic protection, their capacity to store excessive fat is limited. Once this capacity is exceeded, excessive fat begins to accumulate in tissues not suited for lipid storage through systemic venous drainage (Hausman et al., 2014).

Wang et al. (2022) further explored the differences in SAT metabolism between male and female pigs, uncovering key sex-specific pathways and genes. Their conclusions were drawn from a study involving 34 crossbred F2 Duroc x Göttingen minipigs, which were evenly divided into three groups with different obesity indices. They found that males exhibit a greater capacity for angiogenesis (the formation of new blood vessels) and adipogenesis (the formation of fat cells) in SAT. In contrast, females have a stronger autoimmune and proinflammatory response in SAT, driven by the activation of type I interferon response and the production of interferon-stimulated genes. The

findings highlight distinct metabolic and immune regulatory mechanisms in SAT between sexes.

1.2.2. Visceral adipose tissue

Visceral adipose tissue (VAT) in pigs shows diverse metabolic and genomic characteristics that differentiate it from subcutaneous adipose tissue (SAT). VAT demonstrates unique transcriptional profiles, with a significant upregulation of protein-coding genes associated with inflammation and immune response progenitor cells, reflecting a heightened predisposition to inflammatory processes. This is further evidenced by increased infiltration of macrophages, particularly in the greater omental adipose tissue, which shows the highest level of macrophage infiltration (9.81 %) among various visceral fat depots, compared to 7.39 % in mesenteric adipose tissue and 7.18 % in abdominal subcutaneous adipose tissue, as discovered in a study by Jin et al. (2021). However, retroperitoneal adipose tissue was found to exhibit transcriptional patterns similar to metabolically active SAT for genes involved in glucose and lipid metabolism, suggesting variability within VAT depots regarding their metabolic activity (Jin et al., 2021).

In contrast to SAT, mature VAT shows reduced expression of extracellular matrix-related genes, limiting the expansion capacity of adipocytes and leading to metabolic deterioration as the adipose tissue enlarges (Rosen and Spiegelman, 2014). Metabolically, VAT poses a greater risk due to their direct drainage of venous blood to the liver, allowing inflammatory and signalling molecules from VAT to directly affect hepatic metabolism (Ibrahim, 2010). This direct connection intensifies the risk of metabolic dysfunction in comparison to SAT.

In summary, VAT in pigs is characterised by higher inflammatory and immune gene expression, greater macrophage infiltration, and direct metabolic interactions with the liver compared to subcutaneous adipose tissue, all of which contribute to increased metabolic risks.

2. Intrinsic factors

2.1. Influence of sex

Hormonal differences between male and female pigs play a significant role in determining body composition, particularly in the accumulation and distribution of visceral and subcutaneous adipose tissue. Sexual hormones are naturally occurring steroid hormones synthesised from cholesterol in the endocrine cells of the adrenal cortex, Leydig cells in the testicles of boars, and theca cells in the ovaries of female pigs. Besides being essential for reproductive development and performance, these hormones are involved in metabolism, particularly in protein synthesis and muscle growth, known for their anabolic effect (Skoupá et al., 2023). In intact boars, testosterone is predominantly synthesised from androgens in their testicles. Castration results in the absence of most of this steroid hormone in barrows. In female pigs androgens serve as essential substrates for oestrogen synthesis (Pope and Cárdenas, 2006).

In humans it is well known that the distribution of fat storage differs between men and women. Men tend to accumulate more visceral fat in the central abdominal region, whereas women accumulate predominantly subcutaneous fat in the femoral-gluteal region, also known as the gynoid distribution (Lemieux et al., 1993; Mayes and Watson, 2004; Palmer and Clegg, 2015). This difference is mainly due to different expression levels of the enzyme lipoprotein lipase and different ratios of adrenergic receptors in visceral and subcutaneous adipose tissue between men and women, as outlined by Palmer and Clegg (2015).

After menopause, which is characteristic of humans, the levels of androgens and oestrogens decrease, leading to an increase in visceral fat storage in women, similar to that observed in men (Toth et al., 2000). This shift is associated with an increased risk of cardiovascular and metabolic diseases in postmenopausal women (Kamińska et al., 2023). Treatment with oestradiol aims to prevent this, but it is unclear whether this is done by increasing subcutaneous fat storage or by reducing visceral fat (Sebo and Rodeheffer, 2021). In addition, the absence of oestrogen after the menopause leads to reduced energy expenditure and fat oxidation during both exercise and rest

(Abildgaard et al., 2013). Equivalently, aging men experience a decrease in androgen and testosterone levels, which is associated with an increase in central abdominal adipose tissue accumulation due to the absence of fat regulating anabolic effects of steroid hormones (Mayes and Watson, 2004).

The extent to which there are gender differences in the distribution of fat depots in pigs has not been widely investigated. In general, it is expected that barrows will be fatter than gilts due to the lack of steroid hormones associated with castration.

In a study published by Zomeño et al. (2022), growth and performance parameters of different sex types (surgically and immunocastrated males, intact males and females) in crossbred pigs [Piétrain × (Landrace × Duroc)] were analysed. The results showed that castrates had the highest fat deposition at finishing weight, with a back fat thickness over the loin muscle of 18.1 mm compared to 15.0 mm in gilts. This was confirmed on all other anatomical landmarks analysed. There was no major difference in protein deposition and muscle mass development between the sexes, although females showed greater gluteus medius muscle thickness (81.9 mm vs. 78.9 mm) and estimated lean meat content (61.2 % vs. 58.4 %) than surgically castrated barrows. The influence of sex on body composition development was also investigated in a study on Berkshire pigs (Walugembe et al., 2016). At slaughter weights of 122 ± 2.5 kg, no significant differences were found for loin muscle area, measured via ultrasound in cm^2, but they were observed for back fat growth and overall back fat thickness. Barrows demonstrated a faster back fat deposition rate of 0.22 mm per day compared to gilts, with 0.14 mm per day, respectively, resulting in a greater average back fat thickness of 31.5 mm at slaughter weight, compared with 22.6 mm for gilts. Overall, barrows achieved a higher average finishing weight than gilts (125 kg vs. 121 kg, respectively) (Walugembe et al., 2016). A study conducted by Pappenberger (2014) also investigated body composition parameters in hybrid fattening finishing pigs, assessed comparatively with MRI and DXA. They confirmed through DXA evaluations a higher body fat percentage and lower lean meat content in barrows compared to gilts, with 18.0 % fat and 79.7 % lean meat content compared to 15.0 % fat and 82.6 % lean meat content, respectively. Their MRI results revealed the same pattern. This trend was also confirmed

by a DXA analysis in the study of Weigand et al. (2020), who were able to demonstrate a higher total body fat percentage in barrows (16.4 %) compared to gilts (14.1 %). Looking at the abdominal fat distribution in detail, it became apparent that barrows had a significantly higher amount and volume of visceral abdominal fat (volume: 1979 cm³, mass: 1.87 kg) than gilts (volume: 1367 cm³, mass: 1.29 kg), which is consistent with the distribution pattern in humans (Palmer and Clegg, 2015).

In contrast, using CT to measure fat content in Landrace and Duroc barrows and gilts, Kolstad et al. (1996) found an overall higher amount of subcutaneous adipose tissue in gilts than in barrows, while gilts had less intramuscular fat depots than barrows. No significant differences were found for internal abdominal fat depots though. Similar findings were reported in a study conducted by González et al. (2017), which analysed adipogenetic Iberian pigs in terms of the development and degree of subcutaneous fat thickness and muscle growth. Using ultrasound at a wide variety of anatomical locations, it was found that the spayed female pigs had a higher overall subcutaneous fat layer (for example 47.7 mm in gilts vs. 45.2 mm in barrows measured at the 10^{th} intercostal space) and at the same time a larger longissimus muscle area compared to castrated male pigs (16.0 cm^2 vs. 15.6 cm^2 at 14^{th} rib, respectively). However, there was no significant difference in body weight gain between both sexes (González et al., 2017). It is also known that in Göttingen minipigs, females generally accumulate more total body fat than males, which in return are leaner. This is probably due to a difference in hormone concentrations in this breed, with males having very high testosterone concentrations and even higher oestradiol concentrations than female minipigs (Christoffersen et al., 2007). These elevated steroid hormone concentrations protect males from obesity, whereas severe obesity with increased metabolic dysfunctions has been observed in female Göttingen minipigs (Renner et al., 2018). The increased adiposity associated with lower steroid hormone concentrations in minipigs can be considered similarly to the increased risk of adiposity and particularly central abdominal fat accumulation in elderly (post-menopausal) women and men (Christoffersen et al., 2007).

Additionally, sexual steroid hormones are associated with appetite suppression (van den Broeke et al., 2022). The absence of these hormones

in castrated barrows leads to higher voluntary feed intake compared to intact animals, a fact confirmed by several studies.

A direct link between sex hormones and reduced appetite was demonstrated in an experiment by Claus and Weiler (1994). They showed that a single injection of testosterone at a dose of 1 mg per kg in barrows reduced their voluntary feed intake by 21.4 %. An injection of oestradiol (1 mg/kg) similarly reduced their feed intake by 20.2 %. Differences in voluntary feed intake between sexes were highlighted in a study by van den Broeke et al. (2022). Barrows, whether surgically castrated or immunocastrated, generally had a higher feed intake of 2.82 kg per day and 2.97 kg per day, respectively, on a high-energy diet, compared to gilts and intact males, which consumed 2.48 kg per day. A temporary reduction in feed intake during the mating season has also been observed in wild boars, which is associated with increased testosterone levels. Similarly, reduced feed intake was observed in sows, which have cycle-dependent elevated oestradiol levels (Claus and Weiler, 1994).

Additionally, a higher voluntary feed intake can be associated with higher daily gains. In a study by Pauly et al. (2008), barrows had average daily gains (ADG) of 830 g/d compared to 771 g/d in intact boars, while demonstrating a higher voluntary feed intake of 2.23 kg per day compared to 1.87 kg per day, respectively. However, barrows also showed an increased feed conversion ratio (FCR), indicating that they convert feed into lean meat less efficiently than intact boars. On one hand, this leads to a faster growth rate and fewer days needed to reach slaughter weight, but it also results in increased adipose tissue storage. This was demonstrated by a greater back fat thickness (22.1 mm in barrows compared to 13.0 mm in boars) and higher omental fat accumulation (2.3 % compared to 1.2 %, respectively). Böttinger (2006) also discovered a poorer FCR of 3.93 kg/kg in castrated pigs compared to 3.14 kg/kg in female pigs, with females having a higher percentage of whole-body lean tissue, in contrast to a higher percentage of fat in castrated males. In a study on growth differences between pigs of different sexes, Carabús et al. (2017) also came to the conclusion that in castrates fat accumulation occurs quicker during growth and slower in entire males and females, while lean tissue deposition follows the opposite pattern.

The question of whether gender-segregated feeding would make sense in order to increase overall efficiency and feed savings, or whether this categorisation by sex is not sufficient enough due to other parameters within intrasexual groups, which result in different capacities of energy conversion into protein and fat, is still under discussion (Carabús et al., 2017; Reckels et al., 2020).

3. Extrinsic factors

In addition to intrinsic factors like variations between sexes, understanding the complex interplay between extrinsic factors such as feed intake levels, diet composition, housing conditions and environmental elements like seasonal variations in ambient temperatures is essential. These factors collectively shape fat distribution and overall body composition in pigs.

3.1. Nutrition

3.1.1. Feed intake

Understanding the relationship between feed intake and fat deposition in pigs is essential for optimising growth performance and body composition. Alongside genetic factors, nutrient intake plays a crucial role in shaping these outcomes.

Pigs undergo changing metabolic requirements over the rearing and fattening phases. Growing pigs require high levels of energy and protein for rapid growth, whereas mature pigs have reduced protein requirements towards the end of the fattening period (Gilbert et al., 2017). Excessive energy during this phase results in increased fat accumulation in the body. Therefore, tailored diets that match the animal's growth stage and energy demands is crucial for promoting optimised growth, lean mass development and minimizing fat deposition, ultimately resulting in enhanced feed efficiency and cost-effective production rates (Mitchell et al., 2001).

Meeting the metabolic energy demands essentially depends on feed intake levels. The energy density of feed significantly influences feed intake, with a negative correlation observed. Animals compensate for lower energy concentrations by higher feed intake to achieve the required daily energy (Patience et al., 2015). In pigs, lysine functions as a limiting amino acid, affecting protein synthesis. Aiming for the optimal amino acid / energy ratio in a diet formula elevates the protein deposition into growth and lean muscle tissue (Babinszky and Halas, 2009). Additionally, factors such as flavour, palatability, water availability and technical conditions influence feed intake levels (Kamphues and Dobenecker, 2014).

3.1.2. Diet composition

Exploring the impact of diet composition on fat deposition and body composition, specifically high-fat or high-protein diets, provides insights into optimising nutritional strategies aiming for lean muscle development while minimizing fat deposition, as well as into investigations of diet-induced obesity models. Several studies have analysed how feeding of high energy diets, usually containing higher percentage of crude fat and greater amounts NFE (nitrogen-free extract, carbohydrates like sugars and starch) affects pigs' performance and body composition traits.

Van den Broeke et al. (2022) revealed that providing *ad libitum* access to a higher energy diet with 10.2 MJ NE/kg resulted in increased daily energy intake, leading to faster growth and greater fat deposition compared to a lower energy diet of 8.8 MJ NE/kg. Additionally, the high energy diet led to increased total digestibility of crude fat and crude protein, resulting in a more efficient energy conversion ratio. Crude protein content remained constant across both diets. The same trends were observed in a similar study conducted by González et al. (2017) who differentiated between a high energy diet containing elevated oleic acid levels (increased crude fat) and a standard diet with slightly more crude protein. Higher growth rates and increased back fat thickness was found in animals fed the former diet. In juvenile Göttingen minipigs, Christoffersen et al. (2013) also observed that feeding a high-energy diet for just two weeks could induce alterations in glucose and lipid metabolism, leading to an increased body fat percentage. This makes them particularly interesting as an animal model for diet-induced obesity in children and adolescents. Ultimately, after four months of diet feeding at the conclusion of the study, pigs fed the high-energy diet gained approximately 40 % more weight and showed more than twice the body fat percentage and visceral fat amounts compared to those fed the low-energy diet (Christoffersen et al., 2013).

3.1.3. Dietary modifications

Feed composition modifications and a range of supplements can be applied to diets for pigs to improve performance through various mechanisms, especially through increasing feed intake. As reviewed by Nyachoti et al.

(2004), feed additives like exogenous enzymes, which make polysaccharide components in feed easier to digest, or the addition of flavouring agents like dextrose can enhance the palatability of less accepted feed components, resulting in improved feed intake levels.

The composition of the feed can greatly affect the amount of heat generated during digestion, which in turn influences both feed intake and efficiency. This effect can lead to improvements or reductions in efficiency, depending on the heat requirements dictated by the surrounding temperature. Increasing the protein and fibre content in the feed during colder winter months may be beneficial for generating additional heat, while it is not recommended during warmer ambient temperatures (Patience et al., 2015). Moreover, reducing heat stress-induced intestinal barrier dysfunction, and inflammatory response can be achieved through the use of feed additives such as yeast, selenium, vitamin E, and others, as reviewed by Liu et al. (2022).

3.2. Housing

The housing environment for pigs, which ranges from conventional setups to enriched conditions featuring elements like straw beddings or access to the outdoors, and designed for groups of various sizes, intricately shapes feeding and activity behaviours. Subsequently, it can influence fat deposition and body composition. Investigating the dynamic impact of these housing modalities on the pigs' physiological responses is particularly of interest in current research, given the social imperative of non-conventional housing systems designed to promote enhanced animal welfare, proposing a progressive shift in swine husbandry practices (Godyń et al., 2019).

Škrlep et al. (2020a) investigated performance and carcass qualities of (surgically and immunologically) castrated and intact pigs reared in three different housing conditions: standard group housing, enriched housing with doubled space and outdoor access, and standard housing with repeated social mixing. In mixed housing environments, decreased carcass weights and reduced subcutaneous fat accumulation were observed. This was attributed to higher activity levels rising from ranking fights, resulting in increased energy expenditure. Moreover, pigs kept in enriched housing with outdoor access displayed lower amounts of belly and leaf fat due to elevated activity and thermoregulatory needs.

On the other hand, Holinger et al. (2018) found increased back fat thickness and decreased leanness in pigs also housed in mixed environments, although without other negative effects on performance. These findings suggest the potential for elevated chronic stress levels in mixed housing conditions leading to increased obesity, a phenomenon observed in humans as well (Chrousos, 2000; Scott et al., 2012).

Böttinger (2006) investigated the effects of outside-climate housing and conventional indoor housing on body composition parameters in pigs. The findings suggest that especially during summer, temperatures influence body composition, resulting in higher fat tissue percentages in pigs housed in an outside-climate stable, while still having a positive effect on performance parameters like feed efficiency and daily weight gain, compared to animals conventionally indoor housed. Conversely, no significant differences were

found in animals fattened during winter between the two housing systems.

Furthermore, group size significantly influences feed intake levels and feeding behaviour habits, as discussed by Nyachoti et al. (2004) and Fornós et al. (2022). For instance, pigs housed in larger groups exhibit less declines in feed intake levels during colder ambient temperatures due to their ability to huddle together, thereby reducing cutaneous heat loss (Nyachoti et al., 2004). Moreover, hierarchy within group housing settings affects the frequency and duration of feed intake, with lower-ranked animals consuming more frequently and for shorter periods compared to higher-ranked animals (Fornós et al., 2022). Therefore, feed access competence remains a critical factor in large group housings.

3.3. Seasonal variations

Investigating how changes in ambient temperatures affect feed intake levels, nutrient digestibility and changes in energy expenditure offers valuable insights into their impact on fat distribution and overall body composition in pigs.

3.3.1. Feed intake

The pig, as a homeotherm mammal, needs to maintain a constant internal body temperature, even across wide differing ambient temperatures. A balance must be created between heat loss and heat production so that the body temperature can be maintained constantly, with feed intake playing a crucial role in this. The thermoneutral zone is defined as the range of ambient temperatures where an animal can maintain its body temperature without expending extra energy (Noblet et al., 1985). Within this zone, the metabolic rate required for heat production remains constant and minimal, ensuring that neither heat gain nor loss occurs to the environment (Rinaldo and Le Dividich, 1991). The boundaries of the thermoneutral range vary among species and are influenced by factors such as breed, age, body size, weight, and metabolic rate (Patience et al., 2015). Brown-Brandl et al. (2013) reported a comfort thermoneutral zone ranging from 17.4 to 23.2 °C in growing and finishing crossbred pigs. Poullet et al. (2022) stated a temperate environment up to 25°C as thermoneutral for growing-finishing pigs, in which no extra energy is needed for thermoregulation. Within the thermoneutral zone feed intake levels are the limiting factor for growth rates and ultimately body composition traits (Rinaldo and Le Dividich, 1991).

At sub-thermoneutral temperatures, pigs undergo behavioural and physiological adapting mechanisms to increase heat production, primarily by increasing feed intake. This phenomenon has been observed by numerous researchers, providing varied data for different weight and production categories (Ramirez et al., 2022). Patience et al. (2015) reported a 1.5 % increase in feed intake per degree Celsius decrease below the lower critical temperature of pigs. Rinaldo and Le Dividich (1991) observed a feed increase of 13 grams per Celsius degree drop between 25 and 12 °C for pigs weighing 30 kg, while below 18.5 °C, feed intake remained relatively unchanged,

indicating that feed intake levels reached maximum within this weight range. In pigs provided outdoor access, and therefore exposed to colder ambient temperatures during winter, an increased feed intake of approximately 290 grams per day was noted compared to conventionally housed pigs (Lebret et al., 2006). This difference was pronounced in the heavier production class of growing-finishing pigs.

In contrast, with increasing temperatures beyond the upper critical temperature, animals tend to avoid the thermic effect of feed and its induced heat production by decreasing feed intake (Liu et al., 2022). Due to the absence of functional sweat glands, pigs are more sensitive to ambient temperatures beyond their thermal comfort zone (Ross et al., 2017; Gonzalez-Rivas et al., 2020). Consequently, various studies have documented a reduction in feed intake from a temperature of 20 °C upwards (Rauw et al., 2020), again dependent on their body weight and production level. Subsequently, body heat production can be further diminished by decreased weight gain resulting from decreased feed intake and, therefore, reduced nutrient intake (Lebret et al., 2006), as observed by Rinaldo and Le Dividich (1991) in growing pigs, where a decrease in feed intake of approximately 18 % led to a corresponding reduction in growth rates of 15 % in temperatures ranging between 25 and 31.5 °C.

3.3.2. Nutrient digestibility

Not only is reduced feed intake a factor, but impaired intestinal barrier function during heat stress (Pearce et al., 2013) also contributes to reduced growth rates. This dysfunction is likely induced by oxidative stress, leading to a systemic inflammatory response and a compromised amino acid digestibility, along with an altered postabsorptive metabolism (Liu et al., 2022). These factors may lead to disordered protein deposition and a decrease in feed conversation efficiency, ultimately resulting in increased body fat accumulation (Babinszky and Halas, 2009).

3.3.3. Seasonal variations on fat deposition

The extent to which seasonal changes and temperature are related to fat storage in pigs is a major focus of current literature. Controversial findings are being discovered, particularly regarding the response of lipid metabolism to

heat stress.

Several studies have observed reduced fat deposition in pigs experiencing heat stress compared to those kept in thermoneutral environments (Johnson et al., 2015; Čobanović et al., 2020; Albert et al., 2024). Čobanović et al. (2020) studied the impact of different seasons on carcass and meat quality traits of pigs, noticing a decrease in back fat thickness under heat stress during summer, presumably due to reduced feed intake and increased protein catabolism. Likewise, Hungarian Large White and Landrace crossbreds examined during summer demonstrated less back fat thickness compared to those assessed in autumn, with on average 23.42 mm vs. 28.42 mm, respectively (Albert et al., 2024). The author explained this reduction of the insulating layer to the animals' adaption to higher temperatures during summer. Results from seasonal examinations by Wang et al. (2023) further supported this observation. Additionally, Johnson et al. (2015) investigated two groups of growing pigs, one in a thermoneutral environment and another under heat stress. A comparison of tissue accretion and growth rates between the groups examined at a slaughter weight of 60 kg revealed a reduction of approximately 15 % in lipid accumulation in the heat stressed group compared to the pigs kept in thermoneutral ambient temperature. The author suspected that this reduction was due to decreased feed intake, which fails to provide adequate energy for lipid deposition. Interestingly, no difference was observed in protein deposition between the groups. This implies that there is still sufficient energy intake to support lean muscle development during the growth phase, as protein deposition requires less energy than fat deposition (Patience et al., 2015).

Ma et al. (2019) investigated Yorkshire pigs put under heat stress of 35 °C for 30 days compared to a control group kept in a thermoneutral environment of 22 °C, and found similar effects like reduced feed intake by approximately half, resulting in reduced average daily gain and less final body weight, but interestingly increased back fat thickness. Other studies have similarly discovered that heat stress leads to increased fat accumulation and therefore resulting in lower carcass and meat quality, leading eventually to the occurrence of pale, soft and exudative (PSE) meat (Čobanović et al., 2020). Paradoxically, despite a decrease in nutrient intake, animals exposed to heat

stress showed increased basal insulin levels and greater insulin-sensitivity, which is an exceptional non-diabetic condition (Baumgard and Rhoads, 2013; Gonzalez-Rivas et al., 2020). As insulin acts as an antilipolytic hormone, lipid mobilisation is inhibited, reflected in a decrease of non-esterified fatty acid (NEFA) levels in plasma, which are considered indicators of lipolysis (Sanz Fernandez et al., 2015). Furthermore, additional metabolic markers have been identified, indicating that adipose tissue adapts to heat stress and protects itself by increasing lipid storage and reducing mobilisation (Qu and Ajuwon, 2018). Consequently, during heat stress, energy is primarily obtained from protein and carbohydrate metabolism rather than lipid mobilisation, fundamentally due to the substantially higher metabolic heat production associated with energy generated from lipolysis compared to that from protein and carbohydrate metabolism (Gonzalez-Rivas et al., 2020).

In contrast, studies that examined pigs during colder ambient temperatures consistently demonstrated increased fat accumulation, particularly in subcutaneous back fat (Čobanović et al., 2020; Albert et al., 2024).

Age plays an important role of pigs' sensitivity to ambient temperatures. Older pigs have a broader thermoneutral zone and a lower upper critical temperature limit compared to younger ones (Quiniou et al., 2000; Rauw et al., 2020). As pigs age, their subcutaneous fat layer thickens over their entire body, resulting in slowing transmission of heat from their body surface (Pathak et al., 2018). Moreover, older fattening pigs show a greater reduction in feed intake with each degree Celsius rise in ambient temperature compared to younger, growing pigs (Patience et al., 2015).

3.3.3.1. Composition of fatty acids

Environmental factors not only influence the amount and distribution of accumulated fat depots but also affect the composition and concentration of various fatty acids. Zappaterra et al. (2022) analysed, besides genetic influences, further extrinsic factors such as the season at the time of slaughter and diet compositions of fatty acids. These findings revealed an antagonistic correlation between saturated (SFAs) and polyunsaturated fatty acids (PUFAs), specifically n-6 fatty acids, which might be dependent on the animals' carcass fatness (see Chapter II.1.2.1). Pigs slaughtered in autumn

exhibited greater proportions of eicosadienoic acid and other n-6 PUFAs, such as gadoleic and erucic acids, alongside lower amounts of back fat. In contrast, pigs slaughtered in winter showed greater back fat thickness with higher proportions of SFAs, including capric, lauric, myristic, palmitic, and palmitoleic acids. Since adaptive composition changes of fatty acids of back fat takes a long time, the author suggests that the finishing period, especially, influences the fatty acid composition in back fat at slaughter. This results in notable deviations between pigs fattened in summer and slaughtered in autumn and pigs fattened in autumn and slaughtered in (late) winter. Contrary to this, stearic acid, an SFA, was found proportionally more in back fat of pigs slaughtered during summer and early autumn, suggesting its role in improving thermotolerance of adipocyte membranes against rising temperatures (Malekar et al., 2018).

3.3.4. Seasonal variations on body composition

Regarding further components of body composition, such as lean mass and bone mineral, differences due to seasonal variations have been observed.

On one side, Cruzen et al. (2015) reported increased lean tissue percentage and mass in pig carcasses previously exposed to heat stress, in comparison with thermoneutral raised pigs. However, chronic heat stress resulted in overall reduced performance, leading to slower growth rates and smaller carcasses. In the study conducted by Johnson et al. (2015), no difference in lean mass deposition was found in postnatal heat-exposed pigs compared to thermoneutral-held ones. This indicates that although feed intake was reduced, it was still sufficient for maximum muscle mass deposition up to 60 kg live weight. More recent research has confirmed that heat stress induces a highly catabolic state in the body, with muscle catabolism being particularly affected (Qu and Ajuwon, 2018; Liu et al., 2022). As mentioned above, under heat stress, the energy metabolism in pigs shifts from lipolysis to gluconeogenesis preferably sourced from increased oxidation of carbohydrates and through proteolysis-obtained amino acids (Liu et al., 2022), as evidenced by increased oxidation of branched-chain amino acids such as leucine (Fausnacht et al., 2021).

Moreover, there are several potential reasons why seasonal factors could

have an impact on skeletal health. One reason might be the seasonal variations in activity levels, due to adaptation of energy expenditure depending on ambient temperature. It is well known that physical activity closely influences bone remodelling and mineralization by triggering cellular responses in bone tissue that leads to stimulation of osteoblast activity (Lombardi et al., 2019).

Physical activity might also be connected to variations in feed intake, which could affect mineral intake and absorption, subsequently influencing mineral content and density. Changes in feed availability and composition, particularly regarding mineral feed, could affect bone metabolism as well.

Another significant factor in regulating bone metabolism is vitamin D, which is not only achieved through oral intake but also synthesised in the skin of animals via sunlight exposure (Barnkob et al., 2016). Arens et al. (2007) conducted a study on sheep over 18 months in natural light conditions and observed variations in bone mineral density during summer and winter, with higher levels in summer and lower levels in winter. These changes could be influenced by shorter day lengths and correspondingly reduced sunlight exposure. Nevertheless, Delahunty et al. (2009) found seasonal differences in mice, with smaller femoral volumetric bone mineral density (BMD) observed in winter compared to summer, even under laboratory standards with identical temperatures and consistent light-dark cycles. This indicates that seasonal changes in bone metabolism might be influenced by a variety of factors.

4. Methods for assessing adipose tissue and body composition

4.1. Magnetic Resonance Imaging

Magnetic resonance imaging (MRI) is considered the gold standard method for assessing abdominal adiposity in humans due to its ability to directly measure (soft) tissue volumes and areas (Fang et al., 2018; Streicher et al., 2023). As a non-invasive, non-ionizing method, MRI is a safer alternative to computed tomography (CT) examinations in humans. In addition, MRI is increasingly being used to assess body composition in live animals. Due to its high spatial resolution, it is considered the reference method for assessing abdominal adipose tissue in live pigs and other animals (Weigand et al., 2020), effectively replacing the previously and currently used destructive dissection methods for carcass composition analyses (Seidell et al., 1990).

The physical principles of magnetic resonance imaging (MRI) are based on the interaction between the inherent magnetism of atomic nuclei of a sample tissue and an external magnetic field. These interactions can be transformed into electrical signals, which are subsequently detected and processed to produce detailed images. This process allows for the spatial resolution of the sample tissue being examined.

Atomic nuclei consist of protons and neutrons, resulting in a positive charge. However, certain atomic nuclei, for example the most basic atom hydrogen, possess the ability to spin around their own axis due to an uneven number of protons or neutrons. This, combined with their associated electrical charge consequently creates a magnetic moment. This magnetic moment generates a small local magnetic field, similar to that of a bar magnet with north and south poles. In absence of external fields these “bar magnets” spin around their axis randomly orientated in the tissue (M. Scholz et al., 2024). However, when exposed to a strong external magnetic field, such as that generated by an MRI scanner, the protons align their axes with the direction of the magnetic field. This alignment does not line up exactly to the magnetic field, instead, due to the angular momentum of the protons, they orbit around the axis of the main magnetic field in an evasive, rotating manner. This phenomenon is

known as precession (Schild, 1997). The frequency of the precession, also known as the Lamour frequency, is determined by the magnitude of the magnetic field (B_0) and the type of proton. This can be described by the Lamour equation:

$$\omega_0 = \gamma B_0$$

Here, ω_0 represents the angular frequency of the protons in Hertz [Hz], with frequencies typically in the range of Megahertz [MHz]. γ is the gyromagnetic ratio, a constant specific for each nucleus, measured in Megahertz per Tesla [MHz/T]. B_0 is the magnetic field strength in Tesla [T]. Consequently, different atomic nuclei have different Lamour frequencies, which are influenced by the field strength of the external magnetic field.

To achieve nuclear magnetic resonance (NMR), nuclei that possess spin must be excited by applying supplementary energy in form of short, high-frequency energy pulses (B_1) perpendicular to the main magnetic field, at the same frequency as the Lamour frequency of the protons, also known as the resonance frequency. This excitation is obtained through a gradient coil. The nuclei absorb the energy and enter a higher energy state, becoming “excited” (d'Anjou, 2018).

Upon interruption of the high-frequency energy pulses, the protons gradually release the absorbed energy and return to their original alignment within the magnetic field. This process is known as relaxation. Two independent processes occur simultaneously during relaxation. Longitudinal magnetisation, with spins parallel to the magnetic field, begins to rebuild, a phenomenon known as T1-relaxation or spin-lattice relaxation, as protons release the absorbed energy to the surrounding tissue (the “lattice”). This process includes the time required to reach 63 % of its initial level. At the same time, T2-relaxation or spin-spin relaxation occurs, where transverse magnetisation rebuilds to 37 % of its initial value. Subsequently, the magnetic resonance signal decreases through the desynchronisation of the spins (Schild, 1997).

Each nucleus resonates in its specific frequency, meaning that individual tissues exhibit characteristic T1 and T2 relaxation times. Homogenous

tissues, such as liquids or water, typically have longer T2 relaxation times. In summary, tissues with higher water content generally exhibit longer T1 and T2 relaxation times, whereas solid tissues or tissues with higher fat content tend to have shorter T1 and T2 relaxation times. These relaxation times determine the energy emitted when the energy pulse is switched off, generating a signal, which is received by a coil within the MRI machine. The intensity of the signal is then converted into a grayscale, forming contrasts in images based on T1 and T2 relaxation times, enabling the differentiation between various tissues (d'Anjou, 2018).

For the final image reconstruction spatial encoding is essential to localise and visualise the detected signal in a three-dimensional image. This process involves briefly superimposing orthogonal gradient magnetic fields onto the main magnetic field generated by the MRI scanner. These additional fields apply varying field strengths along the three spatial directions: x, y and z. By altering the main magnetic field temporarily, the “local” resonance frequency of protons changes depending on their position. Frequency encoding, phase encoding, and slice selection are achieved by differentiating between three gradient fields produced by coils. Once the signals are encoded with spatial information from the gradient fields, Fourier transformation is employed to convert the data into grayscale images, representing both spatial information and signal intensity (Thrall, 2018; Cole and Hespel, 2020).

4.2. Dual Energy X-ray Absorptiometry

4.2.1. Technical aspects

Dual energy X-ray absorptiometry (DXA) technology relies on the differential attenuation of X-ray energy by various tissues within the body. This attenuation is dependent on several factors. Firstly, it depends on the intensity of energy emitted by the DXA`s X-ray source. Secondly, it is influenced by the evaluated tissue's thickness and density, which is based on its composition.

The DXA machine emits two levels of X-ray energies – a low-energy beam and a high-energy beam. In case of the Lunar *i*DXA from GE HealthCare, the DXA technology used in this study, a 100 kV generator emits photon energy levels of approximately 39 keV and 71 keV by absorbing middle-range energy X-rays using a "K-edge filter" system (see GE Healthcare, 2017 *https://www.gehealthcare.de/-/jssmedia/feature/gehc/products/lunar-idxa/lunartechnology.pdf,* last assessed 20.09.2024).

The context of this lies in the principle of varying intensity levels leading to varying attenuation levels. Higher levels of photon energy are attenuated to a lower extent, while lower photon energy levels are absorbed more, resulting in fewer photons passing through the tissue. As X-rays radiate through the tissues being examined, they are attenuated differently based on the tissue's composition and density. For instance, denser tissues such as bone "absorb" more X-rays compared to lower density tissues like soft tissue (Messina et al., 2020). The DXA machine is designed with a detector positioned opposite to the beam, with the body being examined in between. This detector identifies the energy levels of photons that passed through the tissue calculating the energy attenuation (attenuation coefficients) for both energy levels. It determines the ratio between the high and low energy X-ray attenuation, known as the R-value, which is specific to each tissue within the 3-compartment model of fat mass, non-bone lean mass and bone mineral content (Pietrobelli et al., 1996; Scholz et al., 2015) (Figure 2). By comparing attenuated energy levels to emitted energy photons, a two-dimensional image is produced where different R-values are represented by varying grey values in pixels.

However, since theoretically only two components can be directly measured when applying two photon energy levels, an initial differentiation is made between soft tissue (comprising fat mass and bone-free lean mass) and bone tissue, given that bone mineral possesses a significantly higher R-value than soft tissue (Laskey, 1996). In bone pixels containing both bone mineral and lean soft tissue, the composition of the lean soft tissue is estimated to be similar to that of the surrounding soft tissue pixels (Pomar et al., 2017).

Therefore, the composition of soft tissue can only be determined in areas devoid of bone. The pixels alone cannot distinguish the attenuation properties for fat and lean soft tissue due to the similar R-values of both components. However, specialised algorithms are able to compute these values, relying on previously established and validated R-values using phantoms with known compositions (Laskey, 1996; Pietrobelli et al., 1996). Consequently, the fat content in the soft tissue pixels can be determined, while the lean soft tissue is calculated by the difference between soft tissue and fat tissue (Figure 2).

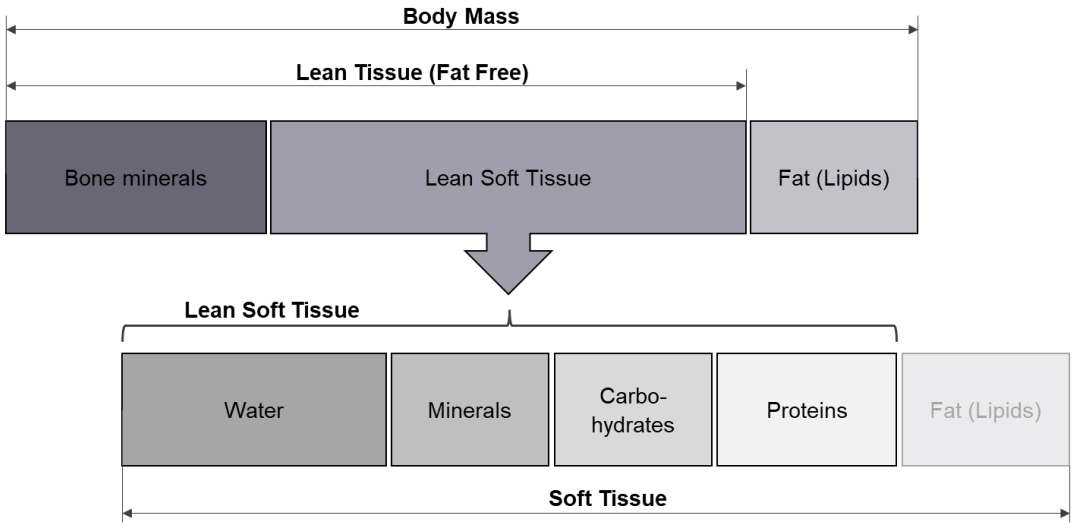

Figure 2: Compartment model of body composition by DXA, modified according to Scholz (2002)

Over the last decades DXA technology has consistently been improved and further evolved. The development from pencil beam technology to fan beam, particularly narrow fan beam technology (patented by GE Lunar) has significantly reduced the examination time while maintaining a low radiation dose, improving image precision without magnification.

Pencil beam technology relies on a single, highly collimated beam of X-rays,

attenuated by a single detector system. Because of its rectilinear beam direction, the body under examination must be X-rayed multiple times in small grids, leading to a prolonged examination time. Conversely, fan beam technology emits X-rays in a fan-shaped pattern and determines them with several detectors, allowing for a single sweep of the X-ray arm over the body of interest, thus reducing examination duration. However, this approach needs increased radiation and results in magnification due to proximity of the body to the X-ray source. These limitations have been addressed with the narrow fan beam technology by GE Lunar, which strikes a balance between pencil beam and fan beam systems, combining precision and speed in examination (Bazzocchi et al., 2016).

4.2.2. Fields of application

DXA was initially introduced into human health research for assessing bone health and osteoporosis (Glüer, 2017). Since then, it has become widely recognised as the standard method for evaluating bone mineral content (BMC) and bone mineral density (BMD), which is calculated by dividing BMC by bone area. This is important for determining the risk of various diseases such as osteoporosis (Slart, Riemer H. J. A. et al., 2025). In addition to its application in humans, DXA has proven to be a reliable tool for measuring BMC and BMD in live pigs, showing high correlations with results from chemical analyses (Schlegel and Gutzwiller, 2020).

Furthermore, DXA is capable of analysing various components of body composition, including lean mass and fat percentage, not only in humans (Thibault et al., 2012) but also in various animal species such as pigs (Soladoye et al., 2016), sheep (Hunter et al., 2011), calves (Kappes et al., 2024), dogs and cats (Speakman et al., 2001; Jeusette et al., 2010). Particularly the field of obesity research in humans and studies investigating therapeutic approaches and nutritional adaptation methods (Hind et al., 2011) have focused on DXA as the method of choice due to its ability to facilitate long-term studies with minimal radiation exposure and rapid application.

Software designed for assessing visceral abdominal fat has been introduced by both main DXA manufacturers (CoreScan™ software by GE Lunar *i*DXA, InnerCore™ by Hologic), aiming to quantify visceral fat amounts and identify

the associated risk of metabolic diseases. In the context of this study, the CoreScan™ software is utilised for determining visceral and subcutaneous fat in the android region. Additionally, the software enables the assessment of the fat distribution in the gynoid region, which is of substantial interest because the distribution of local fat depots and their proportion to each other are significant factors known to be associated with several cardiovascular risk factors in humans (Tchkonia et al., 2013).

To estimate the amount of visceral fat, the CoreScan™ software automatically defines the android area, setting the lower limit at the top of the hip bone and positioning the upper limit at a point 20 % of the distance from the iliac crest to the human's neckline. For the gynoid area, the upper limit is positioned just below the pelvis line, equivalent to 1.5 times the height of the android region. The lower boundary is situated at a distance equivalent to 3.5 times the height of the android region from the pelvis line. Automated calculations are then employed to determine the ratios within these regions, precisely the android-gynoid-ratio (see GE Healthcare, 2024, X-ray Bone Densitometer with enCORE v17 software-User Manual, *https://www.gehealthcare.com/support/manuals*, last assessed 17.03.2025). However, due to differing body proportions between pigs and humans, the android region in pigs, which covers a larger area, requires manual definition. While the software adjusts the gynoid region automatically, it tends to be more caudal ("inferior") than in humans, limiting its suitability for the use in pigs (Figure 3).

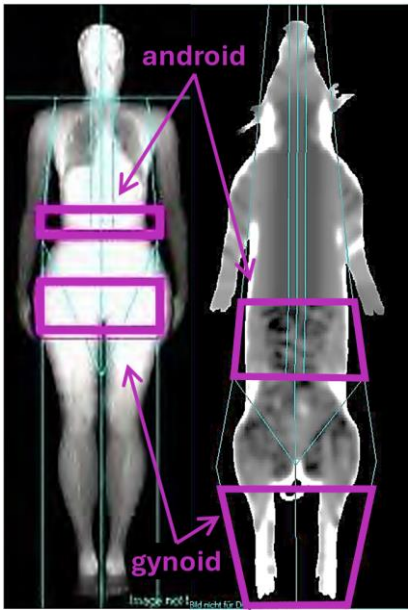

Figure 3: Identification of android and gynoid in humans and pigs by CoreScan™ software

4.2.3. Validation studies

Since the introduction of the GE Lunar *i*DXA CoreScan™ software for measuring abdominal fat distribution, several studies have been conducted to determine its reliability and validate this tool in terms of both precision (consistency of measurements) and accuracy (similarity of DXA measurements to measurements obtained by a gold standard method).

Precision was initially validated by Rothney et al. (2013) shortly after the first cross-sectional validation study with CT (Kaul et al., 2012). They investigated intra- and inter-scanner precision by employing a phantom, specifically designed to imitate and modulate the amount of visceral adipose tissue. Scanning nine possible combinations five times across all ten DXA scanners explored revealed a coefficient of variation (CV) of 4.76 % (47.6 g to 1 kg VAT mass), which closely resembled the findings in the clinical trial conducted by the same authors. Thirty-two obese women, aged between 25 and 45 years old, with an average BMI of 35.1 kg/m² were scanned twice with repositioning between scans, revealing a coefficient of variation of 5.1 % (56.8 g to an average of 1110.4 g VAT mass). Overall, the study found high precision, although it is notably that only a small number of quite similar patients were examined and the phantom used, with a one-dimensional subcutaneous fat layer, does not fully correspond to human anatomy.

On the other hand, in a study by Mellis et al. (2014), a larger and more diverse sample of adults was examined, divided into two groups: a normal-weight group (average BMI of 22.2 kg/m²) and an overweight group (average BMI of 30.0 kg/m²), consisting of a total of 45 adults, including 35 women and 10 men. Again, two consecutive scans were performed with repositioning in between. The overweight group demonstrated a CV of 5.4 %, while the former group showed a CV of 17.0 %, although with smaller precision errors compared to the overweight group (20.9 g versus 43.7 g, respectively). The author attributed this disparity to an inverse relationship between the mean value and the CV, suggesting that when mean values differ across the population, the CV should not be relied upon. Overall, the CoreScan™ software demonstrated satisfactory precision for assessing visceral adipose tissue across a broad range of BMI levels.

Precision and reliability were further investigated by Dordevic et al. (2018), who performed a longitudinal study over three months with 51 weight-stable participants. They compared the results to two consecutive measurements taken with repositioning in between on the same day from 30 participants, all aged between 18 and 65 years old. As expected, higher variability was observed for longitudinal studies compared to same-day assessments, with coefficients of variation for VAT at 42.2 % in the longitudinal group, compared to 16.2 % for same-day scans. For the total of all body segment measurements, CVs ranged from 0.8 % to 5.9 %, compared to under 2 % respectively. Furthermore, the author pointed out that precision is BMI-dependent, particularly challenging for participants with BMIs below 25 kg/m² or those containing less than 500 g VAT. This limitation could impact the results of longitudinal weight intervention studies with short examination intervals or small changes in VAT amounts.

In addition to precision tests for VAT, a more recent study conducted by Henriksen et al. (2021) has also published precision estimates for SAT in both healthy individuals and colorectal cancer patients. The study examined 30 adults in each group, ranging in age from 24 to 77 years old and across various BMI categories from 16.1 to 34.7 kg/m². Similar to the previous studies, two consecutive scans were performed with repositioning in between. The coefficient of variation for VAT and SAT was found to be 5.30 % and 3.46

% among healthy subjects, and 3.56 % and 3.28 % among diseased patients, respectively. Although high precision was found for VAT and SAT, overall, the study revealed that estimates of regional fat distribution had higher precision errors compared to total body fat mass, which is consistent with findings from other studies (Carver et al., 2013; Meredith-Jones et al., 2018). One reason for this might be the narrow anatomical area of the android region, in which VAT is assessed (Rothney et al., 2013), which poses a challenge compared to evaluating total fat across a whole-body scan. Since it is dependent on the estimation of SAT, this can be an error-prone factor, especially in subjects with low BMI and therefore reduced SAT. Additionally, VAT is not as rigid as SAT and may change its visualisation during repositioning, possibly leading to superimposition (Knapp et al., 2015). Ultimately, precision errors can also occur due to incorrect positioning or differing operators between scans.

Initially, Kaul et al. (2012) conducted the first study to validate the accuracy of VAT estimation by the CoreScan™ software compared to CT results, which served as the standard method for assessing visceral adipose tissue. Firstly, a smaller sub-cohort of 10 men was selected to refine and test the previously developed algorithm, the operating principles of which are described above. Subsequently, a validation sample of 109 adults, comprising 48 men and 61 women aged between 18 and 90 years, with a wide range of BMI values between 18.5 and 40 kg/m² but an average of 26.7 kg/m², was selected. VAT values were determined using semi-automated estimation from 5 mm thick DICOM cross-sectional CT images in the android region, with SAT removed and VAT volume calculated. These values were then compared with DXA-derived VAT values obtained through standard procedures. A strong relationship between DXA and CT values was found, with $R^2 = 0.957$ for all included subjects. Additionally, a deviation of 567 cm³ was determined in a Bland-Altman analysis, with 95 % limits of agreement of -355 to 468 cm³. Consequently, a high accuracy for VAT values obtained by DXA could be achieved.

DXA has also been validated for accuracy with MRI, like the study conducted by Reinhardt et al. (2017). They meticulously compared VAT, ensuring the exact same region of interest was used in both MRI and DXA evaluations. In their study involving 40 adults, including 20 men and 20 women aged between

18 and 65 years old, a strong relationship for VAT of $R^2 = 0.948$ was revealed. However, despite finding strong agreement between both methods, a systemic bias was identified, with DXA underestimating leaner patients and overestimating patients with increased VAT levels. A Bland-Altman analysis confirmed a bias of 1104 cm^3 and limits of agreement of 2682 cm^3 and 890 cm^3, suggesting that while DXA is useful for assessing VAT tendencies, it may not provide accurate direct estimates.

Moreover, in a study conducted on adolescents, greater differences between both methods were found in higher BMI categories compared to those of normal weight. Kracht et al. (2021) examined 330 adolescents, including 156 males and 174 females, with an average age of 12.6 years old. They performed examinations for VAT mass distribution, using the CoreScan™ software and compared it with VAT estimates derived from MRI. Again, a high correlation was observed, with a correlation coefficient of 0.78. However, DXA systematically underestimated VAT mass with an average of 0.33 ± 0.39 kg compared to of MRI, which revealed an average of 0.54 ± 0.43 kg, respectively.

To summarise, DXA and particularly in combination with the CoreScan™ software developed for body composition and specifically assessment of fat distribution in the human abdomen, show high precision and accuracy against the gold standard methods like MRI and CT. However, exact measurements partially may be either over- or underestimated, depending on factors like the number of study participants, their age and BMI.

In pigs, DXA can also be used to determine body composition, as mentioned above. Validation studies on accuracy and reproducibility have primarily been conducted on pig carcasses (Marcoux et al., 2003; Soladoye et al., 2016; Kipper et al., 2019). DXA estimates from both carcass and live pigs have then been compared with chemical analysis or dissection, with high accuracy observed.

A study conducted by Soladoye et al. (2016) examined a variety of 648 pigs, with different sire breeds, sexes, and diets, which were slaughtered in two different weight classes. Estimates derived from DXA scans of carcass halves and four primal cuts were compared with dissected and chemically analysed

estimates. Overall, the relationship between DXA-derived estimates for lean and fat was highly correlated with values obtained from dissection for both carcass halves and primal cuts ($R^2 > 0.94$). Additionally, the relationship between DXA-derived and chemically determined fat and lean content of pork bellies was similar, with $R^2 = 0.94$, indicating an accurate prediction by DXA of lean and fat mass in pigs' carcass composition.

Since DXA is an indirect measurement tool and therefore does not provide real values, regression equations need to be used to convert DXA estimates and thus perform a quantitative comparison with destructive methods such as chemical analysis or dissection. It is notable that these regression equations are specific for different breeds, sexes, body sizes, body parts and DXA machines (Lösel et al., 2010; Pomar et al., 2017; Kasper et al., 2021).

Kasper et al. (2021) established their own prediction equations by examining 68 male pigs, which were analysed for body composition across three weight levels of 20, 60 and 100 kg using DXA (GE Lunar *i*DXA). Three days after the initial DXA scan, the pigs were slaughtered and the carcasses, dissected into primal cuts, were scanned via DXA, and subsequently chemically analysed. Prediction equations were established with R^2 values between 0.89 for ash and 0.99 for water and crude protein, respectively, with relatively small prediction errors between 4.3 % and 12.6 %. These results suggest adequate estimates of DXA for live animals and carcass composition. Additionally, existing regression equations from other studies for a similar weight class were compared with the obtained results and evaluated for accuracy. Equations generated using the same DXA technology (narrow fan beam) were found to fit better than those generated using other technologies (pencil beam) (Kasper et al., 2021).

Bernau et al. (2015) conducted a study examining updated regression equations developed from estimates obtained through DXA and MRI. These equations were used for performance tests and investigated using carcass halves of 94 stationary boars from three different F1-crossbred lines. The findings revealed that the equation combining DXA and MRI data had the highest R^2 value of 0.95 and the lowest root mean square error of 0.61 %. This suggests improved predictability compared to the reference "Bonner formula"

for lean meat percentage. Additionally, the updated equation simplifies the model by incorporating only three variables instead of the seven variables present in the reference formula.

To our knowledge, only one validation study to date has explored the accuracy of DXA, particularly the CoreScan™ software, in pigs compared to MRI. This study, conducted by Weigand et al. (2020), preceded this research project, and primarily focused on validating visceral fat measurements. Analysing the exact same android region in 120 MHF1 and MHF2 crossbred pigs, they observed a strong linear relationship between MRI and DXA VAT estimates for both scanning modes used, with R^2 = 0.76 (RMSE = 399.25 cm^3) for the “thick” mode and R^2 = 0.71 (RMSE = 443.42 cm^3) for the “standard” mode, respectively. However, a Bland-Altman analysis revealed a systematic bias and constant overestimation of 579.1 cm^3 for VAT by DXA compared to MRI, the gold standard method. An internal comparison within the software of the two scan modes, “thick” and “standard”, demonstrated a strong relationship (R^2 = 0.95, RMSE = 175 cm^3), with the “standard” mode achieving higher overall values.

At bottom line, DXA and particularly with the CoreScan™ software, proves suitable for evaluating body condition and abdominal fat in humans as well in pigs. However, the obtained values may require adjustment through bias corrections or regression equations, since the technology and accompanying software were developed for humans and primarily designed for them.

4.3. Ultrasound

The principle of ultrasound imaging relies on the reflection of ultrasound waves from tissue surfaces when directed by a transducer beam. More precisely, the basis of this lies in the following: sound moves in cyclical waves, with frequencies for ultrasound imaging exceeding 20 kHz. Within the transducer, piezoelectric crystals generate ultrasound pulses, which are then summarised into an ultrasonic beam (Wagner, 2013). This beam is transmitted through the skin and encounter various tissue surfaces. At tissue boundaries, such as skin-fat or muscle-bone, echoes are created that partially reflect to the transducer. The strength of reflected wavelengths and therefore the ultrasound intensity depends on the varying attenuation coefficient of tissues, determined by tissue density and the acoustic velocity of the echo (Scholz et al., 2015). Tissues with higher density lead to higher acoustic velocity. Variances in tissue acoustic impedance result in differing echo strengths received back at the transducer. The acoustic energy is then converted into signals that form an image pixel. Brighter images represent strong reflections, while black images indicate weak or absent reflections, with their position in the image indicating the tissues` depth. Bone tissue, with its relatively high impedance, appears as bright pixels, followed by muscle, connective tissue, water, and adipose tissue. Contrarily, air demonstrates minimal impedance, resulting in black areas in the image. The choice of ultrasound frequency depends on the tissue of interest, with different frequencies required to obtain the desired depth and resolution. Generally, higher ultrasound frequencies provide greater resolution but decreased depth penetration.

Ultrasound transducers can operate in two modes: A-mode or B-mode. A-mode, also known as amplitude mode, emits a linear beam. The ultrasound wave reaching a tissue boundary is reflected as a peak on a graph, representing the amplitude on a y-axis, while depth is encoded on an x-axis. A-mode enables measurements of tissue distances like fat layers or muscle. In contrast, B-mode, referred to as brightness mode, represents an advancement from A-mode, converting echo intensities from various angles into grayscale brightness values, thus generating a two-dimensional image

and offering further insights into cross-sectional tissue areas. In terms of visualisation, B-mode holds a broader clinical significance compared to A-mode ultrasound, offering a wider range of practical application (Wagner et al., 2020).

With the ability to easily distinguish between adipose tissue, muscle and further types of tissue ultrasound technology emerges a common method for evaluating animal body composition, especially regarding back fat thickness and muscle diameters. Being non-invasive, widely accessible, and cost-effective it can be used for assessing body condition in growing-finishing pigs (Reckels et al., 2020) and sows, particularly relating to the phase of mating and farrowing (Lavery et al., 2019), thus helps to guide for feeding adjustments and monitor overall health status effectively. Moreover, ultrasound is used in performance testing of live animals, as well as for carcass composition evaluation and grading post-slaughter. In the context of breeding selection programs, ultrasound measurements of back fat thickness are essential for selecting animals with reduced back fat thickness (Müller and Polten, 2004; Magowan and McCann, 2006) aiming to optimise economical outcomes. This is particularly of interest given that subcutaneous fat is known to be of high heritability (Malek et al., 2001; Lee et al., 2011). Furthermore, ultrasound technology finds application in human medicine for assessing obesity, providing real-time data acquisition (Ribeiro-Filho et al., 2003; Asano et al., 2017).

III. MATERIAL AND METHODS

1. Animals

This study is part of a genome-wide association study aimed at phenotyping pigs from a purebred parental generation to a multi-hybrid offspring generation, based on four parental breeds frequently occurring in Germany: Large White, German Landrace, Piétrain and Duroc (Figure 4).

An experimental setup for phenotyping the above-mentioned multi-hybrid pigs using MRI and DXA has been previously described by Weigand et al. (2020). However, in this study new aspects have been added, as specified in the following.

All procedures performed on animals in this study were approved by the Animal Ethics Committee of the Government of Upper Bavaria under protocol numbers ROB-55.2-2532.Vet_03-16-81 and ROB-55.2_2532.Vet-03-21-50 between May 2021 and August 2022.

Figure 4: Four-way (multi-hybrid) crossbred pigs of the second generation (MHF2)

1.1. Animal sample

In this study, 138 multi-hybrid four-way crossbred pigs from the second filial generation (MHF2) have been examined. The animals were randomly selected for evaluation based on their birth dates, without consideration for balancing by sex, genotype, or rearing season and year. The dataset includes 46 castrated males and 92 females. Details on their distribution across genotypes and season-year categories are provided in Table 14 in Appendix IX.3.1.

Out of the initial 138 pigs scanned, as detailed in Chapter III.3.2.1 (MRI image analysis), factors such as sudden movements and size limitations during MRI examinations resulted in images being analysable for a subgroup of 67 animals, including 23 castrated male and 44 female pigs. As a result, this study focuses on this group of n = 67 animals, for which imaging data from MRI, DXA, and ultrasound scans are available for comprehensive analysis.

Based on the specific crossbreeding scheme and the consistent genetic composition of the sire (PiDuDLDE), six different combinations are apparent in this study population. The crossbreeding scheme, involving the four parental breeds Piétrain (Pi), Duroc (Du), German Landrace (DL) and Large White (DE), is illustrated in Figure 5.

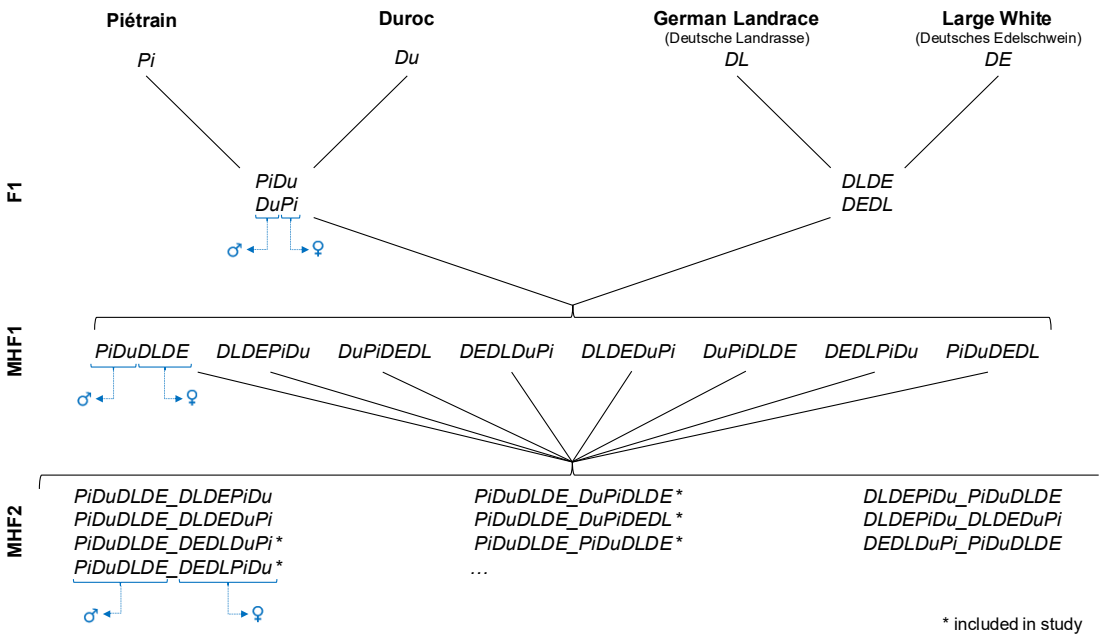

Figure 5: Crossbreeding scheme based on parental breeds Piétrain (Pi), Duroc (Du), German Landrace (DL) and Large White (DE)

The study was conducted at regular intervals between May 2021 and August 2022 and included group evaluations when the subjects reached an average age of 147 days. The renewal of the animal experiment authorization resulted in an unexpected hiatus of two months in data collection, spanning from November to December 2021.

Building on this, the examination days were categorised by month and year of the animals' scans. Two consecutive months were combined to represent a single season, as illustrated in Table 1.

Table 1: Overview of seasons

season	**month**
1	January + February
2	March + April
3	May + June
4	July + August
5	September + October
6*	November + December

(* is not included in this study)

1.2. Rearing period

All pigs included in this study were bred and raised at the Livestock Centre of the Veterinary Faculty of the Ludwig-Maximilians-University Munich, located in Oberschleissheim, Germany. Their handling and rearing adhered with standard practices for pigs at this institution. All male pigs underwent surgical castration on the third or fourth day of life.

1.2.1. Housing

The facility operates on a 3-week farrowing rhythm system. Following a 4-week suckling period, the animals were weaned and relocated to a flat deck area, where they were housed in groups of 25 - 30 animals. At approximately 70 days of age, they were transferred in groups of up to 35 animals to an outside-climate stable, featuring a ground area of approximately 54 m² per stable bay. This stable is divided into two levels, connected by stairs and a ramp. The lower level is covered with straw-bedding and has a roofed micro-climate area suitable for resting (Figure 6). The upper level, fitted with concrete-slatted flooring, serves as the feeding area (Figure 7). It houses a built-in feeding station with two feeders (Double-FITMIX, Mannebeck Landtechnik GmbH, see Table 3) and four nipple drinkers. The outer walls, constructed with air-permeable wood panelling, maintain an internal climate nearly identical to the external temperature conditions.

Figure 6: Outside-climate stable (from upper level)

Figure 7: Outside-climate stable (from lower level)

1.2.2. Feeding

An automatic feeding system named “Double-FITMIX” with two single-spaced feeders for individual feed supply is used to feed the animals, allowing for accurate monitoring of daily feed intake for each pig. A transponder chip in the ear, equipped with tag number recognition, enables the animal to access its assigned feed. An automated evaluation system monitors the daily consumption of each animal and determines the remaining amount for the day. This information is derived from the number of rotations of a screw conveyor responsible for transporting the feed to the pipe opening. The conveyor has been pre-calibrated to dispense 35 grams of pre-fattening feed and 45 grams of finishing feed for every 10 rotations. The system records the remaining percentage of unconsumed feed per day, allowing the calculation of daily feed intake by comparing it with the reference feed curve. In general, the finishing feed is introduced as soon as the pigs reach approximately 70 kg of body weight (Table 2).

Due to technical problems with regular backups of the feeding data, gaps in the recordings were found. Consequently, the daily feed intake was not available for all animals on every day in our study. Therefore, the recorded feeding period was subdivided into feeding weeks, and daily feed intake was analysed within these (see Table 13 in Appendix IX.2). Feeding week 1 began at the time of admission to the outside-climate stable at approximately 70 days of age and was calculated up to the date of the study examination.

Table 2: Composition of ingredients of pelleted diet during the experiment

Ingredients [%]	pre-fattening feed	finishing feed
Barley	31	55
Wheat	22	12
Oat	0	5
Corn	22	11
Soybean extraction meal	21	13.5
Mineral premix [a]	3	2.5
Formi® [b]	1	1

a: SALVANA MASTKRAFT (composition details are displayed in Appendix IX.1)
b: technological feed additive, acidity regulator (potassium diformate), by ADDCON

2. Materials

Table 3: Devices, software, drugs, and consumables

Devices	
Double feeding system, Abruffütterung Typ “FITMIX”	B. Mannebeck Landtechnik GmbH, Schüttorf, Germany
GE Lunar *i*DXA	GE Healthcare GmbH, Düsseldorf, Germany
Magnetom C! 0.35T	Siemens Healthineers AG, Forchheim, Germany
M-Turbo® ultrasound system	FUJIFILM SonoSite, Inc., Bothell, WA, USA
L52x Linear Transducer, 10-5 MHz	FUJIFILM Sonosite, inc., Bothell, WA, USA
Software	
3D-Doctor, Release 4.0	Able Software Corp., Lexington, MA, USA
GE Lunar enCore™ software, Version 17	GE Healthcare GmbH, Düsseldorf, Germany
SAS 9.4 (SAS/STAT® 15.1, User’s Guide, 2018)	SAS Institute Inc., Cary, NC, USA
Siemens MRI syngo© software, Version 06.2008, Order No. A91MR-300-20-7600	Siemens Healthineers AG, Forchheim, Germany
Synedra View Personal Version 16.0.0.3	Synedra information technologies GmbH, Innsbruck, Austria
Drugs	
Stresnil®, 40 mg/ml	Elanco GmbH, Cuxhaven, Germany
Ursotamin®, 100 mg/ml	Serumwerk Bernburg AG, Bernburg, Germany
Consumables	
S-Monovette®, K3 EDTA 9 ml Luer Lock	Sarstedt AG & Co. KG, Nümbrecht, Germany
VasoVet® Braunüle 24G 0,7 x 19 mm Luer Lock	B. Braun Vet Care GmbH, Tuttlingen, Germany

3. Methods

The following chapter outlines the methods used to examine the animals and collect the data for this study.

3.1. Examination day

3.1.1. Preparations

The examination of the MHF2 pigs was performed with an average age of 147 days. One day before the scan the pigs were transferred into an examination stable, where the imaging facilities are located. To minimise the risk of anaesthesia the animals underwent a fasting period of approximately 20 hours. Water was accessible throughout.

Before scanning, a quality-control procedure was carried out on both the DXA and MRI scanners. For the DXA scanner, a quality-control phantom was used in accordance with the manufacturers' instructions, while the MRI local coils were automatically adjusted and shimmed using the Siemens MRI syngo© software tool (Table 3).

3.1.2. Procedures

On the examination day, all pigs underwent a health assessment through a clinical examination conducted by the veterinarian in charge of the testing procedures. To perform the imaging scans sedation was required. Therefore, every pig was weighed with a mechanic livestock scale and dosed individually using Azaperone 40 % (1-2 mg/kg, Stresnil®, Elanco) and Ketamine 10 % (10-15 mg/kg, Ursotamin®, Serumwerk Bernburg) as injection anaesthetics. If needed, Ketamine could be adjusted via a catheter (VasoVet®, B. Braun) in the *vena auricularis*. Examination details such as weight, individual dosage, and the use of anaesthetics, along with rectal body temperature as well as vital signs before and during sedation, were documented on score sheets. Additionally, two blood samples were collected using EDTA-coated tubes (S-Monovette®, Sarstedt) via *vena jugularis externa*, and the number of teats of each animal was counted.

3.1.3. Imaging

3.1.3.1. Ultrasonography

Ultrasonography was performed to measure the back fat thickness and the diameter of the longissimus dorsi muscle of each pig, using the M-Turbo® ultrasound system (M-Turbo®, Fujifilm SonoSite) fitted with a linear-array 10-5 MHz transducer (L52x, Fujifilm SonoSite).

Prior to scanning, the hair was clipped at the scanning sites, and the skin was defatted using alcohol. Specific assessment points were marked in colour on the animals using a template. High-contrast images were then generated after applying an acoustic coupling gel.

The scanning site was evaluated at three identified points: Point B, situated at the midpoint between the elbow and knee along a line, 7 cm lateral from the spine midline; followed by Point A, positioned 12 cm cranial to the midpoint; and Point C, located 12 cm caudal to the midpoint, both also 7 cm from the midline. The aim was to visualise both the back fat thickness, encompassing the skin and the overall subcutaneous adipose tissue including the lumbodorsal fascia, and the diameter of the longissimus dorsi muscle. The selection of scanning points adhered to the specifications of performance testing for pigs as described by Müller and Polten (2004).

The images were saved in DICOM format for further evaluations.

3.1.3.2. Magnetic Resonance Imaging

An open low-field MRI system (Magnetom C!, Siemens, see Table 3) with a field strength of 0.35 Tesla was used to examine the fat distribution. The pigs were placed on the MRI table in a prone position with extended front and hind limbs (Figure 8). To facilitate image comparison across different animals, anatomical landmarks were established to define the region of interest, spanning from the last thoracic vertebra to the iliac crest. Due to the body length of the animals, two scans were performed, labelled as “ViscFat” sequence for the cranial abdominal part and “HamFat” sequence for the caudal abdominal and pelvic part, both employing protocol settings outlined in Table 4.

Figure 8: Animal positioning on MRI table

Table 4: MRI setting protocols of "ViscFat" and "HamFat" sequences

	ViscFat	**HamFat**
Voxel size [mm x mm x mm]	1.9 x 1.6 x 6.0	1.9 x 1.6 x 6.0
Signal-to-noise ratio	1.00	1.00
Number of slices	30	20
Slice thickness [mm]	6	6
Distance factor [%]	20	20
FoV read [mm]	400	400
FoV phase [%]	100	100
Time to Repeat (TR) [ms]	441	370
Time to Echo (TE) [ms]	18	18
Orientation	axial	axial
Examination time [min]	12.13	10.16

3.1.3.3. Dual Energy X-ray Absorptiometry

To analyse the composition of the whole body, a DXA scanner (GE Lunar *i*DXA, GE Healthcare GmbH, see Table 3) was used. In this study, two scanning modes, “thick” and “standard”, were applied to generate data related to the quantity and distribution of fat and lean body mass, as well as bone mineral content and bone mineral density for each pig’s entire body.

To obtain this data, sedated pigs were put on the DXA table in a prone position with the front legs bent backwards to the side of the body and the hind legs extended, as illustrated in Figure 9. Two whole-body scans were conducted, with the “thick” mode taking up to 13 minutes and 45 seconds and producing a dose of 6 µGy, while the “standard” mode required up to 7 minutes and 45 seconds and delivered a dose of 3 µGy.

Figure 9: Animal positioning on DXA scanner table (side)

Figure 10: Animal positioning on DXA scanner table (front)

3.1.4. Recovery and Follow-up

After the imaging procedures were completed, the animals were placed in a straw-bedded box for recovery. Care was taken to ensure clear airways, and the venous catheter was removed. They were monitored by a veterinarian until fully awake and brought back to the outside-climate stable the following day. Their feed intake and movement were observed and noted in the score sheets during the next day.

Until the end of the fattening period the animals were kept in this outside-climate stable and were slaughtered with a weight of approximately 130 kg.

3.2. Image analysis

All collected images were subsequently analysed post-scanning by the same evaluator.

3.2.1. MRI image analysis

All images in DICOM format were transferred to the synedra View Personal software (synedra information technologies GmbH, see Table 3). This software enables an overview of all images from both sequences (“ViscFat” and “HamFat”) and assists in identifying those covering the region of interest, spanning from the last thoracic vertebra to the iliac crest. The total number of images used per pig ranges from 27 to 38 (Table 5), depending on the animal’s body length.

A few images exhibited insufficiently analysable quality due to spontaneous movements during the MRI scanning period. Additionally, the size, particularly the width of the abdomen in animals weighing over 100 kg, posed a challenge. It hindered the adequate visualisation of the entire subcutaneous adipose tissue through MRI and the associated evaluation process. Moreover, the image evaluation proved to be highly time-intensive, as it had to be done by hand, since the software lacked sufficient automated evaluation tools.

Consequently, analysis results from MRI images are available for a total of 67 animals.

Table 5: Number of total MRI images, depending on animal’s body length

	number of images
min	27
max	38
mean	31.657
total	2121
number of animals	67

Using the Able 3D-Doctor© software (Able Software Corp., see Table 3), subcutaneous and visceral adipose tissue were detected and marked in colours (Figure 11). This process was manually evaluated for each animal.

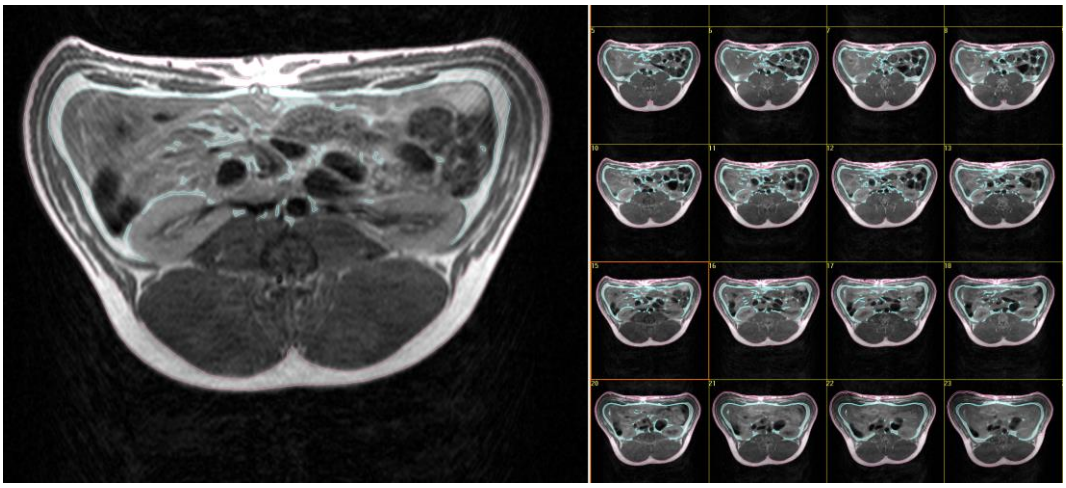

Figure 11: Excerpt from “ViscFat” sequence evaluation

Subcutaneous adipose tissue (SAT) was defined as the fat layer directly beneath the skin, marked in magenta. Visceral adipose tissue (VAT) was defined as the fat inside the abdominal cavity surrounding the intra-abdominal organs, kidneys and beneath the abdominal wall, marked in turquoise.

The software can quantify the volume of SAT (magenta) and VAT (turquoise) in mm^3 (converted into cm^3) based on a 3D-model (Figure 12) constructed by using the number, thickness, and distance of the individual slices of each animal.

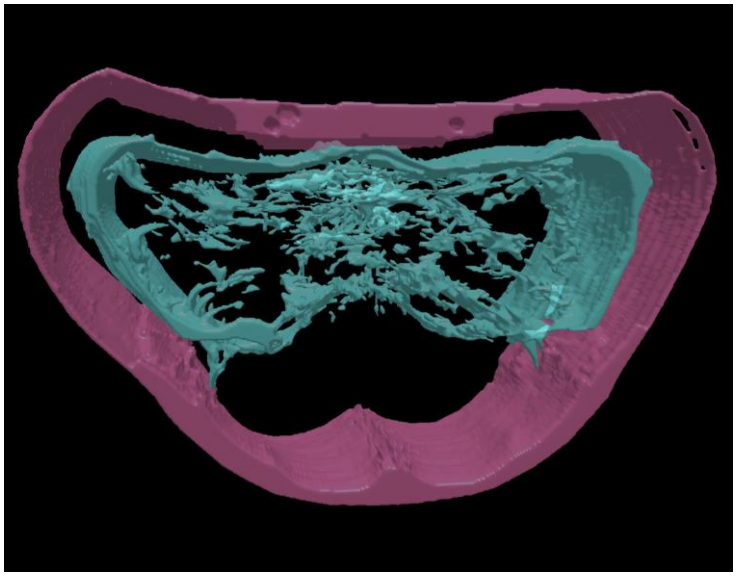

Figure 12: 3D-model with SAT and VAT based on MRI scan

3.2.2. DXA image analysis

The software enCore™ of the Lunar *i*DXA scanner (GE Healthcare GmbH, see Table 3), utilised for data evaluation, offers automated assessments of whole-body composition parameters including weight [kg], fat mass [g], lean mass [g], bone mineral content [g] and bone mineral density [g/cm^2].

Additionally, the CoreScan mode, designed for human adults, enables the analysis of visceral fat mass [g] and volume [cm^3] in the android region.

The CoreScan™ software automatically defines the android region area, as described in Chapter II.4.2.2 (Fields of application). In pigs, the region of interest, in particular the android region, needs to be defined manually in the same way as applied for the MRI evaluation, spanning from the last thoracic vertebra to the iliac crest. The gynoid region is set automatically (II.4.2.2).

The android region contains both visceral adipose tissue (VAT) and subcutaneous adipose tissue (SAT). Employing an algorithm, the software assesses the overall thickness of the abdomen using X-ray attenuation. It considers two parameters: the width of the SAT layer on the lateral aspects of the body and the anterior-posterior thickness of the abdomen. The width of the SAT layer is determined by the fat between the skin line and the outer abdominal wall on both sides of the image. Utilizing the DXA attenuation image provides the anterior-posterior thickness of the abdomen, contributing to the estimation of SAT (see General Electric Company, 2012 patent WO2012092533A1, *https://patents.google.com/patent/WO2012092533A1/en*, last accessed 24.08.2024).

The model integrated into the software subtracts SAT mass from the total abdominal fat mass in the android region (total abdominal adipose tissue, TAT), providing an estimate of VAT mass. Therefore, VAT mass [g] and volume [cm³] can be calculated for the specified region based on the SAT composition. It's essential to highlight that the quantity of VAT is only an estimate and cannot be directly measured.

Conversely, it is then possible to calculate the SAT mass by subtracting the estimated VAT mass [g] from the android fat mass [g] determined by the software. Using the VAT mass and volume information provided by the

CoreScan™ software, its density can be calculated, thus allowing for the estimation of SAT and TAT volume in the android region.

3.2.3. Ultrasound image analysis

The DICOM-formatted images for the focus group of 67 animals were transferred to the synedra View Personal software (synedra information technologies GmbH, see Table 3), employed as the tool for image analysis and measurements. Initial calibration was conducted using the calibration marks present on the ultrasound images.

The back fat may appear in either two or three layers, depending on the animal's condition. Accordingly, separate thickness measurements were conducted for each layer noted as BFT 1 (including the skin and the first outermost layer), BFT 2 (containing the skin and the second layer), and BFT 3 (covering all layers of fat, along with the lumbodorsal fascia, from skin to the muscle). In instances where the entire longissimus dorsi muscle (Mld) was visualised, depending upon the condition of the animal and the scanning site, its diameter was subsequently measured (Figure 13). This was performed at all three scanning sites: B (midpoint), A (cranial) and C (caudal).

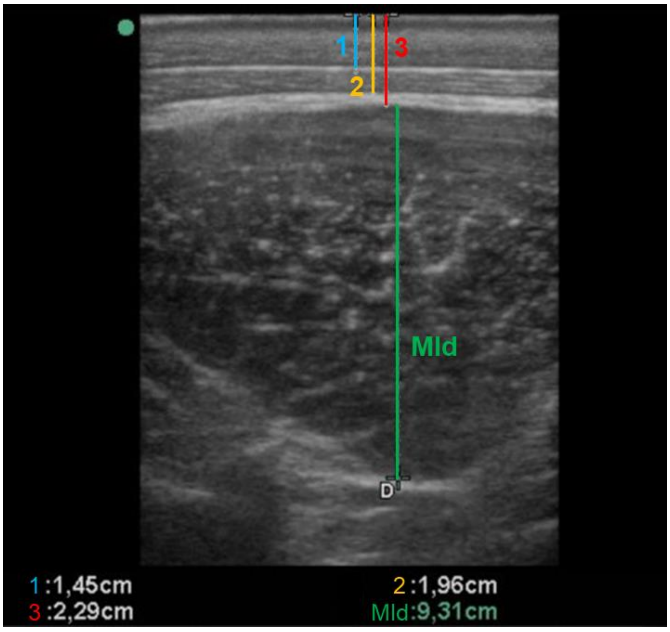

Figure 13: Back fat layers and longissimus dorsi muscle diameter in point B

In the further course of this study the back fat thickness is defined as the sum of skin, entire subcutaneous fat layers, and the lumbodorsal fascia (BFT 3). The different layers of the back fat will not be further discussed, as it falls outside the predetermined scope of this study.

Measurement inaccuracies may arise at scanning point A due to the potential overlap of the longissimus dorsi muscle with other muscles and the overall increase in subcutaneous fat thickness (Müller and Polten, 2004) as measured further cranially (Figure 14).

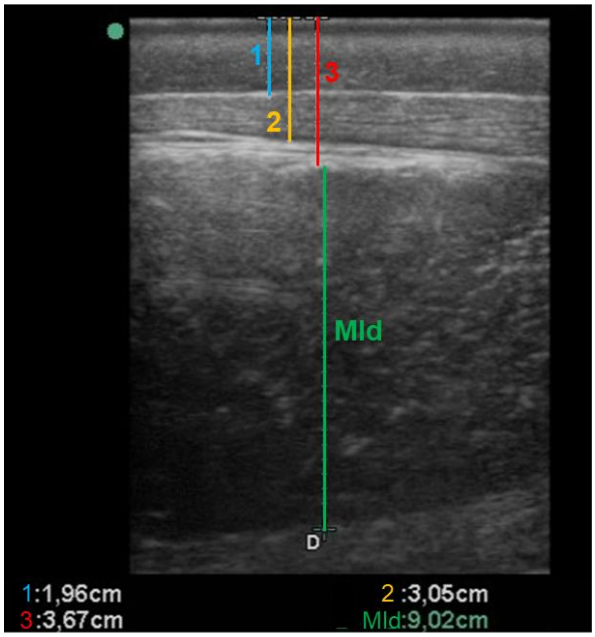

Figure 14: Back fat layers and longissimus dorsi muscle diameter in point A

A Box-Whisker plot in Figure 15 compares all values across the three scanning sites, revealing a broad dispersion of values at point A. Additionally, the median at point A lies outside the boxes of points B and C. Furthermore, measurements at point C show a wider scattering compared to point B.

Consequently, for subsequent analyses focusing on back fat thickness, only measurements from point B were considered instead of using the average of all three scanning sites.

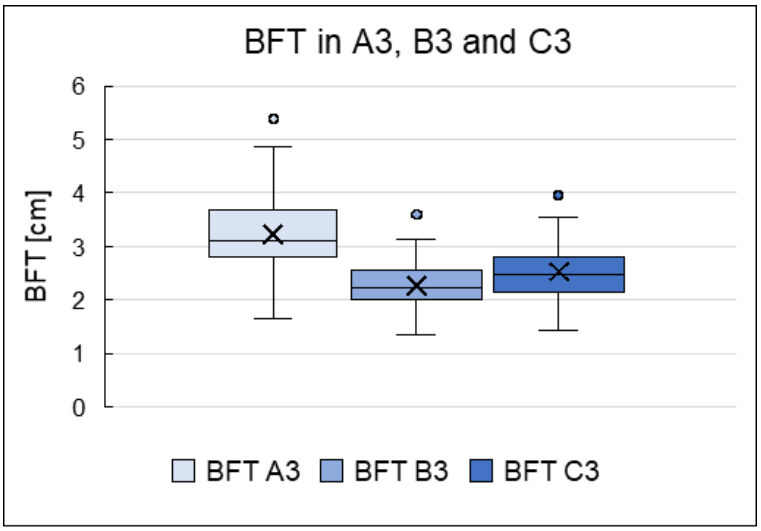

Figure 15: Comparison of back fat thickness at point A, B and C

4. Statistical analysis

The statistical analysis was performed by using the software SAS 9.4 (SAS Institute Inc., see Table 3). All variables were assessed on normal distribution using the Kolmogorov-Smirnov test, complemented by visual inspection through histograms. Additionally, Box-Whisker plots were employed to identify and examine potential outliers.

The dataset in focus includes 67 animals with MRI, DXA and ultrasonography results.

Linear regression models were conducted to assess the relationships among several factors, including general parameters, various body composition parameters, and feeding data. The coefficient of determination (R^2) and the root mean square error (RMSE) were used as a measure of the regression equation's fit between the dependent and independent variables. Additionally, p-values were assessed to determine the statistical significance of the relationships, with a significance level set at $p < 0.05$.

Variance analysis was performed using three linear mixed model procedures with restricted maximum likelihood (REML) estimation, a method that provides more precise estimates of variance components in the presence of random effects. The mixed models were chosen based on the smallest Akaike information criterion (AIC) values. A significance level was set to $p < 0.05$ for both the F-tests and the t-tests.

To enhance the reliability of the analyses, the statistical examinations, particularly the mixed models described in Chapter III.4.1.1 and III.4.1.2, were supplemented with the entire data set, including 138 animals, each with available DXA data. Details of the results can be found in the Appendix IX.3.

Furthermore, a Bland-Altman analysis was conducted to assess the agreement between MRI and DXA in quantifying abdominal adipose tissue variables (VAT, SAT, and TAT) by comparing the means and differences of these variables measured with both methods. Additionally, a modified Bland-Altman plot was performed, with the reference gold standard method of MRI used as the horizontal axis instead of the means of both methods, as described by Johnson, M. and Waller J. (2018). The results of this analysis

are provided in Appendix IX.4 (Figure 64, Figure 65, Figure 66).

4.1. Variance analysis models

In the upcoming section, a more detailed explanation of the linear mixed models used for variance analysis is provided.

4.1.1. Study sample characteristics

The first mixed model assesses the characteristics of the study's focus group considering the variables body weight (weight) [kg], age [d] and number of days spent in the outside-climate stable (stable days) [d]. In this analysis, sex, genotype and the interaction between season and year were applied as fixed effects. The applied mixed model is described by the following equation:

$$y_{ijklm} = Sx_i + G_j + Seas_k * Y_l + e_{ijklm}$$

y_{ijklm} = Considered variable (weight, age, stable days)

Sx_i = Sex (i = 1-2, castrated male / female)

G_j = Genotype (j = 1-6, PiDuDLDE_DLDEPiDu, etc.)

$Seas_k * Y_l$ = Interaction effect between season and year ($k * l$ = 1-7, 4 / 2021, etc.)

e_{ijklm} = Residual error (with m = individual animal)

4.1.2. Abdominal adipose tissue and body composition parameters

For all traits assessed with MRI and DXA, sex, genotype, and the interaction between season and year were defined as fixed effects. In addition, weight was included as a covariate in this model. The following equation describes the applied mixed model:

$$y_{ijklm} = Sx_i + G_j + Seas_k * Y_l + \beta_{ijklm} + e_{ijklm}$$

y_{ijklm} = Considered variable (MRI VAT, MRI SAT, DXA VAT, etc.)

Sx_i = Sex (i = 1-2, castrated male / female)

G_j = Genotype (j = 1-6, PiDuDLDE_DLDEPiDu, etc.)

$Seas_k * Y_l$ = Interaction effect between season and year ($k * l$ = 1-7, 4 / 2021, etc.)

β_{ijklm} = Covariate weight

e_{ijklm} = Residual error

4.1.3. Daily feed intake

Another mixed model was applied for the focus group to examine the effects of sex, genotype, season, and the time during the fattening period (feeding week) on daily feed intake.

In this model, season (treated as a single effect) and feeding week were included as fixed effects, along with sex and genotype. It can be described by the following equation:

$$y_{ijklm} = Sx_i + G_j + Seas_k + FW_l + e_{ijklm}$$

y_{ijklm} = Considered variable (daily feed intake, FI_d)

Sx_i = Sex (i = 1-2, castrated male / female)

G_j = Genotype (j = 1-6, PiDuDLDE_DLDEPiDu, etc.)

$Seas_k$ = Season (k = 1-5)

FW_l = Feeding Week (l = 1-10)

e_{ijklm} = Residual error

IV. RESULTS

All figures and tables presenting the results of the regression analyses include the regression equation with the corresponding coefficient of determination (R^2) and root mean square error (RMSE). In addition, the statistical significance of the regression coefficients (p-value) is provided.

All tables containing results referring to the variance analysis present least squares means (LSM), standard errors of estimation (SEE) and the significance level (p-value) of the variables examined. To determine differences between the examined groups within the independent variables – sex, genotype, and season x year – LSD (least significant difference) post-hoc tests were performed for pairwise group comparisons. If there is a significant difference among the mean values of individual groups, it is represented by using distinct superscripts.

In this chapter, the abbreviations for abdominal adipose tissue variables are defined as follows:

- visceral adipose tissue (VAT)
- subcutaneous adipose tissue (SAT)
- total abdominal adipose tissue (TAT)

To simplify the readability of tables and diagrams, the genotype groups have been abbreviated. The initial segment of the genotype, determined by the sire's crossbred composition and the dam's crossbred composition, remains constant due to the same sire and is therefore omitted. Additionally, the provided numbers in the tables represent individual genotype groups as assigned in the following:

Table 6: Overview of genotype groups

Group number	Genotype
1	PiDuDLDE_DEDLDuPi
2	PiDuDLDE_DEDLPiDu
3	PiDuDLDE_DLDEPiDu
4	PiDuDLDE_DuPiDEDL
5	PiDuDLDE_DuPiDLDE
6	PiDuDLDE_PiDuDLDE

1. Relationships between various phenotyping parameters

1.1. General parameters

1.1.1. DXA modes “thick” and “standard” for VAT and SAT

To evaluate the relationship between VAT and SAT values analysed in DXA “thick” and “standard” mode, a linear regression analysis model (red dashed line) was used.

Figure 16 shows that measuring VAT volume in “standard” mode resulted in higher values than in “thick” mode. The coefficient of determination with R^2 = 0.928 is nearly 1. Any outliers were probably caused by the animals’ strong movement during or towards the end of the scan, with “thick” mode being usually applied before “standard” mode.

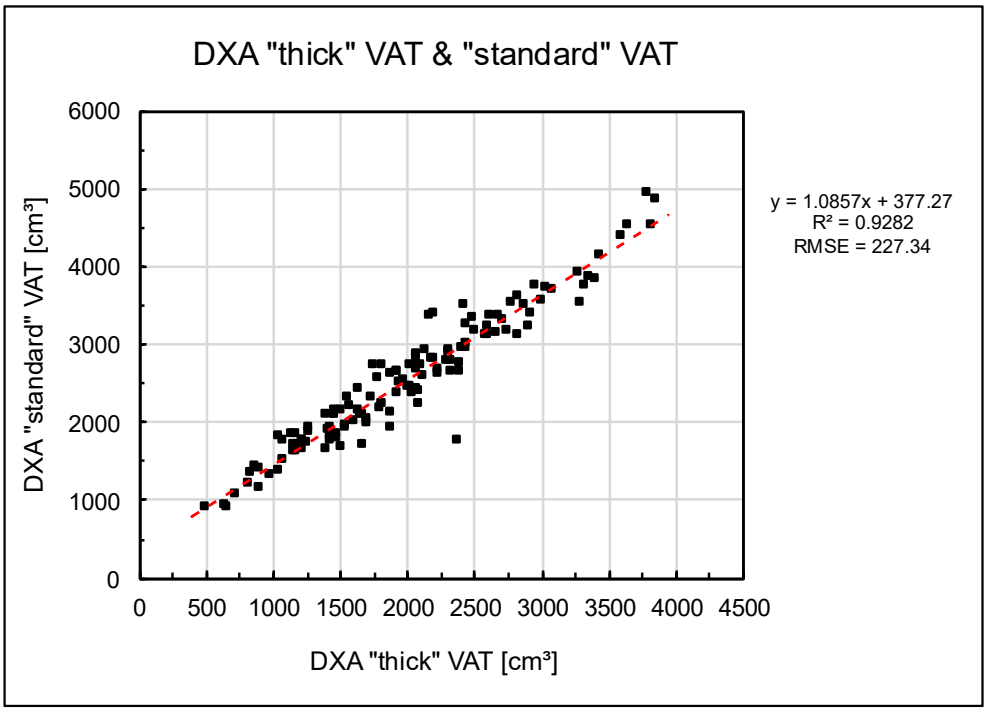

Figure 16: Comparison of DXA modes “thick” and “standard” for estimation of VAT

For enhanced comparability with MRI data, volumes were primarily used in the following analyses. As expected, the relationship between mass and volume is shown with a coefficient of determination of 1 (see IX.3.1 Figure 62).

When comparing the two modes based on the calculated SAT volume data, in Figure 17 it became visible that the “standard” SAT mode supplied negative values, which cannot correspond with reality. Given this discrepancy, the “standard” mode was excluded from the analyses. All data, generated via DXA, were derived from the “thick” mode.

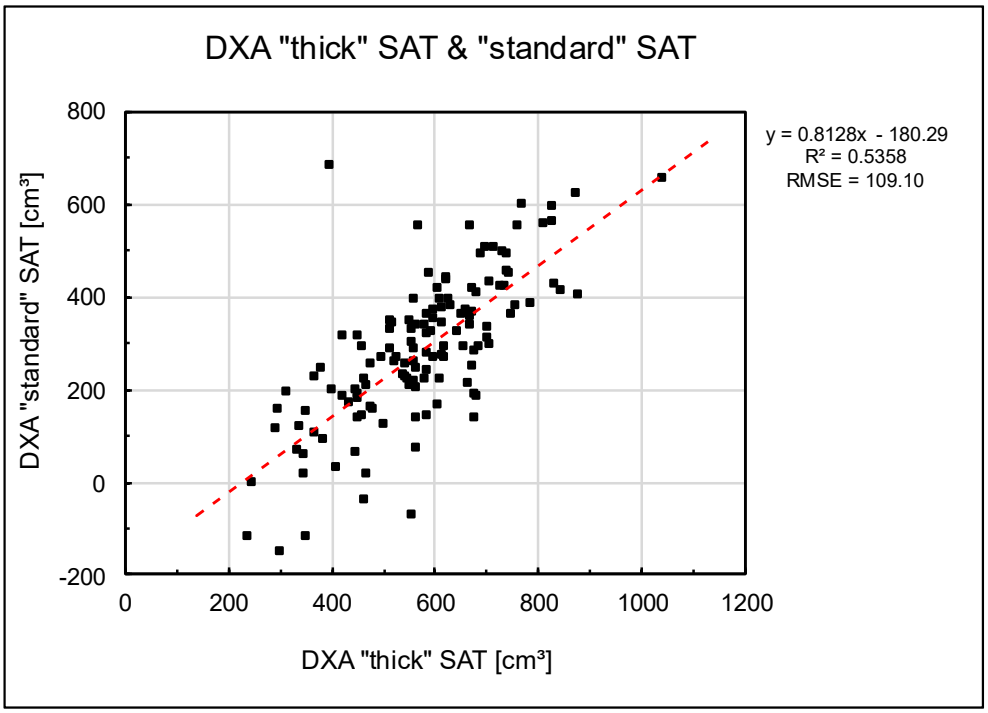

Figure 17: "Standard" mode provides negative SAT values

1.1.2. Body weight and DXA mass

A close relationship between the mechanically determined body weight and the weight generated by DXA in “thick” mode (labelled as DXA mass) is illustrated in Figure 18. DXA mass aligned very closely to the measured body weight. However, minor inaccuracies can occur due to movement. In further analyses of the study the body weight, measured by an animal scale, was used.

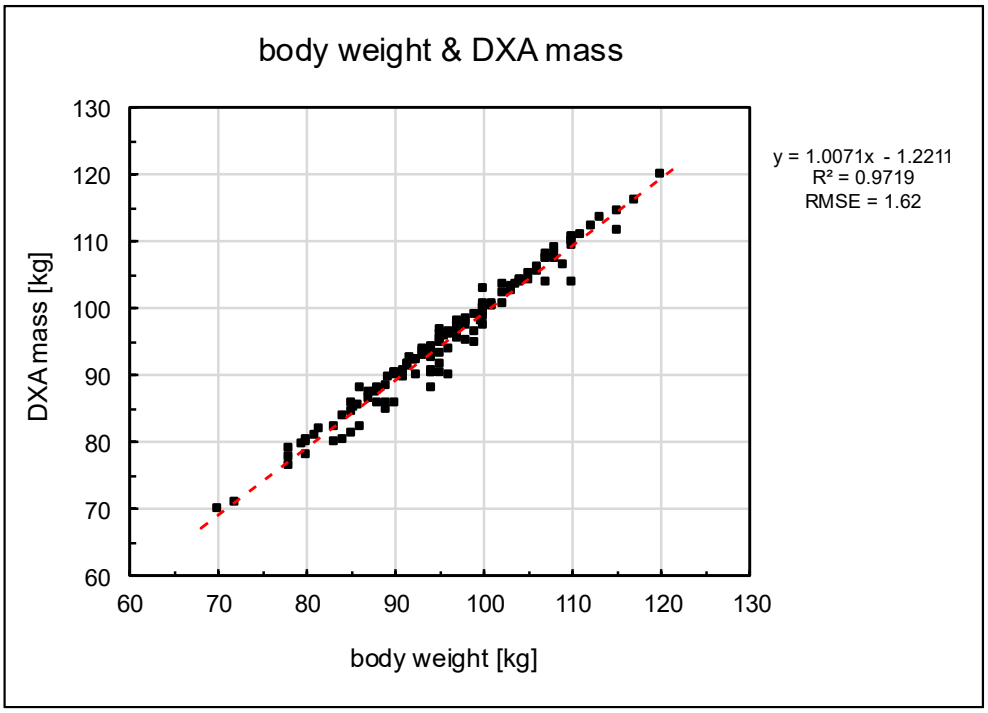

Figure 18: Relationship between scale body weight and DXA mass

1.1.3. Number of MRI images and abdominal adipose tissue volumes

As mentioned in Chapter III.3.2.1, the total number of MRI images depends on the region of interest, which extends from the last thoracic vertebra to the iliac crest. Therefore, the number of images varied depending on the animal's body length. The linear regression analysis in Figure 19 is intended to show the extent to which the number of MRI images had an influence on VAT and SAT volumes.

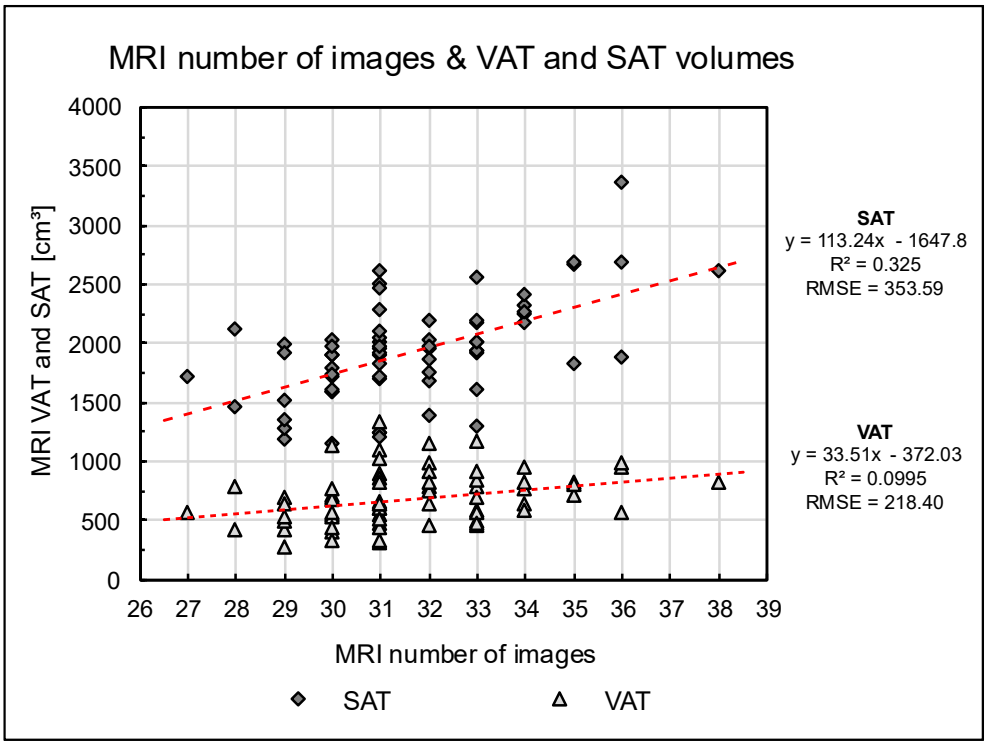

Figure 19: Relationship between total number of MRI images and VAT & SAT

As assumed, the expectation of increased fat volumes in the region of interest with a higher number of images analysed was validated through positive regression coefficients. However, the regression analysis showed a stronger relationship between number of MRI images and SAT volumes compared to VAT volumes. Both models revealed to be statistically significant (SAT $p < 0.001$, VAT $p < 0.05$).

1.2. Abdominal adipose tissue parameters

1.2.1. Relationships between abdominal adipose tissues

This analysis investigates the relationships within abdominal adipose tissue parameters, focusing on the relationship between TAT and its components, VAT and SAT.

For volumes estimated via MRI (Figure 20), the model equations for VAT and SAT exhibit strong positive relationships with TAT. The coefficients' p-values underscore the statistical significance of the observed relationships ($p < 0.0001$).

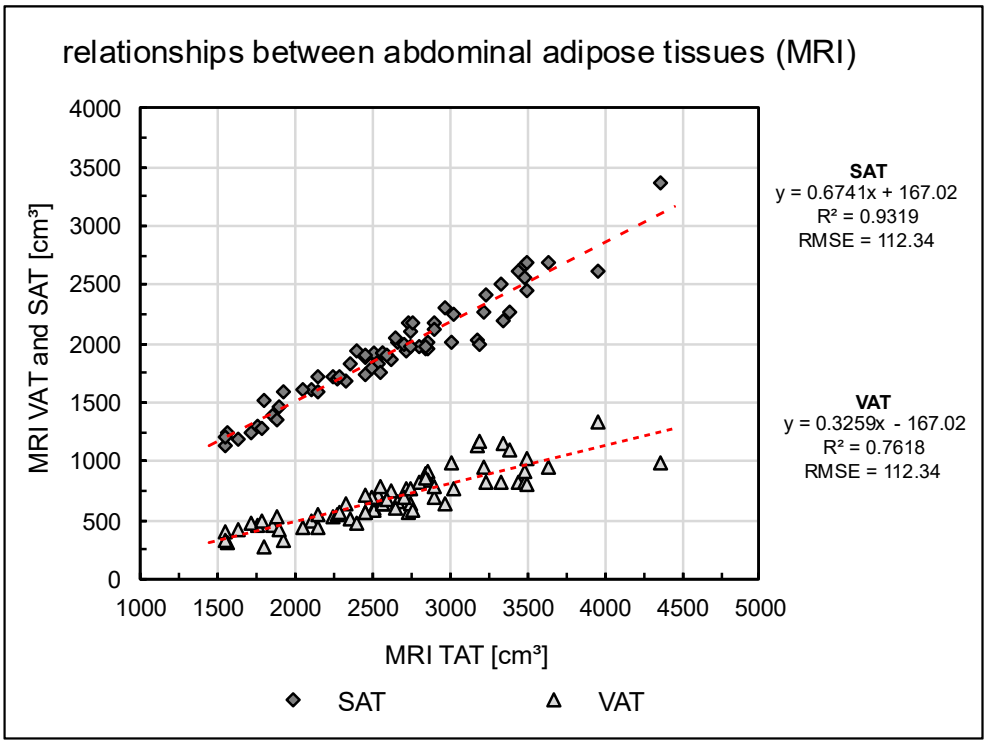

Figure 20: Relationships between abdominal adipose tissues derived by MRI

On the other hand, for DXA estimates, the relationship between TAT and SAT is characterised by a statistically non-significant model ($p = 0.489$). However, the relationship between TAT and VAT remained consistent, reflected in a strong R^2 ($p < 0.0001$) (Figure 21).

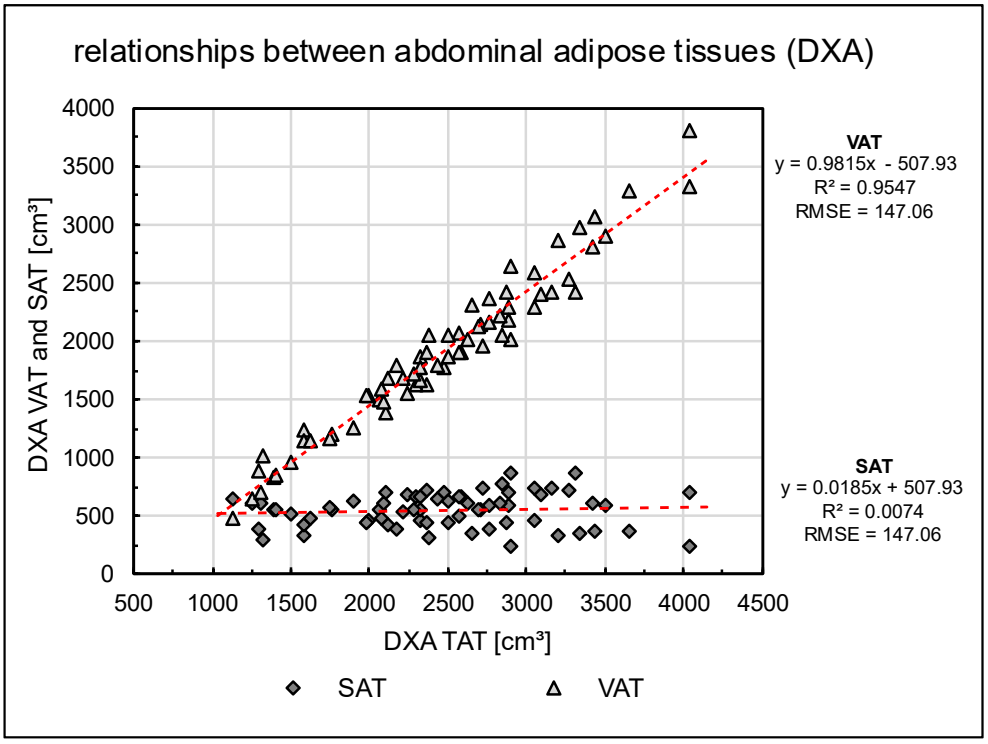

Figure 21: Relationships between abdominal adipose tissues derived by DXA

When examining the relationships between total abdominal adipose tissue and VAT or SAT, derived by DXA in the larger study cohort of 138 animals (Figure 63, Appendix IX.3.3), it became apparent that there were minimal differences in these relationships compared to the results presented in this chapter.

1.2.2. Abdominal adipose tissue volumes measured by MRI vs. DXA

The focus of the following regression analyses is to assess the strength of the relationship between the variables of abdominal adipose tissues (VAT, SAT, and TAT) derived by MRI and DXA. In the following, Chapter IV.5 evaluates if both methods have a close agreement.

Figure 22 shows the regression between VAT measurements in MRI and DXA, which indicates a moderately strong positive relationship ($p < 0.0001$).

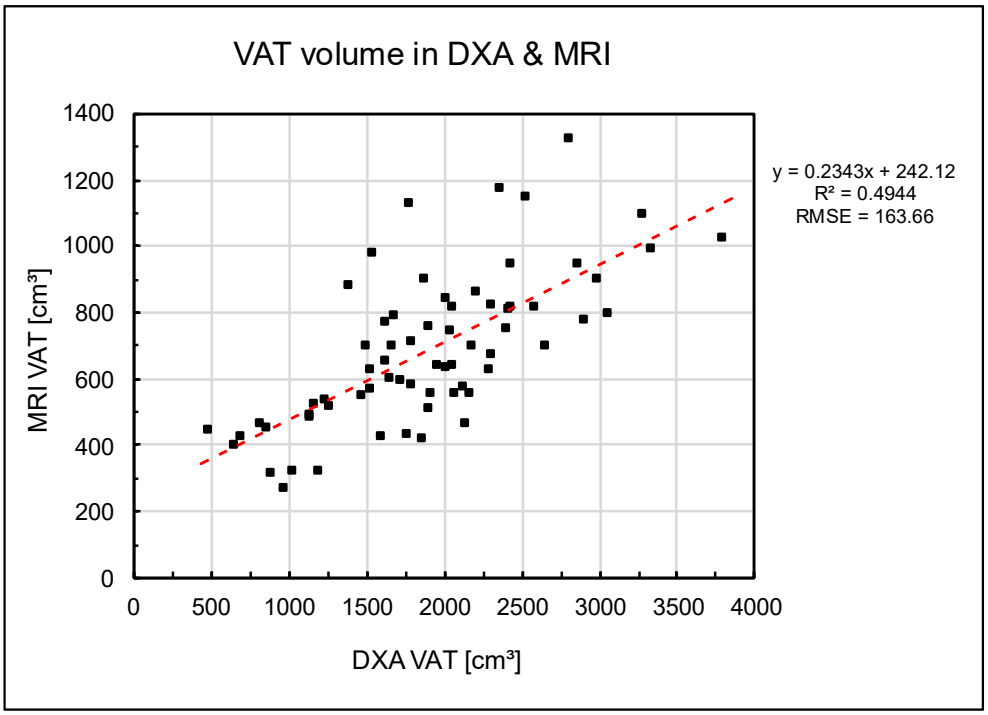

Figure 22: Relationship between DXA-assessed VAT and MRI-assessed VAT

However, SAT demonstrates a smaller R^2 of 0.017 with a non-significant p-value ($p = 0.299$), indicating limitations for this regression model (Figure 23).

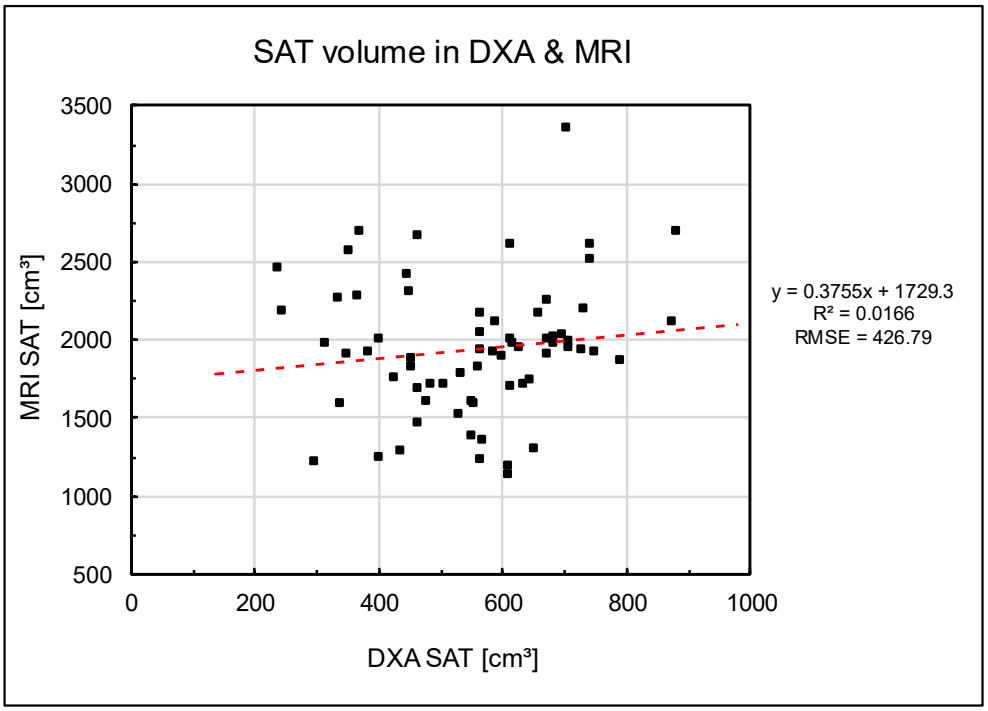

Figure 23: Relationship between DXA-assessed SAT and MRI-assessed SAT

Figure 24 shows the results for TAT, suggesting a positive association ($p < 0.001$) between the DXA-assessed values and MRI-assessed values.

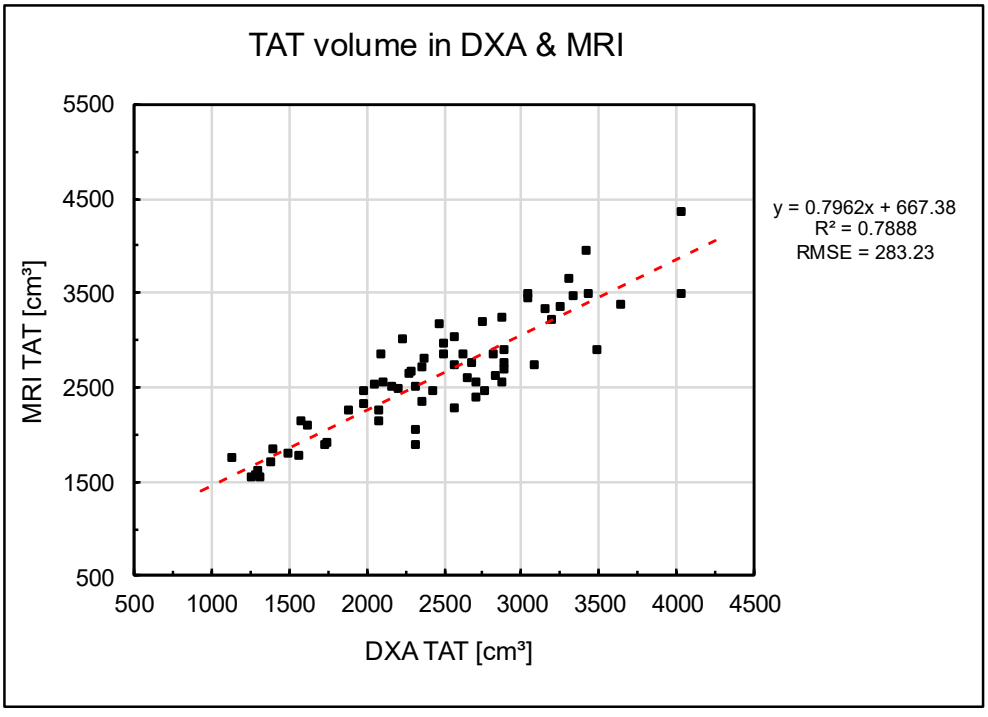

Figure 24: Relationship between DXA-assessed TAT and MRI-assessed TAT

1.3. Back fat thickness and abdominal adipose tissue

This chapter describes a linear regression analysis conducted to determine the degree to which values obtained from back fat thickness measurements aligned with the results of the MRI analysis.

The exploration for MRI subcutaneous fat (SAT) in Figure 25 revealed a positive relationship with back fat thickness assessed by ultrasound (US) ($p < 0.001$).

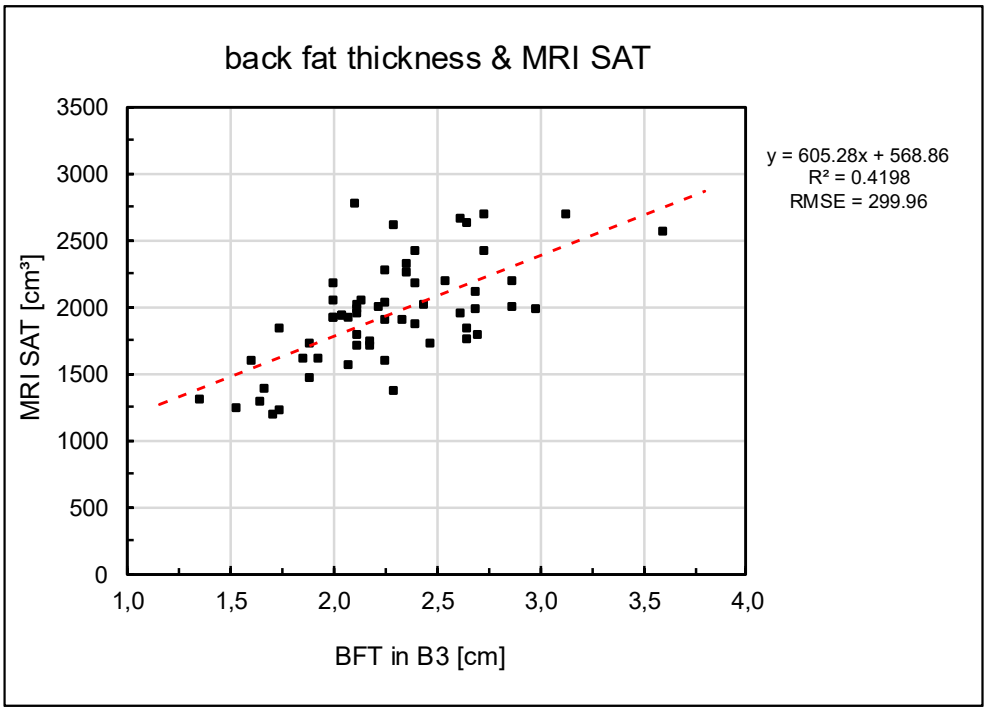

Figure 25: Relationship between US back fat thickness in B3 and MRI SAT

In case of the visceral fat (VAT), the regression model with US back fat thickness showed a slightly weaker relationship ($p < 0.001$) between the variables compared to the previous one with SAT ($R^2 = 0.42$ vs. $R^2 = 0.39$), Figure 26.

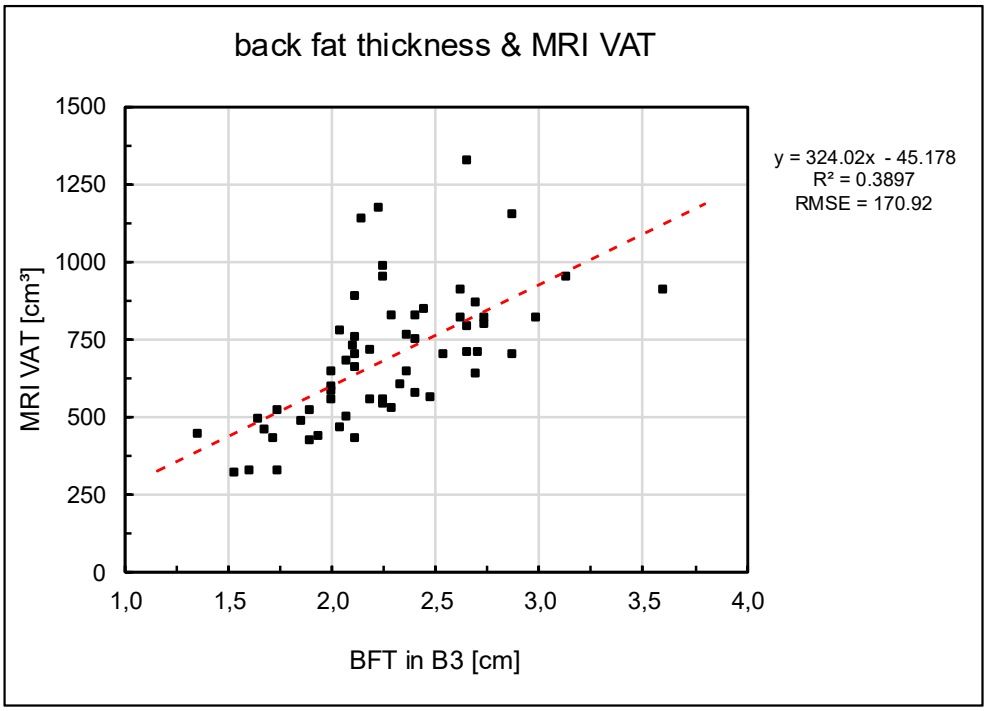

Figure 26: Relationship between US back fat thickness in B3 and MRI VAT

1.4. Weight and body composition parameters

Linear regression analyses of body weight and abdominal adipose tissues, derived by MRI and DXA, revealed differing relationships with body weight. This is reflected in the varying R^2 values obtained (see Table 7), which indicate the strength of these associations.

Table 7: Relationships between body weight and abdominal adipose tissues

		MRI	DXA
VAT	Model Equation	y = 9.8168x - 238.43	y = 51.912x - 2996.9
	R^2	0.1365	0.424
	Root MSE	213.87	524.17
	p-value	0.0021	p < 0.001
SAT	Model Equation	y = 29.561x - 855.17	y = -0.6875x + 618.26
	R^2	0.3541	0.0016
	Root MSE	345.88	147.48
	p-value	p < 0.001	0.7458
TAT	Model Equation	y = 39.378x - 1093.6	y = 51.224x - 2378.7
	R^2	0.3064	0.4166
	Root MSE	513.31	525.1
	p-value	p < 0.001	p < 0.001

Notably, SAT assessed via MRI had the highest coefficient of determination (Figure 28), indicating that a larger proportion of the variability in the SAT distribution is explained by body weight compared to the other parameters.

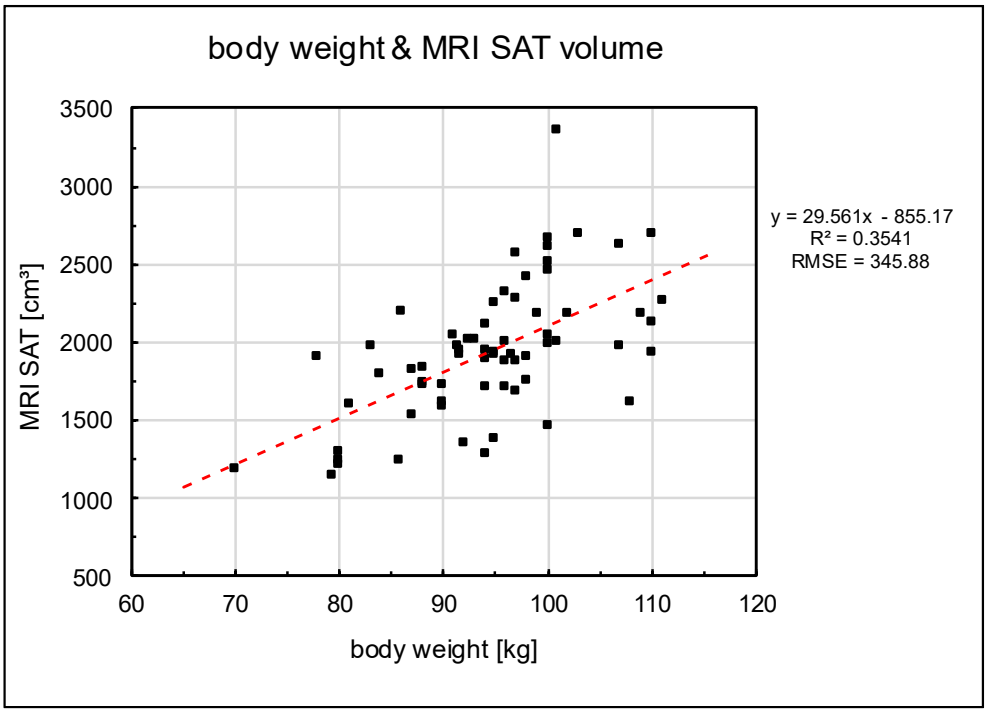

Figure 27: Relationship between body weight and SAT derived by MRI

Conversely, findings from DXA showed a stronger relationship between VAT and body weight (Figure 28), with a higher R^2 value compared to the corresponding MRI measurements.

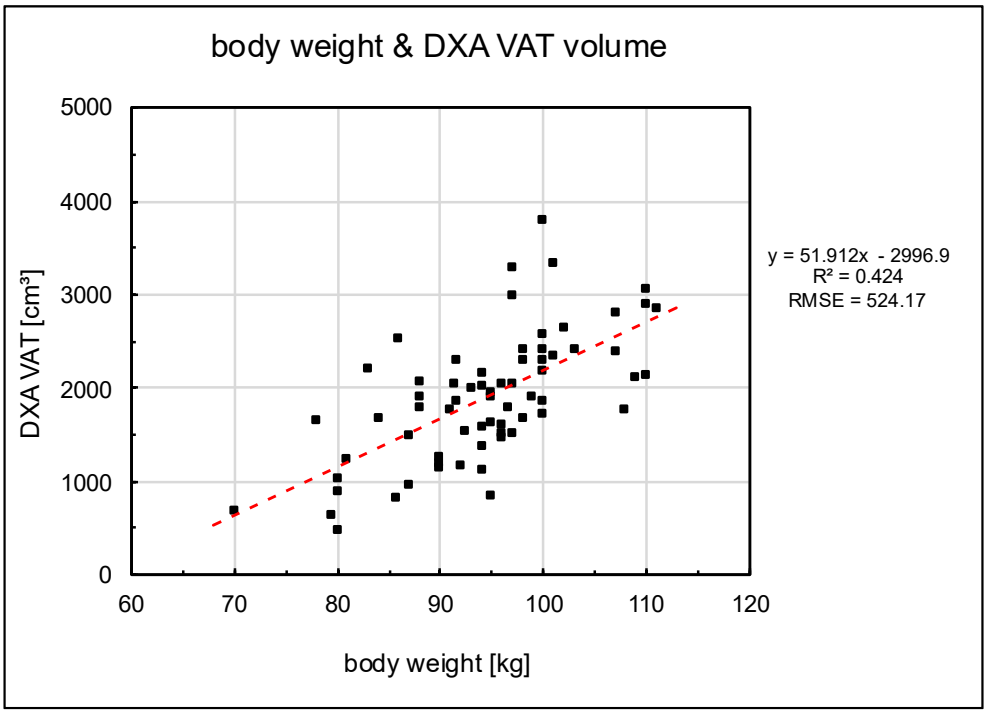

Figure 28: Relationship between body weight and VAT derived by DXA

SAT, however, showed a non-significant relationship ($p > 0.05$) with body

weight in the DXA model (Figure 29). This emphasises the limited ability to explain variations on SAT assessed via DXA based on changes in body weight.

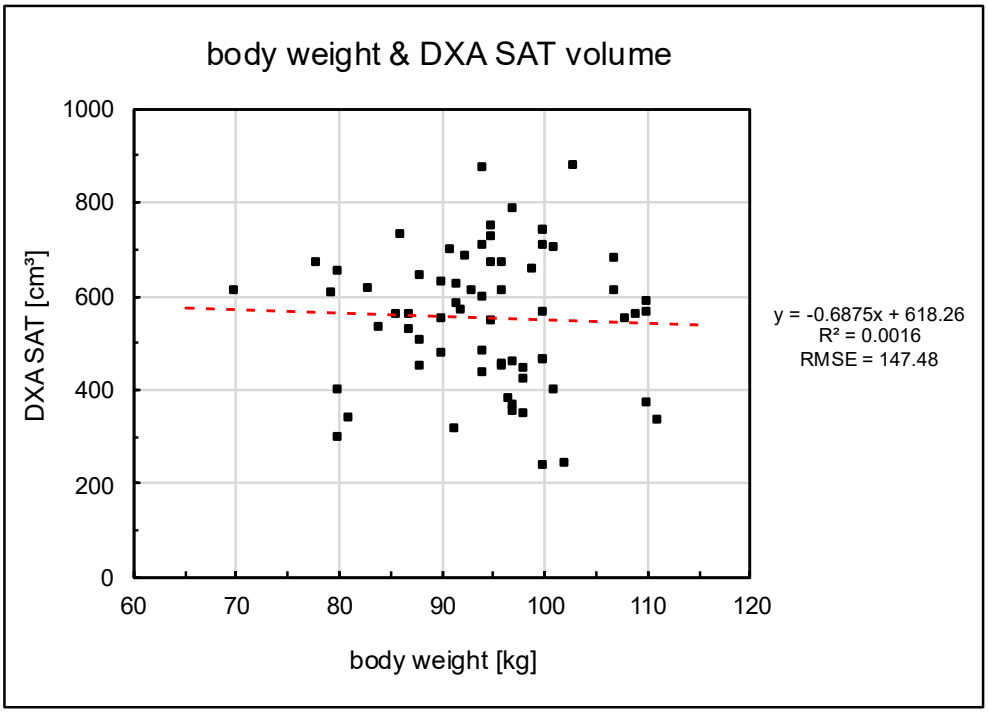

Figure 29: Relationship between body weight and SAT derived by DXA

The DXA model for TAT, described in Table 7, demonstrated a robust relationship with body weight, supported by a high R^2 (DXA TAT = 0.4166) and a very low p-value ($p < 0.001$).

1.5. Average daily feed intake and abdominal adipose tissues

Figure 30 illustrates a positive relationship between the animals' average daily feed intake (FI_avg [g/d]) and the abdominal adipose tissue volumes derived via MRI. Similar positive associations were observed for TAT and SAT ($p < 0.01$). In contrast, the relationship was comparatively weaker for VAT, but still statistically significant with $p < 0.01$.

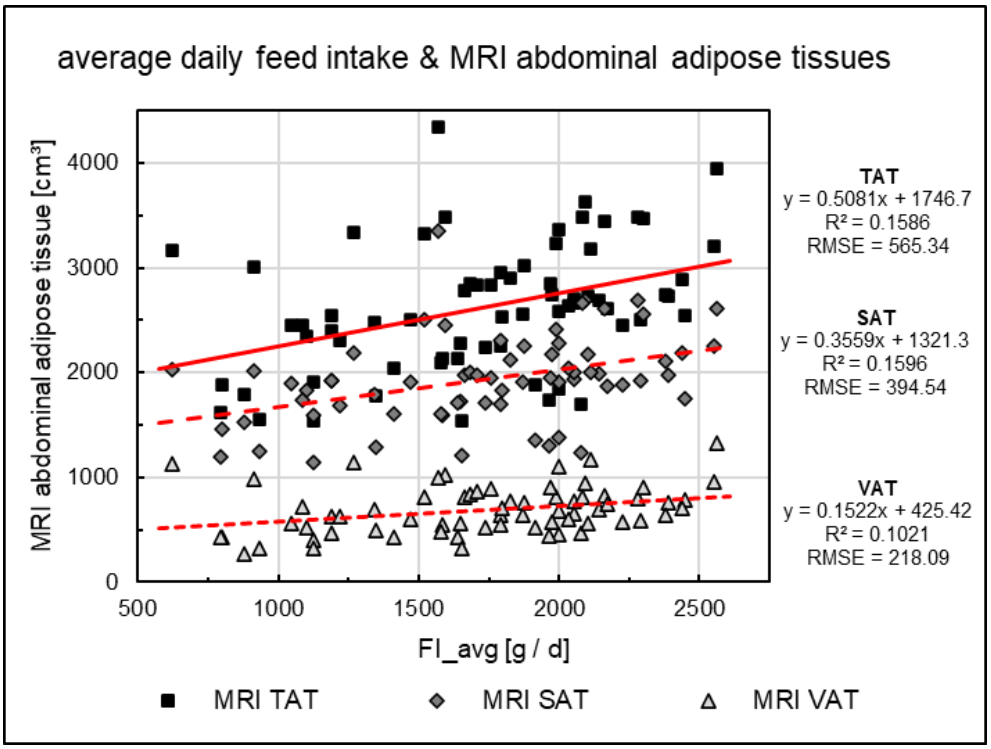

Figure 30: Relationship between average daily feed intake (FI_avg) and VAT, SAT and TAT assessed via MRI

Figure 31 presents the relationship between average daily feed intake and the measurements for abdominal adipose tissue volumes derived by DXA. TAT and VAT demonstrated parallel trends. However, SAT, represented by a negative slope estimate, indicated an inverse relationship compared to MRI.

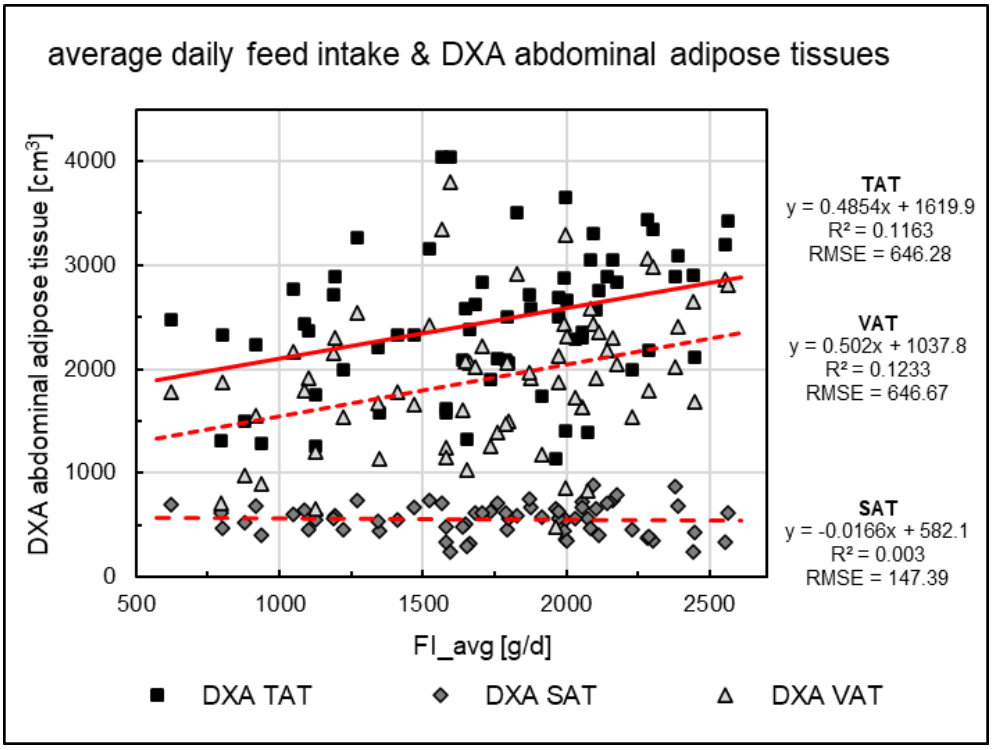

Figure 31: Relationship between average daily feed intake (FI_avg) and VAT, SAT and TAT assessed via DXA

2. Study sample characteristics

To gain a broader understanding of the sample characteristics of the study's focus group at the time of examination, we conducted an analysis of variance for the variables body weight (weight) [kg], age [d], and stable days [d]. It aims to enhance the comprehension of any disparities in the body composition variables and feeding data, which will be explored further in Chapter IV.3 and IV.4.

Table 8 (Chapter IV.2.2.) provides a comprehensive overview of the differences among sexes, genotype groups, and season-year categories regarding the sample characteristic variables.

Stable days are defined as the number of days the animals spent in the outside-climate stable. This duration spanned from the day they were transferred from the flat deck area, with an age of approximately 70 days, into the outside stable up to one day before their examination day, when they were moved into the examination barn.

Detailed information of individual effects from Table 8 is provided in the following sections.

2.1. Weight, age, and stable days

2.1.1. Sex

The animal's sex had no significant impact ($p > 0.05$) on weight, age, or stable days at all (Table 8).

2.1.2. Genotype

There was a significant difference ($p < 0.05$, Table 8) between the animals' genotypes in weight, age, and stable days.

Genotype group 2 (PiDuDLDE_DEDLPiDu) showed the lowest weight (88.08 ± 4 kg), whereas genotype group 6 (PiDuDLDE_PiDuDLDE) had the highest weight of 109.12 kg, notably with the highest standard error of estimation (SEE = 7.57). All other groups fell into a comparable weight range (Figure 32).

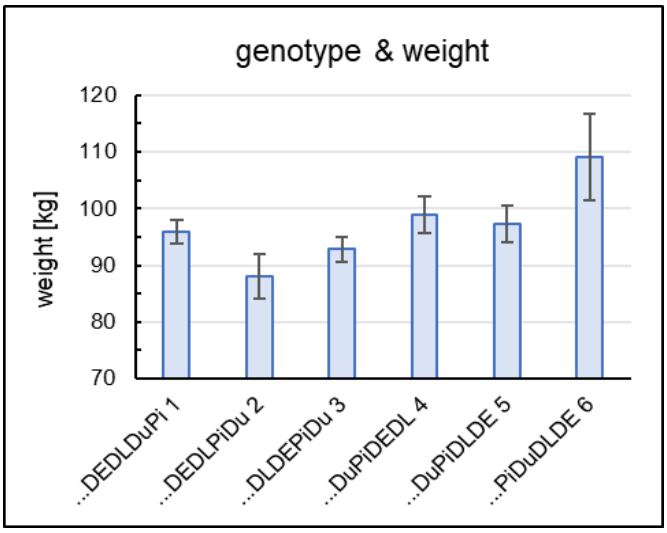

Figure 32: Weight differences among genotypes

Accordingly, Figure 33 shows that animals from genotype group 2 were approximately six days younger (144.61 ± 0.64 d) at the time the scan was performed compared to the oldest genotype group, group 6 (PiDuDLDE_PiDuDLDE, 150.87 ± 1.21 d).

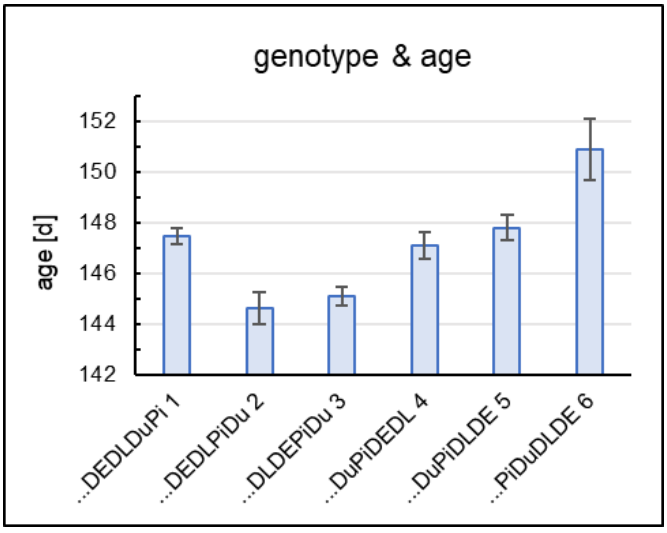

Figure 33: Age differences among genotypes

Even if the analysis revealed noteworthy distinctions ($p < 0.001$, Table 8) among the genotypes concerning the duration in the outside-climate stable (stable days), these differences only amounted to a single day.

2.1.3. Season x year

The influence of season and year in Table 8 is evident, with significant p-values observed for weight ($p < 0.05$), age ($p < 0.0001$), and stable days ($p < 0.0001$).

Figure 34 shows a noticeable difference in weights of animals scanned during season 4 (July and August) in 2021 compared to season 4 in 2022. Animals in season 4 / 2021 were the heaviest (104.61 ± 4.87 kg), while those in season 4 / 2022 were the lightest (88.92 ± 3.42 kg). All other animals fell within a weight range of 94 to 101 kg.

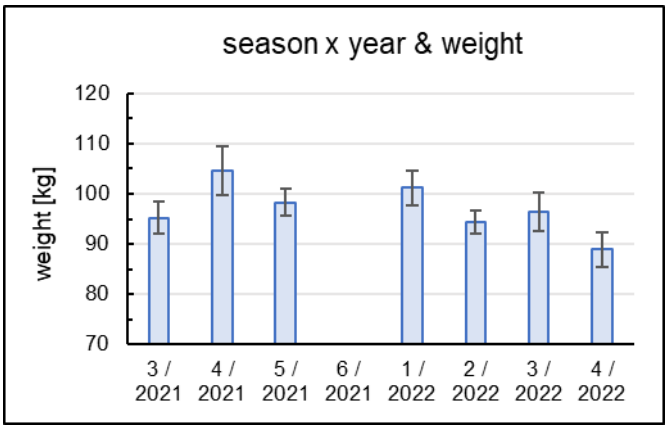

Figure 34: Differences in weight among season-year categories

Animals scanned in early 2022 were, on average, older (150.92 ± 0.56 d) than those scanned in season 3 / 2022 (144.61 ± 0.62 d) (Figure 35). It's worth noting that the scans were conducted only on weekdays due to the extensive preparations required and the availability of assistance.

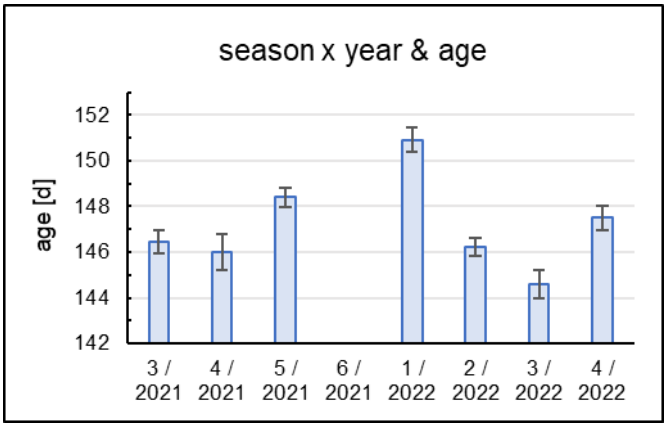

Figure 35: Age differences among season-year categories

Upon examining the differences in the duration spent in the outside-climate stable (Figure 36), substantial variations were observed between the season and year classifications, reaching around 10 days, particularly between season 3 in 2021 and 2022.

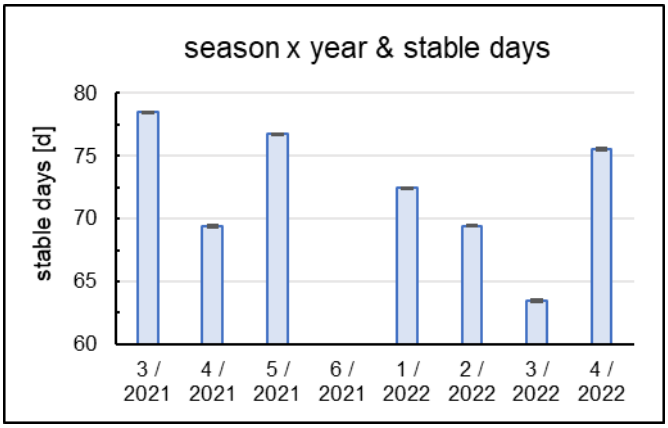

Figure 36: Differences in number of stable days among season-year categories

2.1.4. Comparison with the larger cohort

A comparative analysis of the larger cohort, comprising 138 animals with available DXA analysis values, revealed remarkable similarities when compared to the results displayed for the focus group above. The detailed results are provided in Table 15, Table 16 and Table 17 in the appendix (Chapter IX.3.4).

Notably, sex did not exert a significant influence on any of the study characteristics ($p > 0.05$) (Table 15). However, a nuanced observation emerges when examining the estimated values, indicating a marginal weight disparity between males and females on the day of examination, with slightly heavier males (99.23 ± 1.45 kg) compared to females (97.31 ± 1.13 kg).

Upon inspecting the impact of genotype, a congruent pattern of differences was apparent among the genotype groups, compared to the focus group (Table 16). Genotype group 6 maintained the highest weight (111.42 ± 3.95 kg), while genotype group 2 had the lowest (89.75 ± 3.13 kg). An analogous effect showed the age. Genotype group 2 was the youngest at 144 days old (144.31 ± 0.54 d), while genotype group 6 was the oldest (150.02 ± 0.69 d) on examination day. The number of stable days was consistent, even across

more animals. Notably was only the minor disparity in ranging from 1 to 3 days difference among the genotype groups.

There were few discrepancies between the groupings based on the examination date within the respective season and year when considering the larger cohort (Table 17), compared to the results described in Chapter IV.2.1.3.

2.2. Data overview of variance in study sample characteristics

Table 8: p-values, LSM and SEE of study sample characteristics weight, age and stable days

study sample characteristics										
SEX	p-value	male	female							
weight [kg]	0.6571	97.43 ± 2.28	96.55 ± 1.73							
age [d]	0.4582	147.27 ± 0.37	147.03 ± 0.28							
stable days [d]	0.9006	72.22 ± 0.05	72.21 ± 0.03							
GENOTYPE	p-value	1	2	3	4	5	6			
weight [kg]	0.0462	95.9 ± 2.08 ^{abc}	88.08 ± 4.00 ^{c}	92.79 ± 2.27 ^{bc}	98.85 ± 3.26 ^{ab}	97.20 ± 3.26 ^{abc}	109.12 ± 7.57 ^{a}			
age [d]	<.0001	147.46 ± 0.33 ^{b}	144.61 ± 0.64 ^{c}	145.09 ± 0.36 ^{c}	147.08 ± 0.52 ^{b}	147.80 ± 0.52 ^{b}	150.87 ± 1.21 ^{a}			
stable days [d]	<.0001	72.77 ± 0.04 ^{a}	71.59 ± 0.08 ^{c}	71.68 ± 0.05 ^{c}	71.97 ± 0.07 ^{b}	72.77 ± 0.07 ^{a}	72.49 ± 0.15 ^{a}			
SEASON x YEAR	p-value	3 / 2021	4 / 2021	5 / 2021	1 / 2022	2 / 2022	3 / 2022	4 / 2022		
weight [kg]	0.0417	95.21 ± 3.19 ^{abc}	104.61 ± 4.87 ^{a}	98.31 ± 2.64 ^{ab}	101.24 ± 3.47 ^{ab}	94.33 ± 2.36 ^{bc}	96.31 ± 3.84 ^{abc}	88.92 ± 3.42 ^{c}		
age [d]	<.0001	146.43 ± 0.51 ^{cd}	145.99 ± 0.78 ^{cde}	148.40 ± 0.42 ^{b}	150.92 ± 0.56 ^{a}	146.22 ± 0.38 ^{d}	144.61 ± 0.62 ^{e}	147.50 ± 0.55 ^{bc}		
stable days [d]	<.0001	78.48 ± 0.06 ^{a}	69.44 ± 0.10 ^{e}	76.72 ± 0.05 ^{b}	72.44 ± 0.07 ^{d}	69.44 ± 0.05 ^{e}	63.44 ± 0.08 ^{f}	75.54 ± 0.07 ^{c}		

Significance levels (p-value), least squares means and standard errors of estimation (LSM ± SEE) for study sample characteristics (weight, age, stable days) of the focus group, different superscripts within rows describe significant differences, with p < 0.05
Genotype groups 1 = PiDuDLDE_DEDLDuPi, 2 = _DEDLPiDu, 3 = _DLDEPiDu, 4 = _DuPiDEDL, 5 = _DuPiDLDE, 6 = _PiDuDLDE
Seasons 1 = January + February, 2 = March + April, 3 = May + June, 4 = July + August, 5 = September + October

3. Abdominal adipose tissue and body composition parameters

The least squares means (LSM) provided in the tables of this chapter have been standardised for the body weight of all animals, due to the inclusion of weight as a covariate in this variance analysis model (see Chapter III.4.1.2).

3.1. Abdominal adipose tissue parameters

The following variables summarise the abdominal adipose tissue:

- visceral adipose tissue (VAT)
- subcutaneous adipose tissue (SAT)
- total abdominal adipose tissue (TAT)
- android fat percentage

As described in Chapter III.3.2.1 and III.3.2.2, MRI estimates are given as volumes [cm^3] and DXA estimates are displayed as volumes [cm^3] and masses [g]. The android fat percentage represents the fat mass percentage of total soft tissue in the android area (abdomen).

3.1.1. Sex

Sex had no significant effect on the distribution of abdominal adipose tissue parameters, except for SAT calculated from DXA with $p < 0.0001$ (Table 9). In this case, female animals demonstrated a significantly higher presence of subcutaneous fat (SAT) compared to castrated male animals.

However, when looking at the LSM estimates, differences among MRI and DXA results became obvious (Figure 37). Controversial volumes were derived for VAT, being higher for females measured with MRI (628.50 ± 46.76 cm^3), but lower for females derived by DXA (1756.69 ± 108.49 cm^3) compared to males (1960.87 ± 143.72 cm^3) (see Table 9).

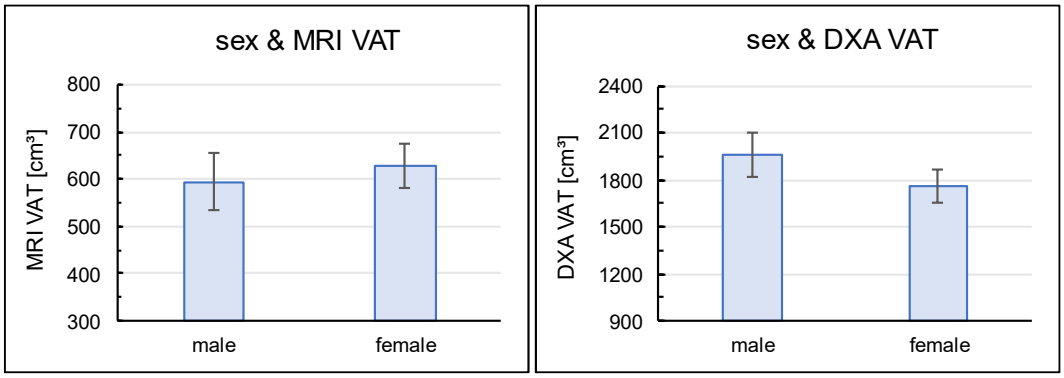

Figure 37: Variance between sexes in VAT via MRI and DXA

3.1.2. Genotype

The animals' genotype structure had a significant effect on all abdominal adipose tissue variables ($p < 0.05$, Table 10). This influence was more pronounced for the variables derived by MRI, as indicated by smaller p-values.

For the abdominal adipose tissue parameters derived by MRI, genotype group 3 and 5 exhibited the highest volumes of VAT (Figure 38) (3 = 768.80 ± 61.06 cm^3, 5 = 772.73 ± 87.64 cm^3), a trend that was similarly reflected in total abdominal adipose tissue (TAT), especially for genotype group 3 (Table 10).

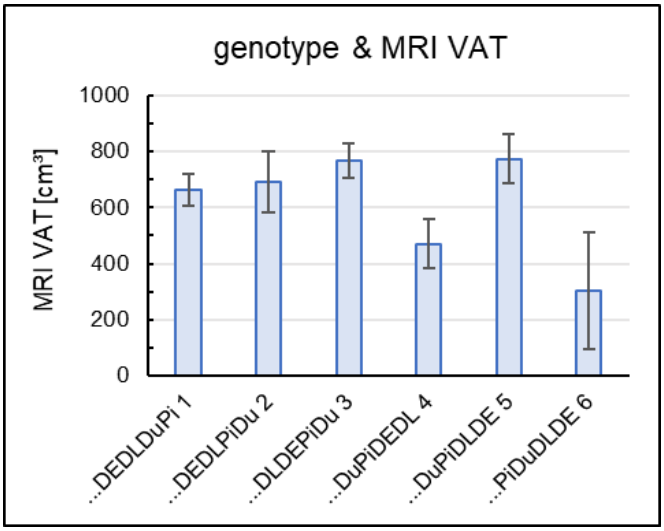

Figure 38: Differences in MRI VAT among genotypes

In the case of SAT, genotypes 1 and 3 showed the highest volumes (1 = 2030.43 ± 89.36 cm^3, 3 = 2082.50 ± 97.92 cm^3, Figure 39). Conversely, both VAT and SAT volumes were comparatively lower for genotypes 4 and 6, a pattern that was consistent in the summary of total abdominal adipose tissue (TAT) (Table 10).

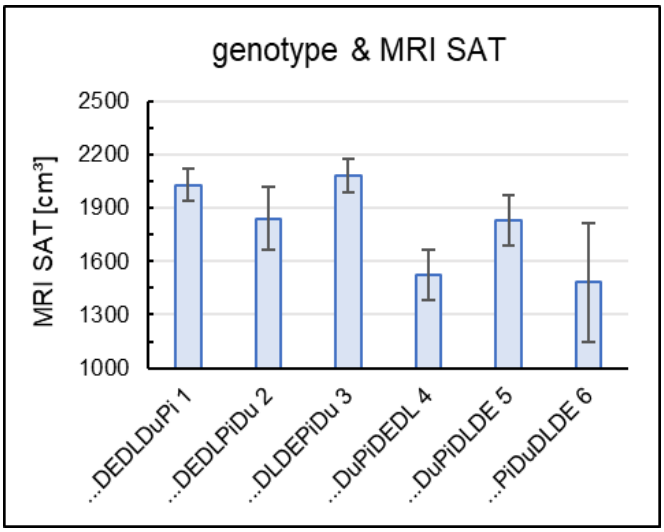

Figure 39: Differences in MRI SAT among genotypes

In contrast to the MRI measurements, DXA values revealed distinct variations among the genotype groups. For VAT (Figure 40), genotype 3 demonstrated the highest volume (2296.89 ± 141.66 cm^3), and this trend was similarly observed in TAT, where genotype 1 followed closely (Table 10).

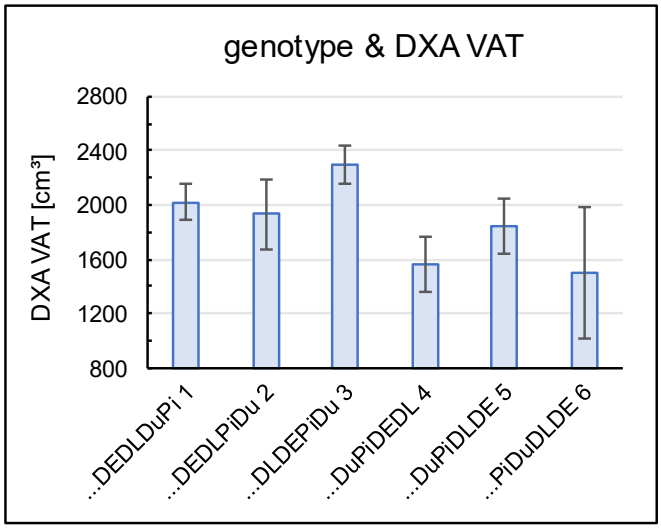

Figure 40: Differences in DXA VAT among genotypes

For SAT genotype 2 showed the highest volume (570.73 ± 59.09 cm^3), surpassing genotypes 1 and 3 (Figure 41). However, it's noteworthy that the

standard error for genotype 2 was higher than that of both genotypes 1 and 3. Genotype 4 was associated with the smallest volumes of VAT and TAT, while for SAT, genotype 5 had an even smaller estimate (4 = 427.05 ± 47.94 cm^3 vs. 5 = 421.35 ± 47.40 cm^3).

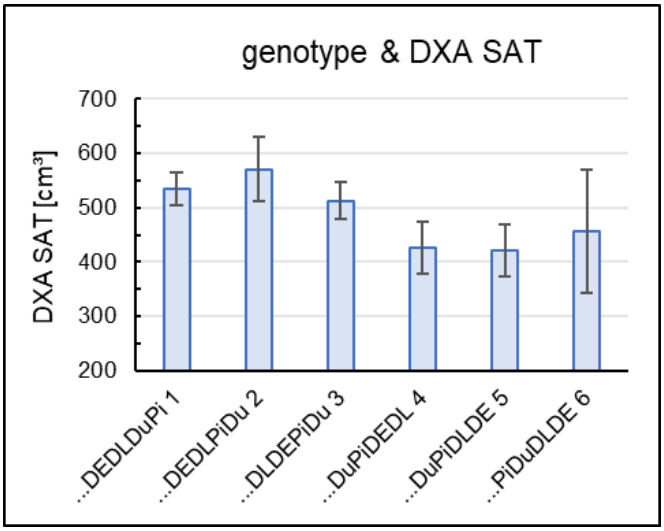

Figure 41: Differences in DXA SAT among genotypes

The fat percentage of the abdomen (android fat [%]) mirrored the same variation observed in TAT, with genotypes 1 and 3 having the highest estimates (1 = 15.60 ± 0.75 %, 3 = 16.19 ± 0.82 %) (Figure 42, Table 10). Genotype 4 and 6 on the other hand, demonstrated substantial differences compared to the rest of the groups with the lowest estimates (4 = 11.79 ± 1.19 %; 6 = 10.73 ± 2.81 %).

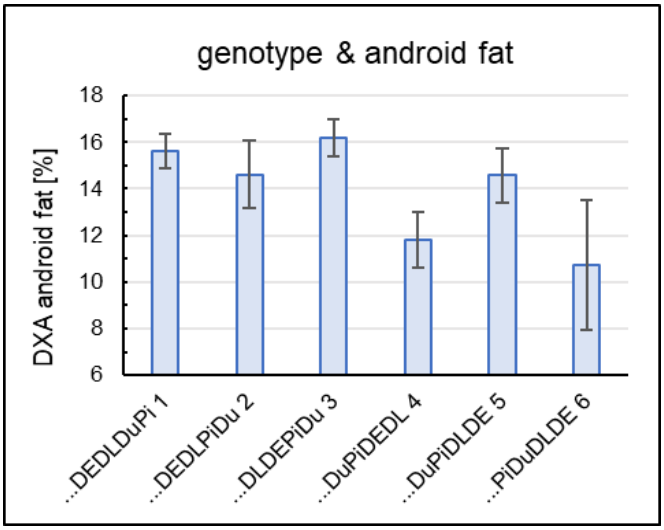

Figure 42: Differences in DXA android fat percentage among genotypes

3.1.3. Season x year

The influence of the combined fixed effect of season x year was significant for most of the abdominal adipose tissue variables. However, there was no significant effect ($p > 0.05$) observed for MRI SAT and for DXA android fat percentage (Table 11).

Overall, a consistent distribution pattern was evident across the range of abdominal adipose tissue variables, visualised using the example of MRI VAT (Figure 43). Animals scanned in season 4 / 2021 predominantly demonstrated the highest volumes for the parameters, followed by season 1 / 2022 and 2 / 2022. In contrast, the group scanned in season 3 / 2022 had the least volume (Table 11).

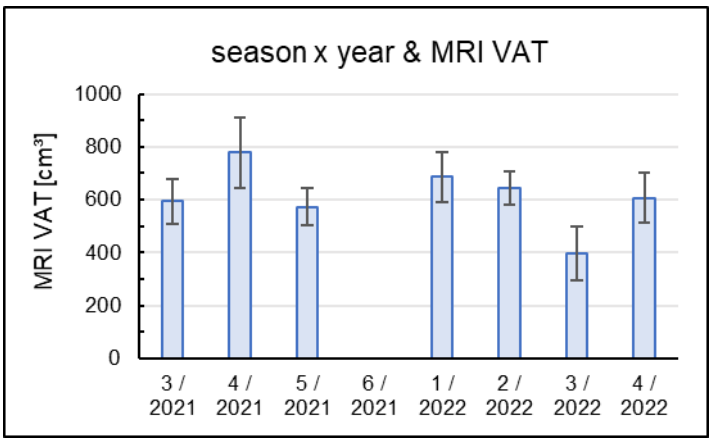

Figure 43: Variations in MRI VAT among season-year categories

An exception to this pattern was observed for DXA SAT, where the group scanned in season 2 / 2022 exhibited the highest SAT volume (Figure 44, Table 11).

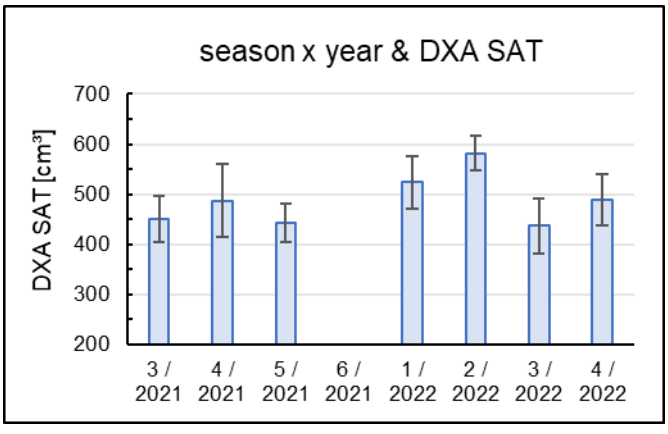

Figure 44: Variations in DXA SAT for season-year categories

3.2. Body composition parameters

To gain a thorough understanding of additional body composition parameters, the same statistical model was employed for the analysis of parameters acquired through the DXA CoreScan® software.

The following parameters were taken into consideration: total body fat (fat) [g], total soft tissue lean mass (lean) [g], bone mineral content (BMC) [g], and bone mineral density (BMD) [g/cm²].

Table 9, Table 10 and Table 11 in Chapter IV.3.3 provide detailed information on the differences among sexes, genotypes, and season-year categories regarding these parameters.

The subsequent paragraphs state relevant details on the respective effects.

3.2.1. Sex

There were no significant differences between male and female animals in the parameters related to body composition. The distribution of values was very similar between the sexes (Table 9).

3.2.2. Genotype

There were significant differences ($p < 0.05$) existing between the genotypes for the variables fat and lean, but not for BMC and BMD ($p > 0.05$) (Table 10).

Mirroring the parallel distribution observed in TAT values (derived by DXA), a similar pattern emerged in total body fat values (Figure 45). Specifically, genotypes 3, 1, and 5 demonstrated the highest amounts, while genotype 4 showed the least (12043 ± 938.73 g) (Table 10).

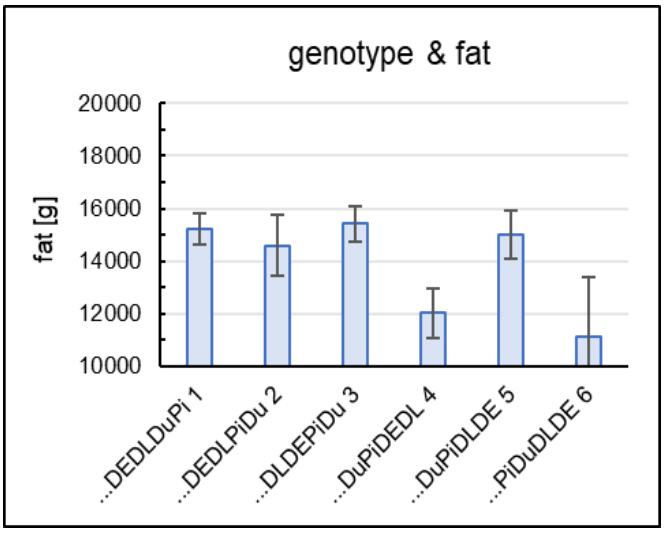

Figure 45: Differences in fat mass among genotypes

In contrast, the situation reversed for lean mass, with genotypes 4 and 6 showing the highest values, and genotype 3 displaying the least (76745 ± 656.93 g) (Figure 46).

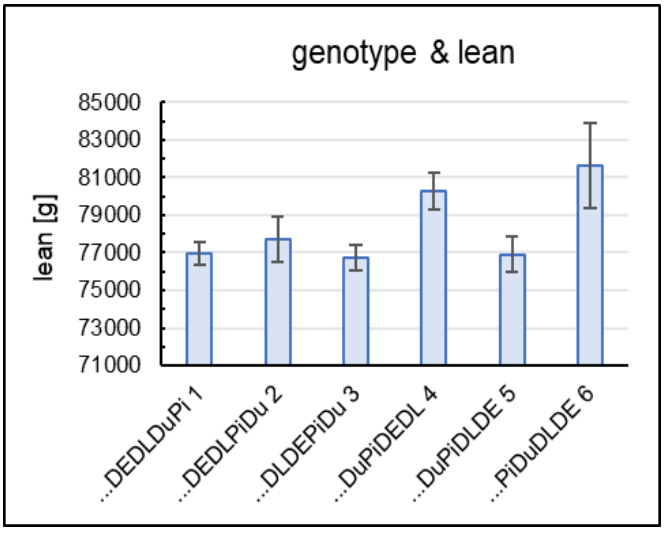

Figure 46: Differences in lean mass among genotypes

3.2.3. Season x year

Details about the distribution of whole-body composition parameters among different season-year-categories are shown in Table 11. The combined effect of season and year had a significant effect ($p < 0.05$) on all the body composition parameters, except for BMD ($p > 0.05$).

Corresponding to the TAT volumes, the animals scanned in season 4 / 2021 showed the highest amount of total body fat (16744 ± 1431.88 g), accompanied by the lowest lean mass (74966 ± 1454.89 g). In contrast, animals scanned in season 3 / 2022 displayed the lowest amount of total body fat (11388 ± 1087.48 g) (Figure 47). The quantities of lean mass remained similar across the different season classes (Figure 48).

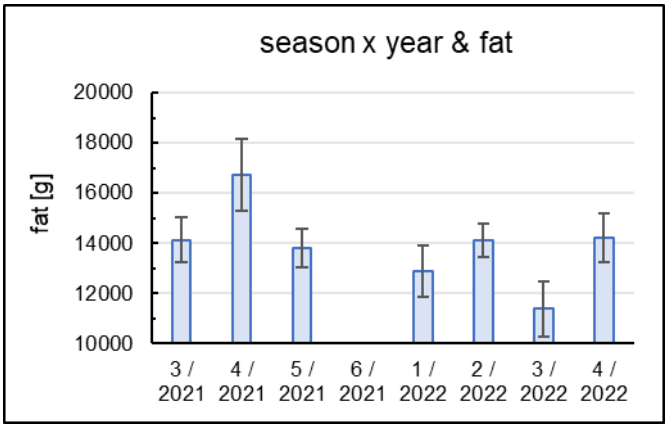

Figure 47: Differences in fat mass among season-year categories

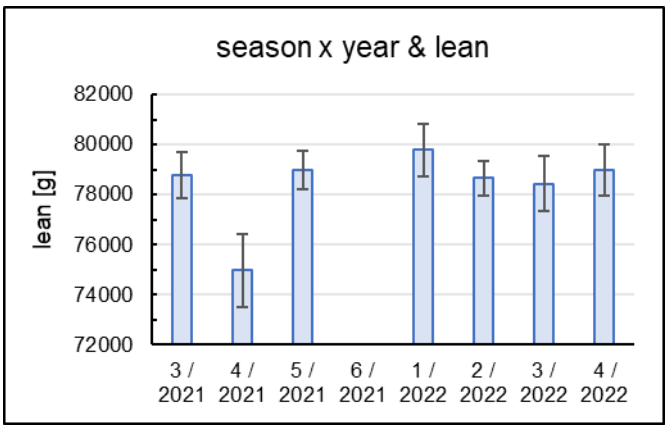

Figure 48: Differences in lean mass among season-year categories

The bone mineral content (BMC) differed significantly among animals scanned in different seasons. Specifically, animals analysed in season 3 of 2022 showed a reduction of approximately 190 g compared to those scanned in season 4 / 2021, which recorded the highest value at 2006.56 ± 66.03 g (Figure 49).

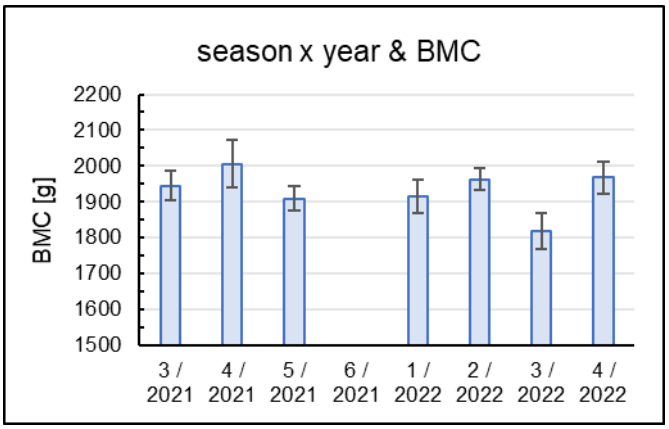

Figure 49: Variations in BMC among season-year category

3.2.4. Comparison with the larger cohort

To gain a comprehensive understanding of the broader population, the analysis was extended to include findings from all 138 animals with available DXA analysis results, using the same statistical model applied as for the initial examination of the focus group. The results are detailed in Appendix IX.3 (Further analyses for the larger cohort), and the key findings are subsequently described.

Differences in abdominal adipose tissue estimates between sexes were evident in the larger cohort (Table 15, Appendix IX.3.4) compared to the study's focus group, as significant differences ($p < 0.001$) were observed between sexes for both VAT and SAT parameters. Precisely, males presented a significantly higher amount of visceral fat (VAT) compared to females, while females demonstrated a greater quantity of subcutaneous fat (SAT) than males (Figure 50). This confirms the tendency already observed in Chapter IV.3.1.1.

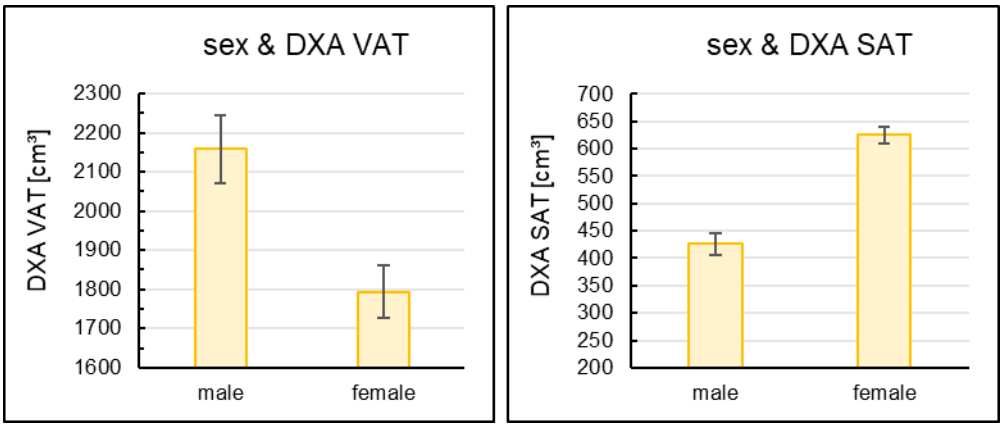

Figure 50: Differences in DXA VAT and DXA SAT between males and females

Examining parameters demonstrating total abdominal fat (total abdominal adipose tissue TAT and android fat %), with likewise significant p-values ($p < 0.05$), indicated that male animals had a higher overall abdominal fat content than females. This trend was also observed for total body fat (fat), where males had higher amounts than females. Conversely, females showed higher amounts of total soft tissue lean mass (lean), though this difference did not reach statistical significance. However, no differences in variation of bone mineral content (BMC) and bone mineral density (BMD) were apparent between the sexes (Table 15, Appendix IX.3.4).

The impact of the genotype structure on the distribution of abdominal adipose tissue variables was consistently affirmed within the broader study cohort (Table 16, Appendix IX.3.4). Notably, genotype groups 3 and 1 exhibited the highest volumes, while groups 4 and 6 displayed the lowest. An exception to this pattern was observed in SAT estimates, with the larger cohort showing higher levels for genotype 1 (590.19 ± 21.77 cm^3) compared to the study's focus group, where genotype group 2 demonstrated the highest SAT levels.

Most notably, in the larger cohort (Table 17, Appendix IX.3.4), an additional significant p-value for BMD ($p < 0.05$) was observed, differing from the non-significance seen within the focus group of 67 subjects (Table 11, Chapter IV.3.3). Otherwise, the distribution of individual parameters between the season-year categories remained consistent, except for lean mass. In this case, the group analysed in 1 / 2022 in the larger cohort exhibited the highest lean mass (79653 ± 811.33 g), while animals scanned in season 4 / 2021 (77821 ± 884.49 g) and season 3 / 2022 (77891 ± 761.84 g) showed the

lowest. As shown in Chapter IV.3.2.3, animals scanned in 4 / 2021 had by far the lowest lean mass estimates within the study's focus group. Regarding BMD, the results mirrored those of BMC, where the group scanned in season 4 / 2021 had the highest (1.1004 ± 0.02 g) and the group of season 3 / 2022 showed the least bone mineral density (1.0262 ± 0.02 g), though these differences were minor.

3.3. Data overview of variance in abdominal adipose tissue and body composition parameters

Table 9: p-values, LSM and SEE of abdominal adipose tissue and body composition variables between sexes

abdominal adipose tissue and body composition

	SEX	p-value	male	female
MRI	VAT [cm³]	0.5234	594.73 ± 61.94	628.50 ± 46.76
	SAT [cm³]	0.3584	1759.25 ± 99.34	1837.37 ± 74.99
	TAT [cm³]	0.3667	2353.98 ± 144.78	2465.87 ± 109.29
DXA	VAT [cm³]	0.1001	1960.87 ± 143.72	1756.69 ± 108.49
	SAT [cm³]	<.0001	363.39 ± 33.50 [b]	611.31 ± 25.29 [a]
	TAT [cm³]	0.7256	2324.26 ± 146.04	2368.00 ± 110.24
	android fat [%]	0.9017	13.87 ± 0.83	13.96 ± 0.63
DXA	fat [g]	0.7991	13978 ± 655.92	13835 ± 495.13
	lean [g]	0.7093	78474 ± 666.46	78262 ± 503.09
	BMC [g]	0.8822	1929.91 ± 30.25	1933.73 ± 22.83
	BMD [g/cm^2]	0.6062	1.0405 ± 0.02	1.0479 ± 0.01

Significance levels (p-value), least squares means and standard errors of estimation (LSM ± SEE) for abdominal adipose tissues and body composition variables assessed with MRI and DXA, different superscripts within rows describe significant differences, with p < 0.05
Abdominal adipose tissues VAT: visceral adipose tissue, SAT: subcutaneous adipose tissue, TAT: total abdominal adipose tissue, android fat percentage: fat mass percentage of the total soft tissue in the android region
Body composition variables fat: total body fat mass, lean: total soft tissue lean mass, BMC: bone mineral content, BMD: bone mineral density

Table 10: p-values, LSM and SEE of abdominal adipose tissue and body composition variables between genotypes

GENOTYPE		p-value	abdominal adipose tissue and body composition					
			1	2	3	4	5	6
MRI	VAT [cm³]	0.0159	663.91 ± 55.72 ^{abc}	691.72 ± 109.26 ^{abc}	768.80 ± 61.06 ^{a}	469.94 ± 88.65 ^{c}	772.73 ± 87.64 ^{ab}	302.58 ± 209.17 ^{bc}
	SAT [cm³]	0.0061	2030.43 ± 89.36 ^{a}	1841.45 ± 175.23 ^{ab}	2082.50 ± 97.92 ^{a}	1521.77 ± 142.18 ^{b}	1831.29 ± 140.56 ^{ab}	1482.43 ± 335.46 ^{ab}
	TAT [cm³]	0.0064	2694.35 ± 130.24 ^{ab}	2533.17 ± 255.38 ^{abc}	2851.30 ± 142.71 ^{a}	1991.70 ± 207.21 ^{c}	2604.03 ± 204.85 ^{abc}	1785.01 ± 488.9 ^{bc}
DXA	VAT [cm³]	0.0254	2023.14 ± 129.28 ^{ab}	1932.25 ± 253.50 ^{ab}	2296.89 ± 141.66 ^{a}	1560.52 ± 205.69 ^{b}	1846.24 ± 203.35 ^{ab}	1493.66 ± 485.31 ^{ab}
	SAT [cm³]	0.0343	534.88 ± 30.13 ^{ac}	570.73 ± 59.09 ^{ab}	513.08 ± 33.02 ^{abc}	427.05 ± 47.94 ^{cd}	421.35 ± 47.40 ^{bd}	457.01 ± 113.12 ^{abc}
	TAT [cm³]	0.0080	2558.03 ± 131.37 ^{a}	2502.98 ± 257.59 ^{ab}	2809.97 ± 143.95 ^{a}	1987.57 ± 209.01 ^{b}	2267.58 ± 206.63 ^{ab}	1950.67 ± 493.14 ^{ab}
	android fat [%]	0.0163	15.60 ± 0.75 ^{a}	14.61 ± 1.47 ^{ab}	16.19 ± 0.82 ^{a}	11.79 ± 1.19 ^{b}	14.57 ± 1.18 ^{ab}	10.73 ± 2.81 ^{ab}
DXA	fat [g]	0.0235	15217 ± 590.03 ^{a}	14591 ± 1156.95 ^{ab}	15413 ± 646.54 ^{a}	12043 ± 938.73 ^{b}	15021 ± 928.05 ^{a}	11153 ± 2214.89 ^{ab}
	lean [g]	0.0155	76988 ± 599.52 ^{bc}	77706 ± 1175.54 ^{abc}	76745 ± 656.93 ^{c}	80269 ± 953.82 ^{a}	76894 ± 942.96 ^{bc}	81609 ± 2250.48 ^{ab}
	BMC [g]	0.4235	1984.18 ± 27.21	1973.18 ± 53.35	1922.85 ± 29.81	1901.58 ± 43.29	1995.17 ± 42.80	1813.95 ± 102.14
	BMD [g/cm²]	0.3036	1.0657 ± 0.02	1.0413 ± 0.03	1.0379 ± 0.02	1.0036 ± 0.02	1.0927 ± 0.02	1.0242 ± 0.06

Significance levels (p-value), least squares means and standard errors of estimation (LSM ± SEE) for abdominal adipose tissues and body composition variables assessed with MRI and DXA, different superscripts within rows describe significant differences, with p < 0.05

Genotype groups 1 = PiDuDLDE_DEDLDuPi, 2 = _DEDLPiDu, 3 = _DLDEPiDu, 4 = _DuPiDEDL, 5 = _DuPiDLDE, 6 = _PiDuDLDE

Abdominal adipose tissues VAT: visceral adipose tissue, SAT: subcutaneous adipose tissue, TAT: total abdominal adipose tissue, android fat percentage: fat mass percentage of the total soft tissue in the android region

Body composition variables fat: total body fat mass, lean: total soft tissue lean mass, BMC: bone mineral content, BMD: bone mineral density

Table 11: p-values, LSM and SEE of abdominal adipose tissue and body composition variables in season-year categories

			abdominal adipose tissue and body composition					
SEASON x YEAR		p-value	3 / 2021	4 / 2021	5 / 2021	1 / 2022	2 / 2022	3 / 2022	4 / 2022
M R I	VAT [cm³]	0.0254	594.79 ± 85.33 ^{ab}	777.75 ± 135.22 ^{a}	573.88 ± 71.81 ^{ab}	686.18 ± 95.86 ^{a}	643.93 ± 63.05 ^{a}	397.05 ± 102.70 ^{b}	607.70 ± 93.52 ^{ab}
	SAT [cm³]	0.1144	1777.60 ± 136.85	2135.75 ± 216.86	1716.31 ± 115.16	1857.99 ± 153.73	1871.00 ± 101.12	1560.48 ± 164.70	1669.05 ± 149.99
	TAT [cm³]	0.0329	2372.39 ± 199.45 ^{ab}	2913.50 ± 316.06 ^{a}	2290.19 ± 167.84 ^{ab}	2544.17 ± 224.06 ^{a}	2514.94 ± 147.37 ^{a}	1957.54 ± 240.04 ^{b}	2276.76 ± 218.59 ^{ab}
D X A	VAT [cm³]	0.0348	1846.27 ± 197.99 ^{b}	2652.46 ± 313.74 ^{a}	1769.43 ± 166.6 ^{b}	1855.79 ± 222.41 ^{b}	1742.58 ± 146.29 ^{b}	1502.86 ± 238.28 ^{b}	1642.10 ± 216.99 ^{b}
	SAT [cm³]	0.0182	450.25 ± 46.15 ^{b}	486.61 ± 73.13 ^{ab}	442.26 ± 38.83 ^{b}	523.90 ± 51.84 ^{ab}	582.24 ± 34.10 ^{a}	436.91 ± 55.54 ^{b}	489.27 ± 50.58 ^{ab}
	TAT [cm³]	0.0253	2296.52 ± 201.18 ^{bc}	3139.07 ± 318.81 ^{a}	2211.69 ± 169.29 ^{bc}	2379.69 ± 226.00 ^{b}	2324.83 ± 148.65 ^{bc}	1939.77 ± 242.13 ^{c}	2131.37 ± 220.49 ^{bc}
	android fat [%]	0.0922	13.90 ± 1.14	17.57 ± 1.81	13.92 ± 0.96	13.35 ± 1.29	13.73 ± 0.85	11.55 ± 1.38	13.40 ± 1.25
D X A	fat [g]	0.0222	14133 ± 903.58 ^{abc}	16744 ± 1431.88 ^{a}	13825 ± 760.36 ^{abc}	12900 ± 1015.05 ^{bc}	14137 ± 667.64 ^{ab}	11388 ± 1087.48 ^{c}	14219 ± 990.31 ^{abc}
	lean [g]	0.0439	78765 ± 918.10 ^{a}	74966 ± 1454.89 ^{b}	78976 ± 772.58 ^{a}	79778 ± 1031.37 ^{a}	78662 ± 678.37 ^{a}	78443 ± 1104.96 ^{a}	78988 ± 1006.22 ^{a}
	BMC [g]	0.0354	1944.66 ± 41.67 ^{ab}	2006.56 ± 66.03 ^{a}	1909.64 ± 35.06 ^{ab}	1914.09 ± 46.81 ^{a}	1962.56 ± 30.79 ^{a}	1817.26 ± 50.15 ^{b}	1967.95 ± 45.67 ^{a}
	BMD [g/cm^2]	0.0650	1.0569 ± 0.02	1.0816 ± 0.04	1.0229 ± 0.02	1.0470 ± 0.03	1.0644 ± 0.02	0.9959 ± 0.03	1.0409 ± 0.03

Significance levels (p-value), least squares means and standard errors of estimation (LSM ± SEE) for abdominal adipose tissues and body composition variables assessed with MRI and DXA, different superscripts within rows describe significant differences, with $p < 0.05$

Seasons 1 = January + February, 2 = March + April, 3 = May + June, 4 = July + August, 5 = September + October

Abdominal adipose tissues VAT: visceral adipose tissue, SAT: subcutaneous adipose tissue, TAT: total abdominal adipose tissue, android fat percentage: fat mass percentage of the total soft tissue in the android region

Body composition variables fat: total body fat mass, lean: total soft tissue lean mass, BMC: bone mineral content, BMD: bone mineral density

3.4. Covariate weight

The covariate weight, applied in the statistical model for abdominal adipose tissue and body composition parameters (III.4.1.2), had a significant effect on all examined parameters except for the estimated SAT derived by DXA (Table 12).

Table 12: Influence of covariate weight on abdominal adipose tissue and body composition variables

Covariate WEIGHT

		p-value
MRI	VAT [cm³]	0.0020
	SAT [cm³]	<.0001
	TAT [cm³]	<.0001
DXA	VAT [cm³]	<.0001
	SAT [cm³]	0.3612
	TAT [cm³]	<.0001
	android fat [%]	0.0002
DXA	fat [g]	<.0001
	lean [g]	<.0001
	BMC [g]	<.0001
	BMD [g/cm^2]	<.0001

Significance levels (p-value) of covariate weight on abdominal adipose tissues and body composition variables assessed with MRI and DXA
Abdominal adipose tissues VAT: visceral adipose tissue, SAT: subcutaneous adipose tissue, TAT: total abdominal adipose tissue, android fat percentage: fat mass percentage of the total soft tissue in the android region
Body composition variables fat: total body fat mass, lean: total soft tissue lean mass, BMC: bone mineral content, BMD: bone mineral density

A different perspective unfolds when considering the larger cohort. In this context, weight consistently showed a significant effect on all variables derived by DXA (Table 18, Appendix IX.3.4).

4. Daily feed intake

The statistical exploration on effects on daily feed intake, using the mixed model described in Chapter III.4.1.3, yielded notable findings, as indicated by significant p-values ($p < 0.001$). These results showed that all four fixed effects in this model – sex, genotype, season and feeding week – played a significant role in the observed variations of the animals' daily feed intake (Table 13 in Appendix IX.2 Data overview of daily feed intake). The results are presented as least squares means with standard errors of estimation (LSM ± SEE) and corresponding p-values.

4.1. Sex

Figure 51 shows that castrated males (males) had a significantly higher daily feed intake compared to female animals (1814.21 ± 32.09 g vs. 1647.64 ± 24.14 g, respectively, $p < 0.0001$).

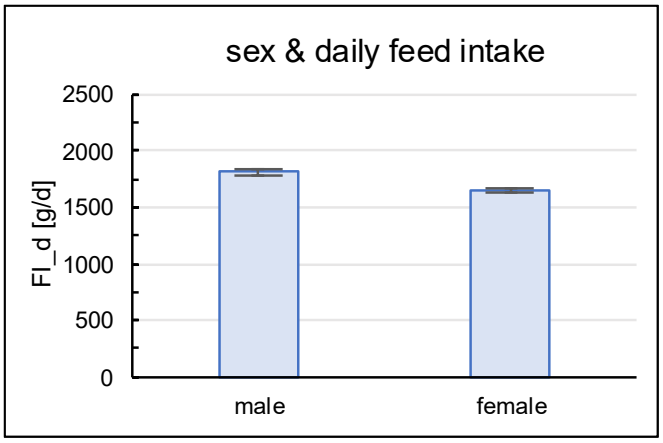

Figure 51: Difference in daily feed intake between sexes

4.2. Genotype

Significant differences were observed between genotypes ($p < 0.0001$). Among the genotypes, genotype group 5 consumed the highest amount of feed per day (1950.68 ± 41.47 g), surpassing genotype group 3 by approximately 330 g. Genotype group 3, in turn, had the lowest daily feed intake among the genotype groups (1621.17 ± 26.08 g).

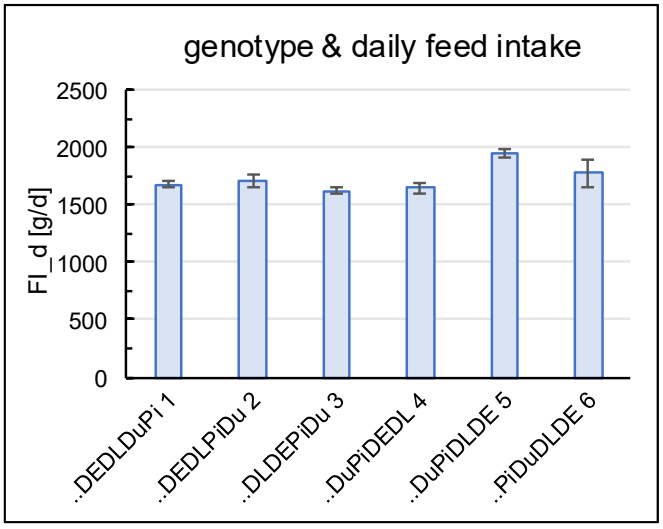

Figure 52: Difference in daily feed intake among genotypes

4.3. Season

It is noteworthy to observe a seasonal pattern when examining the daily feed intake, revealing a decline across the seasons (Figure 53, $p < 0.0001$). Animals which were scanned in season 1 (January or February) and season 2 (March or April) yielded a peak in the amount of daily feed intake, reaching approximately 2050 g per day. This peak was followed by a subsequent reduction leading up to the scanning dates in season 5 (September or October). This period marked the lowest observed daily feed intake. Importantly, it should be emphasised that the animals had been housed and fattened in the outside-climate stable for approximately 2.5 months preceding their scan.

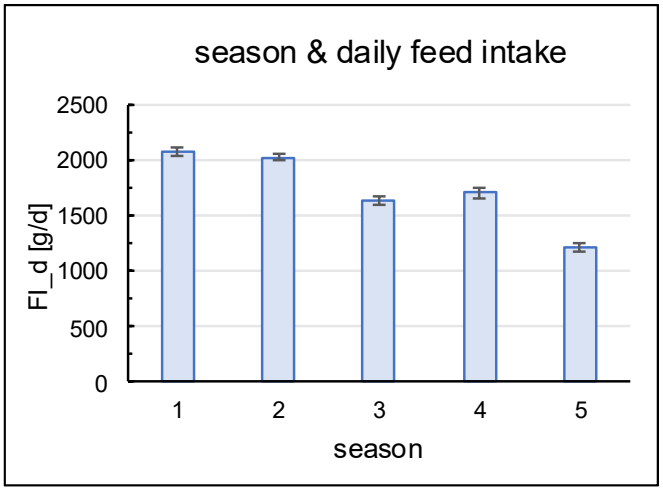

Figure 53: Differences in daily feed intake among seasons

4.4. Feeding week

Throughout the entire fattening period, segmented into ten feeding weeks, a consistent upward trend (Figure 54, $p < 0.0001$) was evident in daily feed intake, reflecting the customised ascending feed curve during this period. Only a minor decline was perceptible in the 10th feeding week.

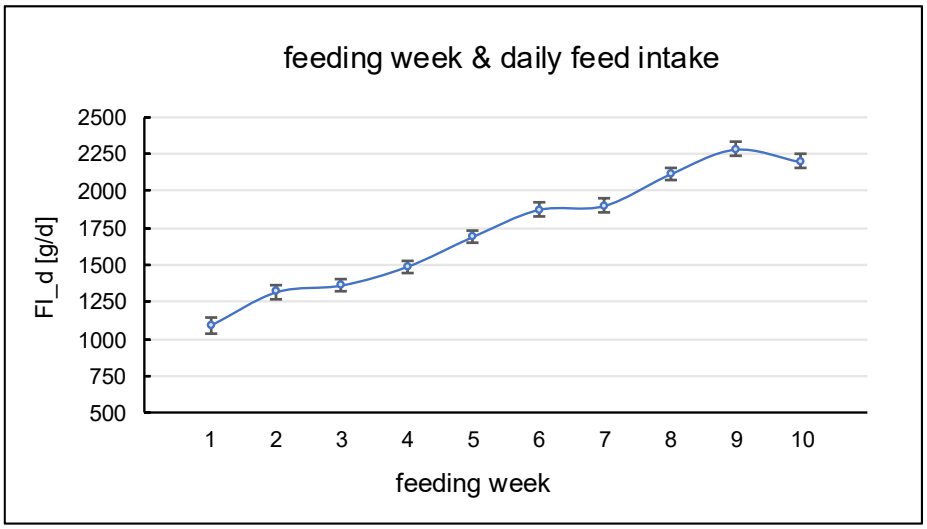

Figure 54: Differences in daily feed intake over ten feeding weeks

5. Method comparison of MRI and DXA

A Bland-Altman analysis was performed to visualise the agreement between the two methods, MRI and DXA, for measuring VAT, SAT, and TAT, and to identify potential systematic bias between them. As described in Chapter III.4 (Statistical analysis), modified Bland-Altman analyses, with differences between the two methods plotted against MRI estimates as the gold standard, are provided in Appendix IX.4.

5.1. Visceral adipose tissue

The Bland-Altman plot for VAT in Figure 55 shows a mean difference (bias, illustrated as a solid grey line) between the two methods of -1218 cm^3 (standard deviation = 549.4 cm^3; $p < 0.001$; 95 % CI: -1084, -1352 cm^3). This indicates a systematic overestimation of VAT volumes by DXA, with an average difference of 1218 cm^3 compared to MRI. The light grey lines represent the limits of agreement, with their 95 % confidence intervals indicated by the dashed lines. The upper limit is -141 cm^3 (95 % CI: 89, -371 cm^3), and the lower limit is -2294 cm^3 (95 % CI: -2064, -2525 cm^3). To assess potential proportional bias, a linear regression analysis was performed, showing a regression slope of -1.13 (SE = 0.07; $p < 0.001$), indicating that as VAT volumes increased, the differences in volume estimates between DXA and MRI became more pronounced.

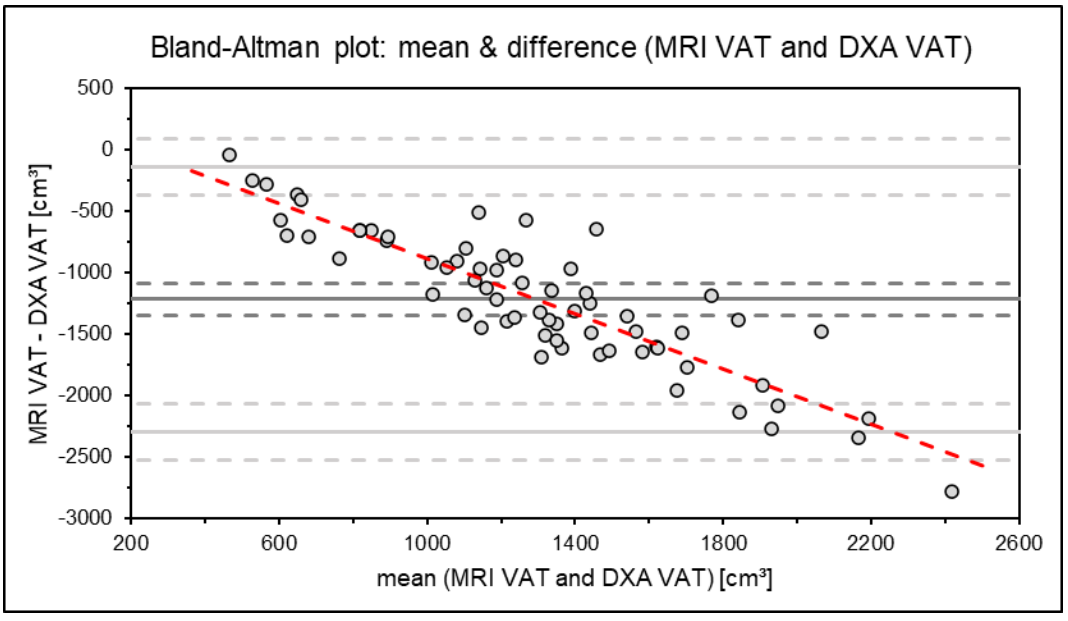

Figure 55: Bland-Altman plot with mean and difference of MRI and DXA for VAT

5.2. Subcutaneous adipose tissue

Figure 56 shows a Bland-Altman plot for SAT assessed with MRI and DXA. The bias between both methods was 1384 cm^3 (standard deviation: 433.3 cm^3; $p < 0.001$; 95 % CI: 1278, 1489 cm^3). The upper limit of 95 % confidence interval for the bias was 2233 cm^3 (95 % CI: 2051, 2415 cm^3), and the lower limit was 534 cm^3 (95 % CI: 353, 716 cm^3). This indicates that SAT was estimated much higher when assessed using MRI than by DXA. There is a positive regression line with a slope of +1.46 (SE = 0.14; $R^2 = 0.63$; $p < 0.001$), suggesting a proportional bias, with larger differences between volume estimates as SAT volumes increase.

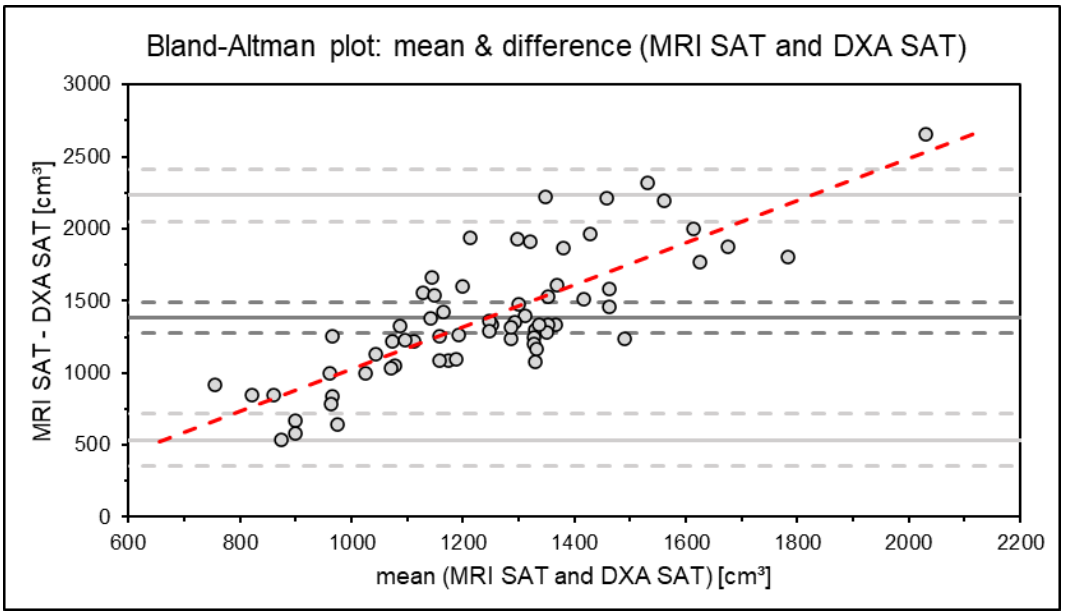

Figure 56: Bland-Altman plot with mean and difference of MRI and DXA for SAT

5.3. Total abdominal adipose tissue

The Bland-Altman plot for TAT in Figure 57 shows an average difference between the two measurement methods of 166 cm³ ($p < 0.001$; 95 % CI: 90, 243 cm³), indicating a statistically significant deviation from zero. The standard deviation (SD) of the bias is 313.6 cm³, resulting in an upper limit of agreement of 781 cm³ (95 % CI: 649, 912 cm³) and a lower limit of agreement of -449 cm³ (95 % CI: -580, -317 cm³). Although the proportional bias was not statistically significant (slope = -0.12; SE = 0.06; $R^2 = 0.054$; $p = 0.059$), the p-value was very close to significance, suggesting a weak trend towards decreasing bias at higher measurement levels.

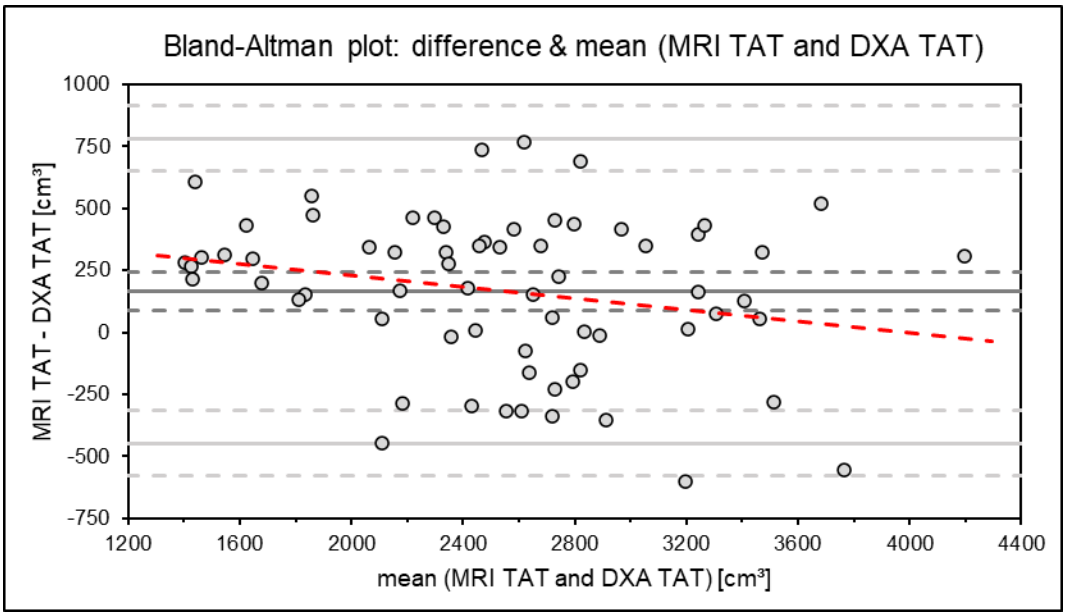

Figure 57: Bland-Altman plot with mean and difference of MRI and DXA for TAT

V. DISCUSSION

The aims of this study were first, to evaluate the ability of dual energy X-ray absorptiometry (DXA) to assess visceral and subcutaneous adipose tissue in pigs compared to the gold standard method of MRI and, second, to determine the impact of sex, genotype, and seasonal variations on body composition phenotypes and the feed intake during fattening of multi-hybrid pigs.

1. Imaging techniques

1.1. MRI

Assessments of adipose tissue, particularly visceral and subcutaneous fat, have long been conducted using magnetic resonance imaging as a non-invasive method. This imaging technique offers several advantages, including being non-ionising, therefore posing no risk in terms of radiation exposure. This makes MRI suitable for longitudinal studies. Furthermore, its high resolution provides excellent contrast among different soft tissues. For these reasons, MRI is considered the gold standard for assessing fat compartments in both human and veterinary research fields (Machann et al., 2013; Scholz et al., 2015; Fang et al., 2018).

Various methods have been proposed for the automated or semi-automated identification and quantification of fat tissue volumes in humans, using MRI (Kullberg et al., 2009; Positano et al., 2009; Wald et al., 2012; Borga et al., 2015). To our knowledge, however, there are currently no accurate automated methods available for animals, particularly for pigs. Therefore, we have chosen to perform a manual analysis of the images, although this process is very time-consuming and greatly relies on the individual's expertise in conducting the image acquisition and evaluation. To minimise discrepancies arising from varying evaluation methods, the analysis was performed by one individual.

Our study revealed mean MRI volumes of 689 cm³ for visceral fat, 1937 cm³ for subcutaneous fat and 2626 cm³ for total abdominal adipose tissue in the region of interest. Compared to the previous study conducted by Weigand et al. (2020), which reported VAT volumes (LSMs) of 1189 cm³ for castrated

males and 1017 cm³ for female pigs, our findings showed lower VAT volumes. Specifically, we observed LSMs of 595 cm^3 in castrated males and 629 cm^3 in females. This difference could potentially be attributed to the fact that our investigation exclusively focused on MHF2 pigs, which Weigand's study found to contain less VAT than the first multi-hybrid filial generation (MHF1), which was also included in their study.

In contrast to other imaging techniques like ultrasound or computed tomography, MRI has consistently shown higher sensitivity to subject motion. This primarily arises from the prolonged duration needed for MR imaging sequences to acquire data for adequate image formation (Zaitsev et al., 2015). In particular, respiratory motion and gastrointestinal peristalsis in the examined pigs may have resulted in variation in image quality. To minimise potential inaccuracies in the calculation of visceral adipose tissue volumes, only images characterised by high quality and strong contrast were included in the evaluation. In addition, challenges appeared in complete visualisation and subsequent evaluation, specifically for subcutaneous adipose tissue due to the size and abdominal circumference of certain animals.

1.2. DXA

Dual energy X-ray absorptiometry has primarily been introduced and is now widely accepted as a method for assessing bone mineral content and density (Glüer, 2017). Its application has expanded to encompass body composition studies by being an easily accessible, fast, and cost-effective tool for evaluating soft tissue body composition parameters in both humans and animals. With its ability to differentiate between adipose (fat), non-adipose (lean) and bone tissue, based on their X-ray attenuation with relatively low radiation, DXA facilitates reproducible data collection, particularly in research settings. By performing whole-body or regional scans along with specialised software analysis, various tissues in specific body regions can be automatically assessed within minutes. This offers a notably faster option compared to MR image analysis of VAT and SAT in pigs, which may take up to 15 hours per animal, depending on the amount of fat distributed and the animal's body length.

The GE Lunar *i*DXA scanner offers theoretically three different scan modes, “thick”, “standard”, and “thin”, which the manufacturer recommends for different body thicknesses. The “thick” mode is recommended for a body thickness of more than 25 cm, “standard” for a body thickness between 16 - 25 cm, and “thin” mode for less than 16 cm of body thickness (Thurlow et al., 2017). However, the “thin” mode does not differ from the “standard” mode, as described by Wenczel (2013). The subject's body thickness is automatically selected based on the subject's entered weight and height, in our case, body length, but it can also be set manually. As described previously, we conducted two scans using “standard” and “thick” modes for comparison, although all animals had a body thickness greater than 25 cm. Our findings revealed a very strong relationship between both modes for VAT (R^2 = 0.93, RMSE = 227.34, Figure 16), with overall greater volumes of VAT observed in “standard” mode compared to “thick” mode, as demonstrated by a slope of +1.09. However, this also resulted in smaller values for SAT in “standard” mode compared to “thick” mode, with a slope of +0.81 and a lower R^2 value of 0.54 (RMSE = 109.10, Figure 17) for the regression equation, with some “standard” SAT values even falling within a negative range. Consequently, the unrealistic results of “standard” mode were not further analysed.

One reason for this unexpected pattern could be that the “standard” mode may not provide sufficient X-ray exposure due to its short scanning time and the related low radiation dose of 3.0 µGy over approximately seven minutes. This may result in poor image quality with not enough X-ray intensity provided for each pixel. In contrast, the “thick” mode offers a higher radiation dose of 6.0 µGy and a longer acquisition time of approximately 14 minutes for a whole-body scan.

1.3. Comparison of MRI and DXA

Upon examining the abdominal adipose tissue variables alongside the methodologies employed, it becomes apparent that notable differences exist between the two methods. Regression analyses and Bland-Altman plots revealed the following disparities:

- For visceral adipose tissue, a relatively strong relationship was observed between MRI and DXA estimates, with an R^2 of 0.49 (RMSE = 163.66, Figure 22), although accompanied by a systematic bias in the Bland-Altman plot (Figure 55). Therefore, the VAT estimates by DXA, particularly the GE Lunar *i*DXA, resulted in a mean overestimation of 1218 cm^3 compared to MRI. The regression slope of -1.13 (R^2 = 0.78, RMSE = 260.43) along the means and differences of both methods suggests that, with increasing volumes of VAT, differences between both methods increase, resulting in greater overestimation errors by DXA.
- For subcutaneous adipose tissue, the relationship between MRI and DXA records was not statistically significant (p = 0.299, Figure 23). Additionally, DXA systematically underestimated the volume of SAT by an average of 1384 cm^3 (Figure 56) compared to MRI. There was a proportional bias with a slope of +1.46 (R^2 = 0.63, RMSE = 266.58), indicating that greater underestimation errors by DXA occur with increasing SAT volume.
- Total abdominal adipose tissue assessed via MRI and DXA revealed a strong relationship between the two methods, with a bias of 166 cm^3 (Figure 57) and an R^2 of 0.79 (RMSE = 283.23, Figure 24). The differences between both methods were independent of TAT volume means (p = 0.059), as indicated by a regression slope of -0.12 (R^2 = 0.054, RMSE = 307.39).

Furthermore, regarding MRI records, regression analyses of the relationships between VAT and TAT, and SAT and TAT, respectively, indicated that SAT shows a comparatively stronger relationship with increasing TAT volume (slope = +0.67, R^2 = 0.93, RMSE = 112.34) than MRI VAT and TAT (slope = +0.33, R^2 = 0.76, RMSE = 112.34, Figure 20). In contrast, DXA estimates revealed a very strong relationship between VAT and TAT volumes (slope =

+0.98, R^2 = 0.96, RMSE = 147.06) compared to SAT (p = 0.489, Figure 21), which remained nearly unchanged even with increasing TAT volumes.

The findings from our study demonstrate that a direct comparison of visceral, subcutaneous, and total abdominal adipose tissue between MRI and DXA is only possible to a limited extent. A relatively strong agreement was observed between the two methods for total abdominal adipose tissue (TAT); however, this was not the case for its components, VAT and SAT. A consistent pattern of VAT overestimation and a corresponding underestimation of SAT was found. Additionally, a systematic proportional bias was discovered in our study for VAT (negative slope) and SAT (positive slope), indicating that larger volumes of VAT or SAT in the animals corresponded to greater overestimation or underestimation errors by DXA relative to MRI, respectively.

Weigand et al. (2020) also reported an average VAT overestimation of approximately 579 cm³ by DXA compared to MRI, accompanied by a proportional bias. Similarly, a study assessing VAT in calves using DXA and MRI demonstrated a similar overestimation by DXA (Kappes et al., 2024).

Several studies in humans have further demonstrated that DXA overestimates VAT, particularly in overweight and obese individuals (Neeland et al., 2016). Knapp et al. (2015) reported higher precision errors in VAT estimation between DXA and MRI with increasing body fat, which were more pronounced than those associated with increased BMI. Additionally, Dias et al. (2019) found that DXA measurements overestimated VAT by approximately 171.5 cm³ compared to MRI among normal-weight and obese children. Furthermore, they observed a weaker correlation between DXA and MRI VAT records among participants in the highest third of body fat percentage (r = 0.38 – 0.47) compared to the overall study sample (r = 0.90).

VAT records in DXA are only provided by the software, which calculates VAT by estimating SAT at the lateral aspects of the android region, taking body depth into account, and then subtracting SAT from total abdominal fat (TAT) (Kaul et al., 2012). Consequently, VAT is not directly measurable or verifiable, and because SAT is not provided separately, its accuracy cannot be assessed either. Therefore, we relied on estimations provided by the CoreScan™ software, meaning VAT accuracy depends on the precise determination of

subcutaneous adipose tissue.

A key consideration when using DXA to detect visceral and subcutaneous adipose tissue is that the scanners and accompanying software are primarily designed for the use in humans (Hunter et al., 2011; Kasper et al., 2021). When comparing fat distribution between humans and pigs, the colour mapping feature of the enCore™ software assists in identifying locally distributed fat depots (Figure 58). However, the distribution of these depots varies between humans and pigs, particularly at the lateral aspects of the android region (as shown in the pink box).

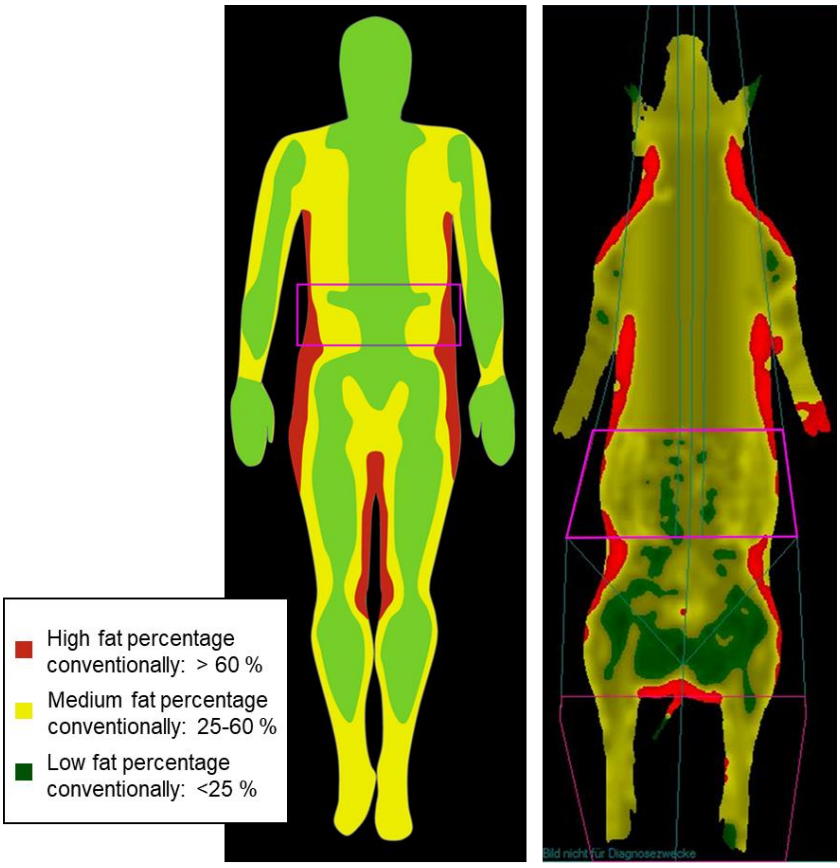

Figure 58: Comparison of fat distribution between humans and pigs with colour mapping scheme, modified according to Bazzocchi et al., 2016

This discrepancy in lateral fat layers, as illustrated by black arrows in Figure 59, may contribute to the underestimation of SAT and the corresponding overestimation of VAT in pigs. This estimation error could be attributed to the two-dimensional nature of DXA. The thick back fat layer of pigs is likely not fully accounted for as subcutaneous fat and may instead be partially classified as VAT. If the lateral fat layer depth is smaller than the back fat depth, SAT would, in most cases, be underestimated.

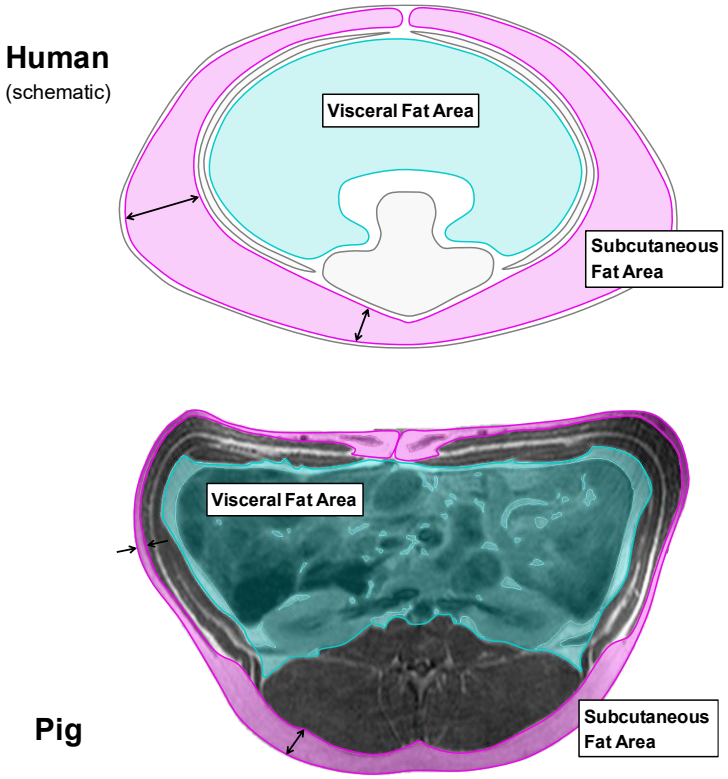

Figure 59: Comparison of schematic abdominal cross-sections in humans and pigs

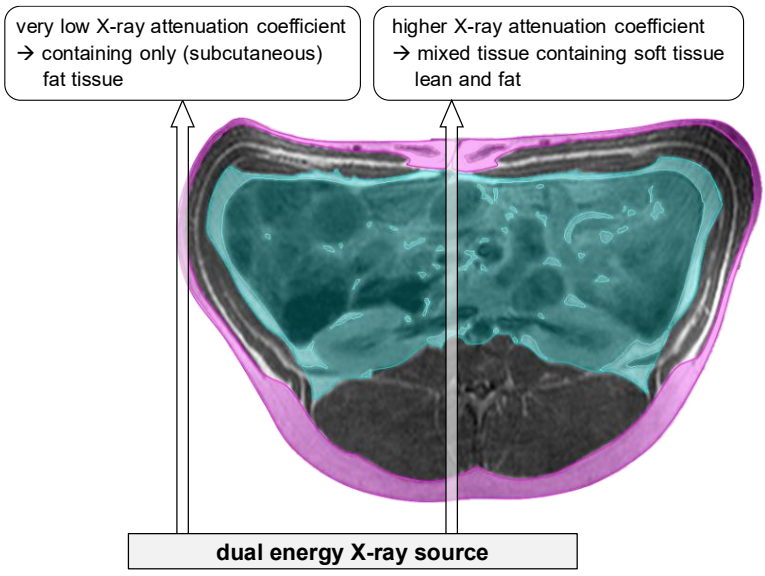

Figure 60: Schematic, simplified principle of DXA

This is due to the detection of very low soft tissue X-ray attenuation coefficients over only a relatively small area of the body, which is associated with a higher proportion of fat tissue compared to the lower attenuation coefficients of mixed soft tissues (Figure 60).

The enCore™ algorithm is optimised for humans in a supine position.

However, the animals were positioned in ventral recumbency primarily to prevent respiratory depression or sudden movements during anaesthesia, ensuring their safety and stability. The positioning, combined with the presence of a thick layer of fat over the back muscles (see Figure 59), may cause overlapping adipose tissue, potentially hindering precise estimation of SAT and, therefore, leading to an underestimation of SAT compared to MRI findings.

Additional limiting factors contributing to VAT overestimation may include the animals' large body dimensions and depth, as also suggested by Knapp et al. (2015) within studies of obese humans. Seibert and Boone (2005) described the beam hardening effect, which explains greater attenuation of low-energy X-rays in thicker tissues compared to high-energy X-rays, resulting in decreased R-values (X-ray attenuation coefficients), and consequently, in an overestimation of fat estimates compared to the actual tissue composition. Due to the proprietary nature of the DXA's system algorithm, modifications for studies involving animals with, for example, broader or thicker bodies than humans are not possible (Kasper et al., 2021).

Lastly, the hydration status of the soft tissue is another known factor influencing DXA accuracy in fat estimation, as variations can be caused by factors such as feed or fluid intake and increased physical activity (Pietrobelli et al., 1998). To mitigate these potential effects, we employed standardised procedures, including overnight fasting periods, before scanning.

1.4. Back fat thickness assessment using ultrasonography

Assessing back fat thickness using ultrasound at the midpoint between the shoulder and ham on the right side of each animal may provide additional information about the thickness of the subcutaneous layer at this specific area. This study investigates whether this assessment can potentially offer insights into the distribution of subcutaneous and visceral adipose tissue in pigs.

We found a moderately strong relationship between back fat thickness measured using ultrasound and subcutaneous adipose tissue determined with MRI, with a coefficient of determination (R^2) of 0.42 (RMSE = 299.96, $p < 0.001$, Figure 25). Similarly, back fat thickness even showed a positive relationship with visceral adipose tissue, with an R^2 of 0.39 (RMSE = 170.92, $p < 0.001$, Figure 26). To fully interpret these results, it would be necessary to compare the direct values with each other using a Bland-Altman analysis. However, assessing the “true” agreement between the two methods of ultrasound and MRI is not possible due to their different units (volume against distance).

Only MRI and CT scans can provide direct measurements of visceral and subcutaneous adipose tissue volumes. Some studies in humans have applied geometric models to convert depth measurements into VAT areas. Asano et al. (2017) assessed the abdominal visceral fat area in 100 males via ultrasound using two different approaches: the elliptical method and the triangle method. The results of these methods were then compared to VAT measurements obtained from CT scans. Relatively high correlations were observed, with correlation coefficients ranging from 0.77 to 0.78 ($p < 0.001$). Additionally, Rolfe et al. (2010) found a strong correlation between ultrasound and MRI measurements of visceral and subcutaneous fat thickness in elderly humans, with an even higher correlation for visceral fat thickness ($r = 0.90$) compared to subcutaneous fat thickness ($r = 0.73$). Furthermore, ultrasound measurements showed much stronger correlations with MRI records than anthropometric measures such as BMI and waist circumference. This was further supported by Asano et al. (2017), who reported that VAT area measured via ultrasound correlated more strongly with CT than waist circumference did.

Although ultrasound is commonly used to assess body condition in pigs, few studies have evaluated the accuracy against “real” values for fat or muscle. Investigating correlations between ultrasound measurements and slaughter data, Reckels et al. (2020) found a strong association. The back fat / muscle ratio demonstrated a notable correlation with fat and meat measures obtained through dissection, suggesting that precise ultrasound measurements have the potential to predict body composition in pigs accurately.

Building on this, ultrasound has already been implemented in pig carcass classification, where payment is based on data obtained from ultrasound scans. In recent years, ultrasound technologies such as the Auto-FOM have been further developed and improved, and they are used to determine the fat and muscle composition of the entire pig carcass (Busk et al., 1999; Höreth, 2013; Dorleku et al., 2023).

Raschka et al. (2016) conducted a study in dairy cows to evaluate the accuracy of ultrasonic measurements in predicting actual fat amounts. They found strong correlations between fat amounts calculated from ultrasound measurements and those from dissection, with coefficients of determination ranging from 0.83 to 0.95 for total subcutaneous adipose tissue, abdominal adipose tissue, and its components such as retroperitoneal, omental, and mesenteric adipose tissue.

Discrepancies between the methods used in our study could be due to the fact that only one scanning site was examined with ultrasound. Given the irregular distribution of subcutaneous fat between sexes and breeds, this site above the caudal rips may not be appropriate for all animals of different sexes and weight classes (Fortin, 1986; González et al., 2017). The evaluation of several sites could improve the verification of subcutaneous fat. Validating ultrasound measurements against MRI, which is considered the gold standard for assessing adipose tissue distribution, is crucial. Discrepancies between ultrasound and MRI measurements may arise due to variations in imaging principles, differing units, and one-sited assessment with ultrasound.

In conclusion, while ultrasound measurements demonstrated the ability to estimate tendencies for abdominal adipose tissue compartments in our study, further research is needed to assess the accuracy and consistency of

ultrasound in measuring abdominal adipose tissue volumes in pigs.

2. The impact of sex, genotype and season on fat distribution, body composition and feed intake

Our study revealed noticeable differences in the distribution of specific fat depots, such as visceral and subcutaneous adipose tissue, as well as several other body composition parameters among castrated male and female pigs, between different genotype groups and across various seasons, during which we examined the animals. The extent to which these factors influenced feed intake among the animals will also be addressed subsequently. Given the complex and interdependent effects of these parameters on the phenotypic appearance, it is crucial to consider the individual findings within a broader context.

2.1. Variations among barrows and gilts

Sex-related differences were statistically significant only for DXA-derived estimates of SAT, with gilts exhibiting greater volumes than barrows (gilts 611 cm^3, barrows 363 cm^3, Table 9), a finding further validated by the larger study cohort of 138 animals (Table 15). Although not reaching statistical significance, differences were observed in the least squares means of the other examined variables such as VAT, TAT and total body fat.

For VAT, results varied depending on the measurement method. DXA-estimated volumes were higher in barrows than in gilts (barrows 1961 cm^3, gilts 1757 cm^3), a pattern that became statistically significant in the larger cohort. Contrarily, MRI-derived VAT estimates were higher in females than in males (gilts 629 cm^3, barrows 595 cm^3), a pattern also observed for MRI-derived SAT records (gilts 1837 cm^3, barrows 1759 cm^3).

Total abdominal fat volumes assessed via MRI and DXA tended to be higher in gilts than in barrows, though these differences remained marginal (MRI: gilts 2466 cm^3, barrows 2354 cm^3, DXA: gilts 2368 cm^3, barrows 2324 cm^3). Interestingly, DXA analysis of the larger sample size revealed a distinct pattern, suggesting that male animals accumulated more total abdominal fat than females (barrows 2584 cm^3, gilts 2420 cm^3, Table 15). This finding aligns with the distribution of total body fat, where males exhibited significantly higher amounts than females (barrows 15152 g, gilts 14264 g). However, lean mass

did not differ significantly between sexes. Nevertheless, in absolute terms, gilts exhibited slightly greater lean mass than barrows (gilts 79199 g, barrows 78514 g).

Diverse findings are also reported in existing literature. In studies investigating the body composition of different sex types, barrows generally show the highest degree of adipose tissue accumulation, ahead of sows and boars (Barton-Gade, 1987; JinLiang Xue et al., 1997; Schinckel et al., 2008). This is mainly due to the lack of anabolic steroid hormones as a result of castration (see Chapter II.2.1). The results of Weigand's study (2020) support this, with castrated males exhibiting higher overall fat volumes, particularly in VAT, body fat percentage and total body fat, compared to females, as estimated by both MRI and DXA. A recent study conducted by Zomeño et al. (2023) examined the carcass characteristics of Iberian pigs. The findings revealed that castrated males displayed slightly more subcutaneous fat across three weight classes (70 kg, 100 kg, 120 kg), even though the gilts had slightly higher carcass weights compared to barrows. In contrast, but correspondingly to our findings, a study conducted by Kolstad et al. (1996) assessed Duroc and Landrace pigs with CT and revealed higher amounts of subcutaneous fat in gilts compared to barrows but found no differences in the amount of internal visceral fat among male and female animals with a live weight of 60 kg. However, in the context of V.1.3 (Comparison of MRI and DXA), it is important to note that DXA estimates for SAT can only be used to determine tendencies rather than for quantitative comparisons.

Given that the initial characteristics of barrows and gilts were almost the same at the time of examination (Table 8), except for a slightly higher average body weight in males (97.43 kg) compared to females (96.55 kg), the observed difference in daily feed intake (barrows 1814 g/d, gilts 1648 g/d, Figure 51) during the recorded period may have contributed to the increased body weight and greater overall fat accumulation among male pigs. Several studies have confirmed that barrows tend to have a higher voluntary feed intake compared to gilts (Dunshea, 2003; van den Broeke et al., 2022). This difference is also attributed to the absence of gonadal steroids in castrated animals, implying they do not underlie the impact of appetite-inhibiting effects of testosterone or oestradiol observed in intact pigs. It is known that feed efficiency is lower in

castrated male pigs compared to intact ones, with females being intermediate. Castrated males consume more feed without compensatory growth, leading to increased body fat and decreased lean content, ultimately resulting in lower slaughter profits (Pauly et al., 2008; Patience et al., 2015; Bonneau and Weiler, 2019). However, Averós et al. (2012) found no disparities in average daily feed intake and feed conversation ratio between sexes in a meta-analysis. Nevertheless, Fornós et al. (2022) recommended considering not only the absolute daily feed intake, but also feed intake behaviours, such as the number of meals per day and duration per meal, as these factors can also influence body composition. Specifically, larger feed intake portions consumed in a shorter time per meal are associated with higher fat accumulation and reduced carcass quality, compared to slower intake of smaller amounts (Fornós et al., 2022). Additionally, barrows were observed to spend a longer duration consuming feed per day compared to gilts, which likely leads to greater feed intake and increased weight gain (Cross et al., 2020). In contrast to our findings, female Göttingen minipigs showed higher metabolised energy feed intake than males when fed *ad libitum*, resulting in greater body weight gain and increased back fat thickness compared to males (Bollen et al., 2005). The authors suggested that this difference between sexes might be related to the higher predisposition for obesity observed in female Göttingen minipigs. This tendency towards obesity in females may lead to increased feed consumption, more frequent meals and longer meal durations contributing to differences in body composition between sexes in Göttingen minipigs.

To further interpret the sex-specific differences in our results, a detailed evaluation of feed intake behaviours and activity level protocols of both sexes would have been beneficial. Overall, it is worth noting that the distribution of animals by sex was not balanced, resulting in a higher number of gilts than barrows (44 vs. 23, in the larger cohort 92 vs. 46, respectively).

2.2. Variations in genotypes

Our study has shown that the applied crossbreeding scheme can achieve a wide variance of phenotypes, even in a relatively small number of animals.

Analysing the distribution among these groups revealed certain patterns. In particular, genotype groups characterised by a high SAT volume, such as groups 3, 5, and 1, also presented elevated estimates of VAT, while the opposite was observed for genotype groups 4 and 6 (Table 10). Additionally, it was observed that animals with higher body fat content tended to have lower lean mass, aligning with expectations (Figure 45, Figure 46).

Genotype group 6 stood out as the oldest group on the day of the study, with an average age of 150 days (Figure 33). Although not showing the highest fat deposition (Table 10), these pigs exhibited the highest body weight (Figure 32), likely due to their greater age and the associated prolonged fattening period, even if only by a few days. However, it's important to note that due to the limited number of observations for this group, estimates are associated with high standard errors.

In general, we investigated the relationship between weight and the distribution of abdominal fat compartments. Moderately strong associations were found for MRI-derived SAT volume (R^2 = 0.35, RMSE = 345.88, Figure 27) and TAT volume (R^2 = 0.31, RMSE = 513.31, Table 7), as well as for DXA estimates of TAT and VAT volumes (both R^2 = 0.42, TAT RMSE = 525.1, VAT RMSE = 524.17, Table 7). With an increase of 51.9 cm^3 of VAT per kilogram body weight assessed via DXA, our findings revealed an even stronger relationship compared to the findings of Weigand et al. (2020), who reported an increase of 18.3 cm^3 per kg (R^2 = 0.29, RMSE = 238.10).

In addition to literature indicating a strong relationship between body weight and fat deposition (Kolstad et al., 1996; Mohrmann et al., 2006), Reckels et al. (2020) reported a significant association between body weight and the diameter of the longissimus dorsi muscle. However, this correlation weakened as fat content in the body composition increased, suggesting that body weight alone is insufficient for a comprehensive assessment of body composition. Therefore, back fat thickness and muscle diameter measurements, along with their ratio, should also be considered when evaluating and classifying body

conditions, particularly for determining feeding efficiency and carcass quality.

2.3. The impact of seasonal variations

Given that the animals in our study were housed in an outside-climate stable during the growth and fattening phase, they were exposed to changes in ambient temperatures throughout the study duration. Consequently, we also investigated the impact of seasonal variations in our study.

Significant differences were observed among the seasons and years during which the animals were examined. Generally, animals fattened and scanned in winter exhibited higher fat deposition compared to those scanned in summer. Notably outlying was the group scanned during season 4 in 2021, representing July and August, which displayed the highest volumes of visceral, subcutaneous, and total abdominal adipose tissue, as well as the highest overall body fat mass and bone mineral content, while exhibiting the lowest lean mass (Table 11). Accordingly, BMD was also the highest in this season-year category (4 / 2021), although the effect of season x year was only significant ($p = 0.0037$) in the larger cohort of 138 observations (Table 17). Conversely, season 4 in 2022, along with season 3 in 2022, showed the least fat deposition overall and the smallest amounts of BMC and BMD (Table 11).

To explain the significant disparity observed in our findings for animals examined in season four between the years 2021 and 2022, we conducted a thorough examination of the detailed average temperature trends spanning the entire study period. We set these trends against the average temperatures recorded over the last 30 years (1991 – 2021, Meteostat, 2024 *https://meteostat.net/de/station/10866?t=2020-12-01/2022-10-31,* last assessed 12.02.2024) for a comparative analysis (Figure 61). Notably, the ambient temperatures during the months of March through May, as well as July and August in 2021, were below average. These months corresponded with the rearing and fattening period for the animals scanned in season 4 in 2021. In contrast, the temperature patterns observed in 2022 displayed an opposite trend, with temperatures being consistently above the averages from May to August.

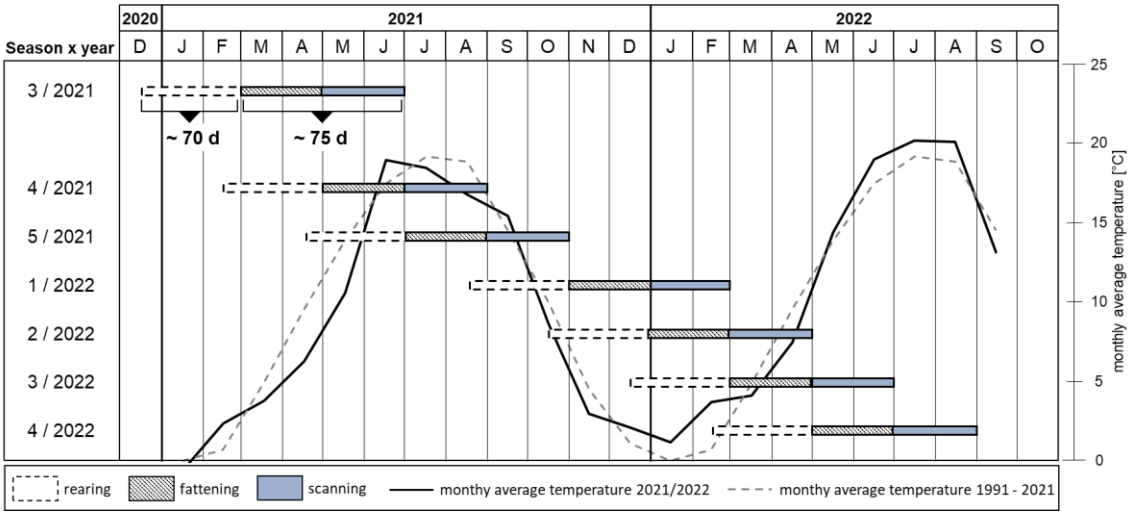

Figure 61: Average temperature during study period and between 1991 and 2021

Additionally, seasonal variances were found to influence feed intake. The daily feed intake demonstrated a decreasing trend across the seasons, with animals scanned in season 1 showing the highest intake and those scanned in season 5 showing the lowest (Figure 53).

Changes in temperature between summer and winter are known to influence the amount of feed intake (Quiniou et al., 2000; Patience et al., 2015; Cross et al., 2020; Albert et al., 2024). On the one hand, due to elevated metabolic and nutrient requirements during winter, feed intake typically increases. Lebret et al. (2006) showed that for every 1° C decrease in temperature the feed intake of pigs increases by approximately 35 g/day. Consequently, during the winter months higher feed intake levels may lead to greater fat deposition, particularly as increased back fat thickness, serving for protection against the cold (Čobanović et al., 2020).

On the other hand, heat stress during summer months leads to reduced feed intake, as has been frequently observed (Quiniou et al., 2000; Barnett et al., 2001; Li and Patience, 2017; Rauw et al., 2020) and aligns with our observations. In connection with heat stress, a reduction in feed intake, attributed to the need to decelerate metabolic heat production, is associated with decreased performance indicators such as reduced average daily weight gain and smaller live weights (Čobanović et al., 2020; Wang et al., 2023). Consequently, decreased growth rates contribute to leaner body compositions (Albert et al., 2024), caused by reduced energy levels available for lipid

deposition (Johnson et al., 2015). However, despite these findings, Qu and Ajuwon (2018) suggested that chronic heat stress prompts a response in adipose tissue, leading to increased lipid storage as a protective mechanism against the stressor. This adaptive response results in higher carcass fat accumulation and wider back fat thickness, a phenomenon which has been repeatedly observed in recent studies (Pearce et al., 2013; Victoria Sanz Fernandez et al., 2015; Gonzalez-Rivas et al., 2020; Liu et al., 2022).

Seasonal variations in climate between summer and winter can also influence physical activity levels. Reduced activity and the resulting decrease in energy expenditure may contribute to weight gain and increased fat storage, which can, in turn, affect each other (Renner et al., 2018). Podder et al. (2022) demonstrated how Ghoongroo pigs adapt their activity levels in a tropical environment, with increased resting and laying down behaviours during winter and increased standing and roaming activities during summer. In the present study, however, activity levels were not recorded. Thus, information in this regard is not available.

Overall, our findings emphasise a pronounced seasonal variation in feed intake, notably influencing adipose tissue deposition. However, the deviation in season 4 in 2021 may be attributed to cooler temperatures during the corresponding fattening period or other factors, such as underlying hereditary traits specific to the pig breed or crossbred population within a given environment (Rauw 2020, Albert 2024, Guan 2024).

In addition to adipose tissues, the evaluation of bone mineral content and bone mineral density is essential for determining bone stability, especially in fattening pigs, and understanding the associated risks of bone fractioning (Nielsen et al., 2007). A comprehensive understanding of the influence of seasonal variations on bone health in pigs is necessary, as this has been addressed in Chapter II.3.3.4. In our study, the findings regarding BMC and BMD levels revealed an association with variations in fat distribution rather than with seasonal changes of winter and summer. Further research is currently being carried out to investigate the relationship between bone metabolism and fat metabolism. A deeper understanding of the connection between obesity and osteoporosis is especially crucial in humans (Gkastaris

et al., 2020). However, conflicting findings are present in the current literature regarding the associations between body fat distribution and BMD. Some studies found a positive association with fat accumulation (Marwaha et al., 2013), suggesting a protective effect on bone strength. Fu et al. (2011) also discovered a positive relationship between total fat mass and BMD, although this association was observed only for premenopausal women. Contrarily, in post-menopausal women, higher fat accumulation in the android region was negatively associated with BMD. Various authors have also reported negative relationships between visceral fat and BMD (Choi et al., 2010; Zhang et al., 2015; Zhu et al., 2020) in humans. Hilton et al. (2022) have noted controversial findings, revealing in individuals of normal-weight a positive correlation between fat mass and BMD. However, after correcting for at and lean mass, a negative association between visceral adipose tissue and total BMD was observed, suggesting a higher risk of VAT on bone health (Hilton et al., 2022). Additionally, Lin et al. (2023) revealed a negative relationship between SAT and BMD, which was in line with findings of Wang et al. (2017). The degree to which bone health is linked to fat distribution, particularly visceral and subcutaneous adipose tissue depots, is currently under investigation. Some studies have suggested that visceral adipose tissue may have a pronounced negative effect on bone density compared to subcutaneous adipose tissue. This could be due to higher levels of pro-inflammatory cytokines and other factors associated with visceral fat accumulation, such as tumour necrosis factor α, interleukin 6, and resistin, as well as reduced anti-inflammatory factors like adiponectin (Neeland et al., 2019).

The extent to which adipose tissue deposits are linked to bone mineral content and density in pigs remains not fully understood. Bernau et al. (2020) discovered significantly higher levels of BMC and BMD in castrated pigs compared to intact boars, the former of which are known to deposit higher overall body fat levels. However, in a study conducted by Dölle (2019) no differences in BMC and BMD were found between barrows and gilts, despite barrows having greater total fat mass and higher overall body weights. Though it was observed that pigs examined during autumn and winter (group 3) exhibited the highest total fat percentage and mass, while also demonstrating the highest BMC and BMD levels. Again, this raises the question of a potential

seasonal influence on this observation. Therefore, further research is needed to comprehensively understand how visceral and subcutaneous fat and seasonal variations influence bone metabolism for further improving porcine health and breeding.

3. Further investigations

Our study focused on phenotyping visceral and subcutaneous adipose tissue in the entire abdominal area of crossbred fattening pigs, ranging from the last thoracic vertebra to the iliac crest. This assessment was conducted using both MRI and DXA, with the latter employing the android determination feature of the CoreScan™ software for the GE Lunar *i*DXA system. This ensured that both methods covered the exact same region of interest. Additionally, we obtained further body composition parameters through whole-body DXA scans. Furthermore, ultrasound measurements provided additional data on local back fat thickness in individual pigs.

In some cases, particularly with larger pigs weighing over 100 kg, complete visualisation of subcutaneous adipose tissue was challenging due to the animals' abdominal width. Consequently, only subjects with fully visualisable subcutaneous adipose tissue were accountable for evaluation using the 3D-Doctor© software. To address this limitation in future studies with similar trial designs, considerations should be made to either employ an MRI with larger table dimensions or coils, or to perform examinations at earlier stages when the animals are smaller.

The enlarged subcutaneous fat layer located above the longissimus dorsi muscles may not be accurately determined by DXA due to the ventral recumbency of the pigs, potentially resulting in underestimation of SAT as previously discussed in Chapter V.1.3. To verify this, future investigations could explore other positioning options, such as lateral-lateral or dorsal recumbency, as previously examined in dog and cat carcasses (Raffan et al., 2006; Bjørnvad et al., 2017), to evaluate the accuracy and precision of DXA.

Besides collecting imaging data, blood samples were taken from all animals examined, as well as their progenitors (MHF1). Genomic analysis of these samples could allow conclusions to be drawn about specific genes and quantitative trait loci (QTLs*)*. When combined with phenotypic data, such analysis could provide information about potential QTLs associated with increased or decreased visceral and subcutaneous adipose tissue deposition in pigs, as previously demonstrated for body composition traits in whole-body and regional DXA phenotypes (Rothammer et al., 2014; Rothammer et al.,

2017). Beyond the genetic component, blood samples could also be valuable for analysing other blood parameters that reflect the influence of extrinsic factors on fat distribution over the study period.

Furthermore, recording the birth weights of piglets across the different seasons would be of interest, as the progeny of sows that gestate under heat stress have been observed to be lighter weighted compared to those gestated under thermoneutral conditions (Lucy and Safranski, 2017). Additionally, progeny from sows mated in early summer, which then gestate under hot summer conditions, have been found to develop increased back fat thickness by the time of slaughter (Liu et al., 2020).

MRI-based abdominal or whole-body scans can provide detailed information about specific anatomical structures and tissue depositions. Particularly in larger cohort epidemiological or phenotypic studies, semi-automated segmentation and analysis can be time-consuming and more dependent on the evaluating individual compared to automated information-extracting solutions. In recent years, deep learning has been continuously developed for the automated segmentation of large MRI datasets in humans offering fast and precise high-quality segmentation solutions in medical imaging (Rickmann et al., 2022). This technology could also play an important role in phenotyping studies in pigs and other animals, helping to better understand the connection between anatomical structures and pathological conditions, thereby enhancing fundamental research and breeding studies.

VI. SUMMARY

Phenotyping of the Visceral and Subcutaneous Adipose Tissue in Pigs using Magnetic Resonance Imaging (MRI) and Dual Energy X-ray Absorptiometry (DXA)

Over the last thirty years, the global rise in obesity rates has led to immense health and economic challenges. Human obesity results from a complex interplay of genetic, lifestyle and dietary factors, with visceral obesity, characterised by excessive adipose tissue accumulation around internal organs, being particularly concerning due to its association with metabolic disorders. The pig serves as a valuable model for human obesity research due to their anatomical, physiological, and genetic similarities to humans. This thesis aims to evaluate dual energy X-ray absorptiometry (DXA) as a non-invasive and fast method for quantifying visceral and subcutaneous adipose tissue (VAT and SAT) and other body composition parameters in pigs in comparison to magnetic resonance imaging (MRI), alongside using ultrasonography as another non-invasive method for measuring back fat thickness. By phenotyping a diverse pig population, this study further investigates how intrinsic factors such as sex and genotype, along with extrinsic factors including ambient temperatures and feed intake, influence adipose tissue deposition and body composition.

In this study, 138 multi-hybrid crossbred pigs from the second filial generation (MHF2), derived from the parental breeds Piétrain, Duroc, German Landrace and Large White, were examined using MRI, DXA and ultrasonography. All animals were raised and managed under uniform conditions. The average age at the time of examination was 147 days, and due to varying birth dates, examinations were conducted across different seasons and years. Feed intake during the fattening period was recorded for all animals prior to scanning. For a focus group of 67 animals, MRI cross-sections of the abdominal region, with the region of interest spanning from the last thoracic vertebra to the iliac crest, were manually analysed and reconstructed into 3D images using the 3D-Doctor© software (Able Software Corp.), allowing the quantification of VAT and SAT volumes. Whole-body DXA scans were

performed with the GE Lunar *i*DXA CoreScan™ software, which automatically calculates VAT within the same region of interest. This is done by estimating SAT through a specific geometrical algorithm and subsequently subtracting it from total abdominal adipose tissue (TAT). Assessment of further body composition parameters, including fat mass, lean mass, bone mineral content and bone mineral density, were automatically derived by DXA. Moreover, ultrasound measurements of the back fat thickness were performed.

The comparison of the methods using linear regression models revealed a moderately strong relationship between MRI and DXA estimates for VAT volumes (R^2 = 0.49) and a strong relationship for TAT volumes (R^2 = 0.79). In contrast, the relationship between SAT records was weak (R^2 = 0.017). MRI data showed that SAT increases more (slope = +0.67, R^2 = 0.93) than VAT (slope = +0.33, R^2 = 0.76) as total abdominal adipose tissue rises, while DXA estimates demonstrated a larger increase in VAT (slope = +0.98, R^2 = 0.96) compared to SAT (slope = +0.019, p = 0.489). In addition, the results of a Bland-Altman analysis suggested that DXA systematically overestimates VAT (bias = 1218 cm^3) and underestimates SAT (bias = 1384 cm^3) compared to MRI, especially at higher fat levels. In contrast, for TAT, a stronger agreement was observed, with a smaller bias of 166 cm^3. Additionally, the study found a moderately strong relationship between back fat thickness assessed with ultrasonography and both SAT (R^2 = 0.42) and VAT (R^2 = 0.39) derived from MRI.

Regarding the evaluation of effects influencing the phenotype, both intrinsic and extrinsic factors were considered by applying mixed model procedures. Although our study revealed only a minor effect of sex on body composition and fat distribution, seasonal variations had a significant impact on these traits. Animals fattened and scanned during winter showed overall greater adipose tissue deposition compared to those examined in summer. Additionally, both sex and season influenced feed intake, with barrows demonstrating a higher feed intake (approximately 1814 g/d) compared to gilts (approximately 1647 g/d). In general, a higher feed intake was observed during winter compared to summer. By applying a specific crossbreeding scheme in our study, a wide variation of phenotypes was generated, with the genotype composition significantly affecting most of the examined variables.

In conclusion, the findings of this thesis suggest that the GE Lunar *i*DXA CoreScan™ software is not suitable for accurately quantifying subcutaneous adipose tissue (SAT) in pigs, as it tends to underestimate SAT, leading to an overestimation of visceral adipose tissue (VAT). The analysis of total abdominal adipose tissue (TAT) shows a moderate to strong agreement between the two methods of MRI and DXA. While ultrasound provides distance measurements of back fat only, tendencies for abdominal fat compartment volumes can be indicated due to the moderately strong relationship observed between back fat thickness and abdominal adipose tissues. Furthermore, our findings enhance the understanding of the intrinsic and extrinsic factors influencing adipose tissue dynamics and body composition and may contribute to the improvement of pig breeding programs and economic aspects of livestock management, as well as to obesity research relevant to both humans and animals.

VII. ZUSAMMENFASSUNG

Phänotypisierung des viszeralen und subkutanen Fettgewebes bei Schweinen mittels Magnetresonanztomographie (MRT) und Dualenergie-Röntgenabsorptiometrie (DXA)

In den letzten dreißig Jahren hat der weltweite Anstieg von Adipositasraten beim Menschen zu enormen gesundheitlichen und wirtschaftlichen Herausforderungen geführt. Fettleibigkeit entsteht durch ein komplexes Zusammenspiel genetischer, lebensstil- und ernährungsbedingter Faktoren. Besonders kritisch ist dabei die viszerale Adipositas, welche sich durch eine übermäßige Fettansammlung um die inneren Organe auszeichnet, da sie eng mit Stoffwechselstörungen gekoppelt ist. Das Schwein dient infolge seiner anatomischen, physiologischen und genetischen Ähnlichkeit mit dem Menschen als wertvolles Modell für die Erforschung der menschlichen Fettleibigkeit. Ziel dieser Doktorarbeit ist es, die Dualenergie-Röntgenabsorptiometrie (DXA) als nicht-invasive und schnelle Methode zur Quantifizierung des viszeralen und subkutanen Fettgewebes (VAT und SAT) und anderer Parameter der Körperzusammensetzung bei Schweinen im Vergleich zur Magnetresonanztomographie (MRT) zu evaluieren, sowie Ultrasonographie als weitere nicht-invasive Methode zur Messung der Rückenfettdicke zu bewerten. Durch die Phänotypisierung einer heterogenen Schweinepopulation befasst sich diese Studie außerdem mit intrinsischen Einflüssen wie Geschlecht und Genotyp sowie mit extrinsischen Faktoren wie Umgebungstemperatur und Futteraufnahme, welche die Fettverteilung und die Körperzusammensetzung beeinflussen.

In dieser Studie wurden 138 multi-hybrid gekreuzte Schweine zweiter Filialgeneration (MHF2) aus den Rassen Piétrain, Duroc, Deutsche Landrasse und Deutsches Edelschwein mittels MRT, DXA und Ultraschall untersucht. Alle Tiere wurden hierfür unter identischen Bedingungen aufgezogen und gehalten. Das Durchschnittsalter zum Zeitpunkt der Untersuchung betrug 147 Tage. Die Untersuchungen wurden aufgrund unterschiedlicher Geburtsdaten über verschiedene Jahreszeiten und Jahre hinweg durchgeführt. Die Futteraufnahme wurde für alle Tiere während der Mastperiode vor dem

Untersuchungsscan aufgezeichnet. Zur Quantifizierung von VAT- und SAT-Volumen wurden für die Fokusgruppe von 67 Tieren im Bereich zwischen des letzten Brustwirbels und dem Beckenkamm MRT-Querschnitte der Bauchregion manuell ausgewertet und anschließend mittels der Software 3D-Doctor© (Able Software Corp.) in 3D-Modelle umgewandelt. Ganzkörper-DXA-Scans wurden mit der GE Lunar *i*DXA CoreScan™-Software analysiert, die das viszerale Fett innerhalb des identisch festgelegten Analysebereichs automatisch berechnet. Dies erfolgt, indem das subkutane Fett mithilfe eines spezifischen geometrischen Algorithmus ermittelt und anschließend vom gesamten abdominalen Fettgewebe (TAT) subtrahiert wird. Weitere Parameter der Körperzusammensetzung, darunter Fettmasse, Magermasse, Knochenmineralgehalt und Knochenmineraldichte, wurden vom DXA automatisiert ausgewertet. Darüber hinaus wurden Ultraschallmessungen der Rückenfettdicke durchgeführt.

Der Methodenvergleich unter Verwendung linearer Regressionsmodelle ergab eine moderat starke Beziehung zwischen MRT- und DXA-Werten für VAT-Volumen (R^2 = 0,49), sowie eine starke Beziehung für TAT-Werte (R^2 = 0,79). Im Gegensatz dazu war die Beziehung beider SAT-Volumen schwach (R^2 = 0,017). Die MRT-Daten verdeutlichten, dass SAT mit zunehmendem Gesamtabdominalfett (TAT) stärker anstiegt (Regressionskoeffizient = +0,67, R^2 = 0,93) im Vergleich zu VAT (Regressionskoeffizient = +0,33, R^2 = 0,76). Die geschätzten DXA-Werte zeigten hingegen einen stärkeren Anstieg von VAT (Regressionskoeffizient = +0,98, R^2 = 0,96) im Vergleich zu SAT (Regressionskoeffizient = +0,019, p = 0,489). Darüber hinaus ergab die Bland-Altman-Analyse, dass DXA, im Vergleich zum MRT, VAT systematisch über- (Mittelwert der Differenzen = 1218 cm^3) und SAT unterschätzte (Mittelwert der Differenzen = 1384 cm^3), insbesondere bei höheren Fettgehalten. Im Gegensatz dazu wies TAT eine stärkere Übereinstimmung mit einer geringeren Abweichung von lediglich 166 cm^3 auf. Darüber hinaus ergab die Ultraschalluntersuchung eine mittelstarke Beziehung zwischen Rückenfettdicke und sowohl MRT-SAT (R^2 = 0,42) als auch MRT-VAT (R^2 = 0,39).

Zur Analyse der Effekte auf den Phänotypen wurden sowohl intrinsische als auch extrinsische Faktoren mittels Varianzanalyse untersucht. Während das

Geschlecht in unserer Studie nur geringe Auswirkungen auf Körperzusammensetzung und Fettverteilung zeigte, hatten saisonale Unterschiede einen signifikanten Einfluss auf diese Merkmale. Tiere, welche im Winter gemästet und gescannt wurden, wiesen insgesamt höhere Fetteinlagerungen auf als jene, die im Sommer untersucht wurden. Zudem beeinflussten sowohl das Geschlecht als auch die Jahreszeit die Futteraufnahme. Kastrierte Eber fraßen im Durchschnitt mehr (ca. 1814 g/Tag) als Sauen (ca. 1647 g/Tag) und im Winter wurde generell eine höhere Futteraufnahme festgestellt als im Sommer. Durch die Anwendung eines gezielten Kreuzungsschemas entstand in unserer Studie eine große Vielfalt an Phänotypen, bei welcher der Genotyp einen signifikanten Einfluss auf die meisten Variablen hatte.

Zusammenfassend zeigen die Ergebnisse dieser Doktorarbeit, dass die GE Lunar *i*DXA CoreScan™-Software nicht geeignet ist, um das subkutane Fett (SAT) bei Schweinen präzise zu quantifizieren, da SAT unterschätzt wird und infolgedessen es zu einer Überschätzung des viszeralen Fetts (VAT) kommt. Für die Messung des totalen abdominalen Fettgewebes (TAT) ergab unsere Analyse eine mäßige bis gute Übereinstimmung zwischen den beiden Methoden MRT und DXA. Obwohl Ultraschall lediglich Distanzmessungen des Rückenfetts erlaubt, lassen sich aufgrund der moderaten Beziehung zwischen Rückenfettdicke und abdominalem Fettgewebe dennoch Tendenzen für deren Volumen ableiten. Darüber hinaus führen unsere Ergebnisse zum besseren Verständnis von intrinsischen und extrinsischen Faktoren, welche die Dynamik von Fettgewebe und Körperzusammensetzung beeinflussen, und können zur Optimierung von Schweinezuchtprogrammen und ökonomischen Aspekten der Nutztierhaltung, sowie zur Adipositasforschung beitragen, die für Mensch und Tier von Bedeutung ist.

VIII. REFERENCES

Abildgaard, J., Pedersen, A.T., Green, C.J., Harder-Lauridsen, N.M., Solomon, T.P., Thomsen, C., Juul, A., Pedersen, M., Pedersen, J.T., Mortensen, O.H., Pilegaard, H., Pedersen, B.K., Lindegaard, B., 2013. Menopause is associated with decreased whole body fat oxidation during exercise. American journal of physiology. Endocrinology and metabolism 304, E1227-36.

Aigner, B., Renner, S., Kessler, B., Klymiuk, N., Kurome, M., Wünsch, A., Wolf, E., 2010. Transgenic pigs as models for translational biomedical research. Journal of Molecular Medicine 88, 653–664.

Alalwan, T.A., 2020. Phenotypes of Sarcopenic Obesity: Exploring the Effects on Peri-Muscular Fat, the Obesity Paradox, Hormone-Related Responses and the Clinical Implications. Geriatrics 5, 8.

Albert, F., Kovács-Weber, M., Bodnár, Á., Pajor, F., Egerszegi, I., 2024. Seasonal Effects on the Performance of Finishing Pigs' Carcass and Meat Quality in Indoor Environments. Animals 14, 259.

Allen, C.E., 1976. Cellularity of adipose tissue in meat animals. Federation proceedings 35, 2302–2307.

Anderson, D.B., Kauffman, R.G., 1973. Cellular and enzymatic changes in porcine adipose tissue during growth. Journal of lipid research 14, 160–168.

Arens, D., Sigrist, I., Alini, M., Schawalder, P., Schneider, E., Egermann, M., 2007. Seasonal changes in bone metabolism in sheep. The Veterinary Journal 174, 585–591.

Asano, T., Kubota, N., Koizumi, N., Itani, K., Mitake, T., Yuhashi, K., Liao, H., Mitsuishi, M., Takeishi, S., Takahashi, T., Ohnishi, S., Sasaki, S., Sakuma, I., Kadowaki, T., 2017. Novel and Simple Ultrasonographic Methods for Estimating the Abdominal Visceral Fat Area. International journal of endocrinology 2017, 8796069.

Averós, X., Brossard, L., Dourmad, J.Y., Greef, K.H. de, Edwards, S.A., Meunier-Salaün, M.C., 2012. Meta-analysis on the effects of the physical environment, animal traits, feeder and feed characteristics on the feeding behaviour and performance of growing-finishing pigs. Animal. 6, 1275–1289.

Babinszky, L., Halas, V., 2009. Innovative swine nutrition: some present and potential applications of latest scientific findings for safe pork production. Italian Journal of Animal Science 8, 7–20.

Barnett, J.L., Hemsworth, P.H., Cronin, G.M., Jongman, E.C., Hutson, G.D., 2001. A review of the welfare issues for sows and piglets in relation to housing. Australian Journal of Agricultural Research 52, 1–28.

Barnkob, L.L., Argyraki, A., Petersen, P.M., Jakobsen, J., 2016. Investigation of the effect of UV-LED exposure conditions on the production of vitamin D in pig skin. Food chemistry 212, 386–391.

Barton-Gade, P.A., 1987. Meat and fat quality in boars, castrates and gilts. Livestock Production Science 16, 187–196.

Baumgard, L.H., Rhoads, R.P., 2013. Effects of heat stress on postabsorptive metabolism and energetics. Annual review of animal biosciences 1, 311–337.

Bazzocchi, A., Ponti, F., Albisinni, U., Battista, G., Guglielmi, G., 2016. DXA: Technical aspects and application. European Journal of Radiology 85, 1481–1492.

Bee, G., Gebert, S., Messikommer, R., 2002. Effect of dietary energy supply and fat source on the fatty acid pattern of adipose and lean tissues and lipogenesis in the pig. Journal of Animal Science 80, 1564–1574.

Bellinger, D.A., Merricks, E.P., Nichols, T.C., 2006. Swine models of type 2 diabetes mellitus: insulin resistance, glucose tolerance, and cardiovascular complications. ILAR Journal 47, 243–258.

Bernau, M., Kremer, P.V., Lauterbach, E., Tholen, E., Petersen, B., Pappenberger, E., Scholz, A.M., 2015. Evaluation of carcass composition of intact boars using linear measurements from performance testing, dissection,

dual energy X-ray absorptiometry (DXA) and magnetic resonance imaging (MRI). Meat science 104, 58–66.

Bernau, M., Schrott, J., Schwanitz, S., Kreuzer, L.S., Scholz, A.M., 2020. "Sex" and body region effects on bone mineralization in male pigs. Archives Animal Breeding 63, 103–111.

Bjørnvad, C.R., Nielsen, M.E., Hansen, S.E.M., Nielsen, D.H., 2017. The effect of position on the precision of dual-energy X-ray absorptiometry and correlation with body condition score in dogs and cats. Journal of Nutritional Science 6, e20.

Blüher, M., 2014. Are metabolically healthy obese individuals really healthy? European Journal of Endocrinology 171, R209-19.

Bollen, P.J.A., Madsen, L.W., Meyer, O., Ritskes-Hoitinga, J., 2005. Growth differences of male and female Göttingen minipigs during ad libitum feeding: a pilot study. Laboratory animals 39, 80–93.

Bonneau, M., Weiler, U., 2019. Pros and Cons of Alternatives to Piglet Castration: Welfare, Boar Taint, and Other Meat Quality Traits. Animals 9, 884.

Borga, M., Thomas, E.L., Romu, T., Rosander, J., Fitzpatrick, J., Dahlqvist Leinhard, O., Bell, J.D., 2015. Validation of a fast method for quantification of intra-abdominal and subcutaneous adipose tissue for large-scale human studies. NMR in biomedicine 28, 1747–1753.

Böttinger, M., 2006. Untersuchung des Einflusses verschiedener Produktionssysteme auf das Wachstum beim Schwein unter Verwendung der Dualenergie-Röntgenabsorptiometrie zur Messung von Fett, Magerweichgewebe und Knochenmineralansatz.

Brown-Brandl, T.M., Eigenberg, R.A., Purswell, J.L., 2013. Using thermal imaging as a method of investigating thermal thresholds in finishing pigs. Biosystems Engineering 114, 327–333.

Busk, H., Olsen, E.V., Brøndum, J., 1999. Determination of lean meat in pig carcasses with the Autofom classification system. Meat science 52, 307–314.

Cancello, R., Zulian, A., Gentilini, D., Maestrini, S., Della Barba, A., Invitti, C., Corà, D., Caselle, M., Liuzzi, A., Di Blasio, A.M., 2013. Molecular and morphologic characterization of superficial- and deep-subcutaneous adipose tissue subdivisions in human obesity. Obesity 21, 2562–2570.

Candek-Potokar, M., Monin, G., Zlender, B., 2002. Pork quality, processing, and sensory characteristics of dry-cured hams as influenced by Duroc crossing and sex. Journal of Animal Science 80, 988–996.

Čandek-Potokar, M., Lebret, B., Gispert, M., Font-i-Furnols, M., 2024. Challenges and future perspectives for the European grading of pig carcasses - A quality view. Meat science 208, 109390.

Carabús, A., Sainz, R.D., Oltjen, J.W., Gispert, M., Font-I-Furnols, M., 2017. Growth of total fat and lean and of primal cuts is affected by the sex type. Animal 11, 1321–1329.

Carver, T.E., Christou, N.V., Andersen, R.E., 2013. In vivo precision of the GE iDXA for the assessment of total body composition and fat distribution in severely obese patients. Obesity 21, 1367–1369.

Chau, Y.-Y., Bandiera, R., Serrels, A., Martínez-Estrada, O.M., Qing, W., Lee, M., Slight, J., Thornburn, A., Berry, R., McHaffie, S., Stimson, R.H., Walker, B.R., Chapuli, R.M., Schedl, A., Hastie, N., 2014. Visceral and subcutaneous fat have different origins and evidence supports a mesothelial source. Nature cell biology 16, 367–375.

Choi, H.S., Kim, K.J., Kim, K.M., Hur, N.W., Rhee, Y., Han, D.S., Lee, E.J., Lim, S.-K., 2010. Relationship between visceral adiposity and bone mineral density in Korean adults. Calcified Tissue International 87, 218–225.

Christoffersen, B., Golozoubova, V., Pacini, G., Svendsen, O., Raun, K., 2013. The young Göttingen minipig as a model of childhood and adolescent obesity: influence of diet and gender. Obesity 21, 149–158.

Christoffersen, B.O., Grand, N., Golozoubova, V., Svendsen, O., Raun, K., 2007. Gender-associated differences in metabolic syndrome-related parameters in Göttingen minipigs. Comparative medicine 57, 493–504.

Chrousos, G.P., 2000. The role of stress and the hypothalamic-pituitary-adrenal axis in the pathogenesis of the metabolic syndrome: neuro-endocrine and target tissue-related causes. International journal of obesity and related metabolic disorders 24 (Suppl 2), S50-S55.

Cinti, S., 2000. Anatomy of the adipose organ. Eat Weight Disord 5, 132–142.

Claus, R., Weiler, U., 1994. Endocrine regulation of growth and metabolism in the pig: a review. Livestock Production Science 37, 245–260.

Čobanović, N., Stajković, S., Blagojević, B., Betić, N., Dimitrijević, M., Vasilev, D., Karabasil, N., 2020. The effects of season on health, welfare, and carcass and meat quality of slaughter pigs. International journal of biometeorology 64, 1899–1909.

Cole, R., Hespel, A.-M., 2020. Principles of Computed Tomography and Magnetic Resonance Imaging. In: Holland, M., Hudson, J. (Eds.): Feline Diagnostic Imaging. Wiley, pp. 13–26.

Cross, A.J., Brown-Brandl, T.M., Keel, B.N., Cassady, J.P., Rohrer, G.A., 2020. Feeding behavior of grow-finish swine and the impacts of heat stress. Translational animal science 4, 986-992.

Cruzen, S.M., Boddicker, R.L., Graves, K.L., Johnson, T.P., Arkfeld, E.K., Baumgard, L.H., Ross, J.W., Safranski, T.J., Lucy, M.C., Lonergan, S.M., 2015. Carcass composition of market weight pigs subjected to heat stress in utero and during finishing. Journal of animal science 93, 2587–2596.

d'Anjou, M.-A., 2018. Principles of Computed Tomography and Magnetic Resonance Imaging. In: Textbook of Veterinary Diagnostic Radiology. Elsevier, pp. 71–95.

Delahunty, K.M., Horton, L.G., Coombs, H.F., Shultz, K.L., Svenson, K.L., Marion, M.A., Holick, M.F., Beamer, W.G., Rosen, C.J., 2009. Gender- and compartment-specific bone loss in C57BL/6J mice: correlation to season? Journal of Clinical Densitometry 12, 89–94.

Després, J.-P., Lemieux, I., 2006. Abdominal obesity and metabolic syndrome. Nature 444, 881–887.

Dias, K.A., Ramos, J.S., Wallen, M.P., Davies, P.S.W., Cain, P.A., Leong, G.M., Ingul, C.B., Coombes, J.S., Keating, S.E., 2019. Accuracy of Longitudinal Assessment of Visceral Adipose Tissue by Dual-Energy X-Ray Absorptiometry in Children with Obesity. Journal of obesity 2019, 2193723.

Ding, R., Zhuang, Z., Qiu, Y., Ruan, D., Wu, J., Ye, J., Cao, L., Zhou, S., Zheng, E., Huang, W., Wu, Z., Yang, J., 2022. Identify known and novel candidate genes associated with backfat thickness in Duroc pigs by large-scale genome-wide association analysis. Journal of animal science 100, skac012.

Dölle, T., 2019. Untersuchungen zu Klauengesundheit, Knorpelvolumina und Körperzusammensetzung beim Mastschwein in verschiedenen Haltungssystemen unter Verwendung von Magnetresonanz-Tomographie und Dualenergie-Röntgenabsorptiometrie. Tierärztliche Fakultät, Ludwig-Maximilians-Universität München.

Dordevic, A.L., Bonham, M., Ghasem-Zadeh, A., Evans, A., Barber, E., Day, K., Kwok, A., Truby, H., 2018. Reliability of Compartmental Body Composition Measures in Weight-Stable Adults Using GE iDXA: Implications for Research and Practice. Nutrients 10, 1484.

Dorleku, J.B., Wormsbecher, L., Christensen, M., Campbell, C.P., Mandell, I.B., Bohrer, B.M., 2023. Comparison of an advanced automated ultrasonic scanner (AutoFom III) and a handheld optical probe (Destron PG-100) to determine lean yield in pork carcasses. Journal of Animal Science 101, skad058.

Duarte, J.L.G., Cantet, R.J.C., Rubio, Y.L.B., Bates, R.O., Ernst, C.W., Raney, N.E., Rogberg-Muñoz, A., Steibel, J.P., 2016. Refining genomewide association for growth and fat deposition traits in an F pig population. Journal of Animal Science 94, 1387–1397.

Dunshea, D. (Ed.), 2003. A REVIEW - FAT DEPOSITION AND METABOLISM IN THE PIG. Conference: Australasian Pig Science Association At: Fremantle.

Fang, H., Berg, E., Cheng, X., Shen, W., 2018. How to best assess abdominal obesity. Current opinion in clinical nutrition and metabolic care 21, 360–365.

Fausnacht, D.W., Kroscher, K.A., McMillan, R.P., Martello, L.S., Baumgard, L.H., Selsby, J.T., Hulver, M.W., Rhoads, R.P., 2021. Heat Stress Reduces Metabolic Rate While Increasing Respiratory Exchange Ratio in Growing Pigs. Animals 11, 215.

Fontanesi, L., Schiavo, G., Galimberti, G., Calò, D.G., Scotti, E., Martelli, P.L., Buttazzoni, L., Casadio, R., Russo, V., 2012. A genome wide association study for backfat thickness in Italian Large White pigs highlights new regions affecting fat deposition including neuronal genes. BMC Genomics 13, 583.

Fornós, M., Sanz-Fernández, S., Jiménez-Moreno, E., Carrión, D., Gasa, J., Rodríguez-Estévez, V., 2022. The Feeding Behaviour Habits of Growing-Finishing Pigs and Its Effects on Growth Performance and Carcass Quality: A Review. Animals 12, 1128.

Fortin, A., 1986. Development of backfat and individual fat layers in the pig and its relationship with carcass lean. Meat science 18, 255–270.

Fox, C.S., Massaro, J.M., Hoffmann, U., Pou, K.M., Maurovich-Horvat, P., Liu, C.-Y., Vasan, R.S., Murabito, J.M., Meigs, J.B., Cupples, L.A., D'Agostino, R.B., O'Donnell, C.J., 2007. Abdominal visceral and subcutaneous adipose tissue compartments: association with metabolic risk factors in the Framingham Heart Study. Circulation 116, 39–48.

Fu, X., Ma, X., Lu, H., He, W., Wang, Z., Zhu, S., 2011. Associations of fat mass and fat distribution with bone mineral density in pre- and postmenopausal Chinese women. Osteoporosis International 22, 113–119.

GE Healthcare, 2017. Lunar Technology Advantages, https://www.gehealthcare.de/-/jssmedia/feature/gehc/products/lunar-idxa/lunartechnology.pdf. Accessed 20 September 2024.

GE Healthcare, 2024. X-ray Bone Densitometer with enCORE v17 software - User Manual, https://www.gehealthcare.com/support/manuals?search=eyJzZWFyY2hUZXJtIjoiTFU0MzYxNkVOX3ZfMTdTUDUiLCJsYW5ndWFnZU5hbWUiOiJFbmdsaXNoIChFTikifQ%3D%3D&srsltid=AfmBOorJ2T_4FIgIM-kN-pJgDPB7OB-MbkEGJEqZzVYt9YMN3y0-iiIC. Accessed 17 March 2025.

General Electric Company, 2012. Method and system to estimate visceral adipose tissue by restricting subtraction of subcutaneous adipose tissue to coelom projection region, https://patents.google.com/patent/WO2012092533A1/en. Accessed 24 August 2024.

Gilbert, H., Billon, Y., Brossard, L., Faure, J., Gatellier, P., Gondret, F., Labussière, E., Lebret, B., Lefaucheur, L., Le Floch, N., Louveau, I., Merlot, E., Meunier-Salaün, M.-C., Montagne, L., Mormede, P., Renaudeau, D., Riquet, J., Rogel-Gaillard, C., van Milgen, J., Vincent, A., Noblet, J., 2017. Review: divergent selection for residual feed intake in the growing pig. Animal 11, 1427–1439.

Gispert, M., Font i Furnols, M., Gil, M., Velarde, A., Diestre, A., Carrión, D., Sosnicki, A.A., Plastow, G.S., 2007. Relationships between carcass quality parameters and genetic types. Meat science 77, 397–404.

Gkastaris, K., Goulis, D.G., Potoupnis, M., Anastasilakis, A.D., Kapetanos, G., 2020. Obesity, osteoporosis and bone metabolism. Journal of musculoskeletal & neuronal interactions 20, 372–381.

Glüer, C.-C., 2017. 30years of DXA technology innovations. Bone 104, 7–12.

Godyń, D., Nowicki, J., Herbut, P., 2019. Effects of Environmental Enrichment on Pig Welfare-A Review. Animals 9, 383.

González, A., Ayuso, D., Peña, F., Martínez, A.L., Izquierdo, M., 2017. Effects of gender and diet on back fat and loin area ultrasound measurements during the growth and final stage of fattening in Iberian pigs. Archives Animal Breeding 60, 213–223.

Gonzalez-Rivas, P.A., Chauhan, S.S., Ha, M., Fegan, N., Dunshea, F.R., Warner, R.D., 2020. Effects of heat stress on animal physiology, metabolism, and meat quality: A review. Meat science 162, 108025.

Hausman, G.J., Basu, U., Wei, S., Hausman, D.B., Dodson, M.V., 2014. Preadipocyte and adipose tissue differentiation in meat animals: influence of species and anatomical location. Annual review of animal biosciences 2, 323–351.

Henriksen, H.B., Alavi, D.H., Blomhoff, R., 2021. Precision of Lunar Dual-energy X-ray Absorptiometry (iDXA) in measuring body composition among colorectal cancer patients and healthy subjects. Clinical Nutrition ESPEN 44, 316–323.

Hilton, C., Vasan, S.K., Neville, M.J., Christodoulides, C., Karpe, F., 2022. The associations between body fat distribution and bone mineral density in the Oxford Biobank: a cross sectional study. Expert Review of Endocrinology & Metabolism 17, 75–81.

Hind, K., Oldroyd, B., Truscott, J.G., 2011. In vivo precision of the GE Lunar iDXA densitometer for the measurement of total body composition and fat distribution in adults. European Journal of Clinical Nutrition 65, 140–142.

Hinrichs, A., Kessler, B., Kurome, M., Blutke, A., Kemter, E., Bernau, M., Scholz, A.M., Rathkolb, B., Renner, S., Bultmann, S., Leonhardt, H., Angelis, M.H. de, Nagashima, H., Hoeflich, A., Blum, W.F., Bidlingmaier, M., Wanke, R., Dahlhoff, M., Wolf, E., 2018. Growth hormone receptor-deficient pigs resemble the pathophysiology of human Laron syndrome and reveal altered activation of signaling cascades in the liver. Molecular metabolism 11, 113–128.

Holinger, M., Früh, B., Stoll, P., Pedan, V., Kreuzer, M., Bérard, J., Hillmann, E., 2018. Long-term effects of castration, chronic intermittent social stress, provision of grass silage and their interactions on performance and meat and adipose tissue properties in growing-finishing pigs. Meat science 145, 40–50.

Höreth, R., 2013. AutoFom-I und AutoFom-III im Praxisvergleich. Mitteilungsblatt Fleischforschung Kulmbach 52, 221–231.

Hunter, T.E., Suster, D., Dunshea, F.R., Cummins, L.J., Egan, A.R., Leury, B.J., 2011. Dual energy X-ray absorptiometry (DXA) can be used to predict live animal and whole carcass composition of sheep. Small Ruminant Research 100, 143–152.

Ibrahim, M.M., 2010. Subcutaneous and visceral adipose tissue: structural and functional differences. Obesity reviews 11, 11–18.

Jeusette, I., Greco, D., Aquino, F., Detilleux, J., Peterson, M., Romano, V., Torre, C., 2010. Effect of breed on body composition and comparison between various methods to estimate body composition in dogs. Research in veterinary science 88, 227–232.

Jin, L., Tang, Q., Hu, S., Chen, Z., Zhou, X., Zeng, B., Wang, Y., He, M., Li, Y., Gui, L., Shen, L., Long, K., Ma, J., Wang, X., Chen, Z., Jiang, Y., Tang, G., Zhu, L., Liu, F., Zhang, B., Huang, Z., Li, G., Li, D., Gladyshev, V.N., Yin, J., Gu, Y., Li, X., Li, M., 2021. A pig BodyMap transcriptome reveals diverse tissue physiologies and evolutionary dynamics of transcription. Nature Communications 12, 3715.

Jin, L., Wang, D., Zhang, J., Liu, P., Wang, Y., Lin, Y., Liu, C., Han, Z., Long, K., Li, D., Jiang, Y., Li, G., Zhang, Y., Bai, J., Li, X., Li, J., Lu, L., Kong, F., Wang, X., Li, H., Huang, Z., Ma, J., Fan, X., Shen, L., Zhu, L., Jiang, Y., Tang, G., Feng, B., Zeng, B., Ge, L., Li, X., Tang, Q., Zhang, Z., Li, M., 2023. Dynamic chromatin architecture of the porcine adipose tissues with weight gain and loss. Nature Communications 14, 3457

JinLiang Xue, Gary D. Dial, James E. Pettigrew, 1997. Performance, carcass, and meat quality advantages of boars over barrows: A literature review. Journal of Swine Health and Production 5.

Johnson, J.S., Sanz Fernandez, M.V., Gutierrez, N.A., Patience, J.F., Ross, J.W., Gabler, N.K., Lucy, M.C., Safranski, T.J., Rhoads, R.P., Baumgard, L.H., 2015. Effects of in utero heat stress on postnatal body composition in pigs: I. Growing phase. Journal of animal science 93, 71–81.

Johnson, M., Waller J., 2018. Simple Methods for Repeatability and Comparability: Bland-Altman Plots, Bias, and Measurement Error, https://support.sas.com/resources/papers/proceedings18/1815-2018.pdf. Accessed 16.04.24.

Juska, R., Juskiene, V., Leikus, R., 2013. The influence of a free-range housing system on pig growth, carcass composition and meat quality. Journal of Applied Animal Research 41, 39–47.

Kamińska, M.S., Schneider-Matyka, D., Rachubińska, K., Panczyk, M., Grochans, E., Cybulska, A.M., 2023. Menopause Predisposes Women to Increased Risk of Cardiovascular Disease. Journal of clinical medicine 12, 7058.

Kamphues, J., Dobenecker, B. (Eds.), 2014. Supplemente zur Tierernahrung. Für Studium und Praxis. M.& H. Schaper, Hannover, Germany.

Kappes, R., Schneider, V., Schweizer, H., Nüske, S., Knob, D.A., Thaler Neto, A., Scholz, A.M., 2024. Effect of β-casein A1 or A2 milk on body composition, milk intake, and growth in Holstein, Simmental, and crossbred dairy calves of both sexes. Journal of dairy science 107, 4033–4044.

Kasper, C., Schlegel, P., Ruiz-Ascacibar, I., Stoll, P., Bee, G., 2021. Accuracy of predicting chemical body composition of growing pigs using dual-energy X-ray absorptiometry. Animal 15, 100307.

Kaul, S., Rothney, M.P., Peters, D.M., Wacker, W.K., Davis, C.E., Shapiro, M.D., Ergun, D.L., 2012. Dual-energy X-ray absorptiometry for quantification of visceral fat. Obesity (Silver Spring, Md.) 20, 1313–1318.

Kim, S.-H., Chung, J.-H., Song, S.-W., Jung, W.S., Lee, Y.-A., Kim, H.-N., 2016. Relationship between deep subcutaneous abdominal adipose tissue and metabolic syndrome: a case control study. Diabetology & metabolic syndrome 8, 10.

Kipper, M., Marcoux, M., Andretta, I., Pomar, C., 2019. Assessing the accuracy of measurements obtained by dual-energy X-ray absorptiometry on pig carcasses and primal cuts. Meat science 148, 79–87.

Knapp, K.M., Welsman, J.R., Hopkins, S.J., Shallcross, A., Fogelman, I., Blake, G.M., 2015. Obesity increases precision errors in total body dual-energy x-ray absorptiometry measurements. Journal of Clinical Densitometry 18, 209–216.

Koch, T., Lakshmanan, S., Brand, S., Wicke, M., Raum, K., Mörlein, D., 2011. Ultrasound velocity and attenuation of porcine soft tissues with respect to structure and composition: I. Muscle. Meat science 88, 51–58.

Kogelman, L.J.A., Kadarmideen, H.N., Mark, T., Karlskov-Mortensen, P., Bruun, C.S., Cirera, S., Jacobsen, M.J., Jørgensen, C.B., Fredholm, M., 2013. An f2 pig resource population as a model for genetic studies of obesity and obesity-related diseases in humans: design and genetic parameters. Frontiers in genetics 4, 29.

Kolstad, K., Jopson, N.B., Vangen, O., 1996. Breed and sex differences in fat distribution and mobilization in growing pigs fed at maintenance. Livestock Production Science 47, 33–41.

Kouba, M., Bonneau, M., 2009. Compared development of intermuscular and subcutaneous fat in carcass and primal cuts of growing pigs from 30 to 140kg body weight. Meat science 81, 270–274.

Kracht, C.L., Katzmarzyk, P.T., Staiano, A.E., 2021. Comparison of abdominal visceral adipose tissue measurements in adolescents between magnetic resonance imaging and dual-energy X-ray absorptiometry. International Journal of Obesity 45, 104–108.

Kullberg, J., Brandberg, J., Angelhed, J.-E., Frimmel, H., Bergelin, E., Strid, L., Ahlström, H., Johansson, L., Lönn, L., 2009. Whole-body adipose tissue analysis: comparison of MRI, CT and dual energy X-ray absorptiometry. The British journal of radiology 82, 123–130.

Laskey, M.A., 1996. Dual-energy X-ray absorptiometry and body composition. Nutrition 12, 45–51.

Lavery, A., Lawlor, P.G., Magowan, E., Miller, H.M., O'Driscoll, K., Berry, D.P., 2019. An association analysis of sow parity, live-weight and back-fat depth as indicators of sow productivity. Animal 13, 622–630.

Lebret, B., Meunier-Salaün, M.C., Foury, A., Mormède, P., Dransfield, E., Dourmad, J.Y., 2006. Influence of rearing conditions on performance, behavioral, and physiological responses of pigs to preslaughter handling, carcass traits, and meat quality. Journal of animal science 84, 2436–2447.

Lee, K.-T., Byun, M.-J., Kang, K.-S., Park, E.-W., Lee, S.-H., Cho, S., Kim, H., Kim, K.-W., Lee, T., Park, J.-E., Park, W., Shin, D., Park, H.-S., Jeon, J.-T., Choi, B.-H., Jang, G.-W., Choi, S.-H., Kim, D.-W., Lim, D., Park, H.-S., Park, M.-R., Ott, J., Schook, L.B., Kim, T.-H., Kim, H., 2011. Neuronal genes for subcutaneous fat thickness in human and pig are identified by local genomic sequencing and combined SNP association study. PLoS ONE 6, e16356.

Lemieux, S., Prud'homme, D., Bouchard, C., Tremblay, A., Després, J.P., 1993. Sex differences in the relation of visceral adipose tissue accumulation to total body fatness. The American journal of clinical nutrition 58, 463–467.

Leymaster, K.A., Mersmann, H.J., 1991. Effect of limited feed intake on growth of subcutaneous adipose tissue layers and on carcass composition in swine. Journal of animal science 69, 2837–2843.

Li, Q., Patience, J.F., 2017. Factors involved in the regulation of feed and energy intake of pigs. Animal Feed Science and Technology 233, 22–33.

Lim, U., Monroe, K.R., Buchthal, S., Fan, B., Cheng, I., Kristal, B.S., Lampe, J.W., Hullar, M.A., Franke, A.A., Stram, D.O., Wilkens, L.R., Shepherd, J., Ernst, T., Le Marchand, L., 2019. Propensity for Intra-abdominal and Hepatic Adiposity Varies Among Ethnic Groups. Gastroenterology 156, 966-975.E10.

Lin, Y., Zhong, X., Lu, D., Yao, W., Zhou, J., Wu, R., Feng, F., 2023. Association of visceral and subcutaneous fat with bone mineral density in US adults: a cross-sectional study. Scientific Reports 13, 10682.

Liu, F., Ford, E.M., Morrison, R.S., Brewster, C.J., Henman, D.J., Smits, R.J., Zhao, W., Cottrell, J.J., Leury, B.J., Dunshea, F.R., Bell, A.W., 2020. The Greater Proportion of Born-Light Progeny from Sows Mated in Summer Contributes to Increased Carcass Fatness Observed in Spring. Animals 10, 2080.

Liu, F., Zhao, W., Le, H.H., Cottrell, J.J., Green, M.P., Leury, B.J., Dunshea, F.R., Bell, A.W., 2022. Review: What have we learned about the effects of heat stress on the pig industry? Animal 16 Suppl 2, 100349.

Lombardi, G., Ziemann, E., Banfi, G., 2019. Physical Activity and Bone Health: What Is the Role of Immune System? A Narrative Review of the Third Way. Frontiers in endocrinology 10, 60.

Lösel, D., Kremer, P., Albrecht, E., Scholz, A.M., 2010. Comparison of a GE Lunar DPX-IQ and a Norland XR-26 dual energy X-ray absorptiometry scanner for body composition measurements in pigs – in vivo. Archives Animal Breeding 53, 162–175.

Lucia Rolfe, E. de, Sleigh, A., Finucane, F.M., Brage, S., Stolk, R.P., Cooper, C., Sharp, S.J., Wareham, N.J., Ong, K.K., 2010. Ultrasound measurements of visceral and subcutaneous abdominal thickness to predict abdominal adiposity among older men and women. Obesity 18, 625–631.

Lucy, M.C., Safranski, T.J., 2017. Heat stress in pregnant sows: Thermal responses and subsequent performance of sows and their offspring. Molecular reproduction and development 84, 946–956.

M. Scholz, A., Kušec, G., D. Mitchell, A., Baulain, U., 2024. Tracing the Inside of Pigs Non-Invasively: Recent Developments. In: Kušec, G. (Ed.): Tracing the Domestic Pig. IntechOpen.

Ma, X., Wang, L., Shi, Z., Chen, W., Yang, X., Hu, Y., Zheng, C., Jiang, Z., 2019. Mechanism of continuous high temperature affecting growth performance, meat quality, and muscle biochemical properties of finishing pigs. Genes & nutrition 14, 23.

Machann, J., Horstmann, A., Born, M., Hesse, S., Hirsch, F.W., 2013. Diagnostic imaging in obesity. Best practice & research. Clinical endocrinology & metabolism 27, 261–277.

Machann, J., Thamer, C., Schnoedt, B., Stefan, N., Stumvoll, M., Haring, H.-U., Claussen, C.D., Fritsche, A., Schick, F., 2005. Age and gender related effects on adipose tissue compartments of subjects with increased risk for type 2 diabetes: a whole body MRI/MRS study. Magma 18, 128–137.

Magowan, E., McCann, M., 2006. A comparison of pig backfat measurements using ultrasonic and optical instruments. Livestock Science 103, 116–123.

Malek, M., Dekkers, J.C., Lee, H.K., Baas, T.J., Rothschild, M.F., 2001. A molecular genome scan analysis to identify chromosomal regions influencing economic traits in the pig. I. Growth and body composition. Mammalian genome 12, 630–636.

Malekar, V.C., Morton, J.D., Hider, R.N., Cruickshank, R.H., Hodge, S., Metcalf, V.J., 2018. Effect of elevated temperature on membrane lipid saturation in Antarctic notothenioid fish. PeerJ 6, e4765.

Marcoux, M., Bernier, J.F., Pomar, C., 2003. Estimation of Canadian and European lean yields and composition of pig carcasses by dual-energy X-ray absorptiometry. Meat science 63, 359–365.

Marwaha, R.K., Garg, M.K., Tandon, N., Mehan, N., Sastry, A., Bhadra, K., 2013. Relationship of body fat and its distribution with bone mineral density in Indian population. Journal of Clinical Densitometry 16, 353–359.

Mayes, J.S., Watson, G.H., 2004. Direct effects of sex steroid hormones on adipose tissues and obesity. Obesity reviews 5, 197–216.

McEvoy, F.J., Strathe, A.B., Madsen, M.T., Svalastoga, E., 2007. Changes in the relative thickness of individual subcutaneous adipose tissue layers in growing pigs. Acta Veterinaria Scandinavica 49, 32.

Mellis, M.G., Oldroyd, B., Hind, K., 2014. In vivo precision of the GE Lunar iDXA for the measurement of visceral adipose tissue in adults: the influence of body mass index. European Journal of Clinical Nutrition 68, 1365–1367.

Meredith-Jones, K., Haszard, J., Stanger, N., Taylor, R., 2018. Precision of DXA-Derived Visceral Fat Measurements in a Large Sample of Adults of Varying Body Size. Obesity 26, 505–512.

Messina, C., Albano, D., Gitto, S., Tofanelli, L., Bazzocchi, A., Ulivieri, F.M., Guglielmi, G., Sconfienza, L.M., 2020. Body composition with dual energy X-ray absorptiometry: from basics to new tools. Quantitative imaging in medicine and surgery 10, 1687–1698.

Meteostat, 2024. Wetterdaten Archiv - Flughafen München. Dezember 2020 - Oktober 2022, f. Accessed 12 February 2024.

Millet, S., Moons, C.P.H., van Oeckel, M.J., Janssens, G.P.J., 2005. Welfare, performance and meat quality of fattening pigs in alternative housing and management systems: a review. Journal of the Science of Food and Agriculture 85, 709–719.

Mitchell, A.D., Scholz, A.M., Wange, P.C., Song, H., 2001. Body composition analysis of the pig by magnetic resonance imaging. Journal of Animal Science 79, 1800–1813.

Mittal, B., 2019. Subcutaneous adipose tissue & visceral adipose tissue. The Indian journal of medical research 149, 571–573.

Mohrmann, M., Roehe, R., Susenbeth, A., Baulain, U., Knap, P.W., Looft, H., Plastow, G.S., Kalm, E., 2006. Association between body composition of growing pigs determined by magnetic resonance imaging, deuterium dilution technique, and chemical analysis. Meat science 72, 518–531.

Monziols, M., Bonneau, M., Davenel, A., Kouba, M., 2007. Comparison of the lipid content and fatty acid composition of intermuscular and subcutaneous adipose tissues in pig carcasses. Meat science 76, 54–60.

Mourot, J., Kouba, M., Peiniau, P., 1995. Comparative study of in vitro lipogenesis in various adipose tissues in the growing domestic pig (Sus domesticus). Comparative Biochemistry and Physiology Part B: Biochemistry and Molecular Biology 111, 379–384.

Müller, S., Polten, S., 2004. Vergleichsuntersuchungen zur Ultraschall-Speckdickenmessung beim Schwein im Rahmen der Eigenleistungsprüfung. Archives Animal Breeding 47, 249–263.

Neeland, I.J., Grundy, S.M., Li, X., Adams-Huet, B., Vega, G.L., 2016. Comparison of visceral fat mass measurement by dual-X-ray absorptiometry and magnetic resonance imaging in a multiethnic cohort: the Dallas Heart Study. Nutrition & diabetes 6, e221.

Neeland, I.J., Ross, R., Després, J.-P., Matsuzawa, Y., Yamashita, S., Shai, I., Seidell, J., Magni, P., Santos, R.D., Arsenault, B., Cuevas, A., Hu, F.B., Griffin, B., Zambon, A., Barter, P., Fruchart, J.-C., Eckel, R.H., 2019. Visceral and ectopic fat, atherosclerosis, and cardiometabolic disease: a position statement. The lancet. Diabetes & endocrinology 7, 715–725.

Nielsen, D.H., McEvoy, F.J., Madsen, M.T., Jensen, J.B., Svalastoga, E., 2007. Relationship between bone strength and dual-energy X-ray absorptiometry measurements in pigs. Journal of animal science 85, 667–672.

Noblet, J., Le Dividich, J., Bikawa, T., 1985. Interaction between energy level in the diet and environmental temperature on the utilization of energy in growing pigs. Journal of Animal Science 61, 452–459.

Nyachoti, C.M., Zijlstra, R.T., Lange, C.F.M. de, Patience, J.F., 2004. Voluntary feed intake in growing-finishing pigs: A review of the main determining factors and potential approaches for accurate predictions. Canadian Journal of Animal Science 84, 549–566.

Okunogbe, A., Nugent, R., Spencer, G., Powis, J., Ralston, J., Wilding, J., 2022. Economic impacts of overweight and obesity: current and future estimates for 161 countries. BMJ Global Health 7, e009773.

Oliveira, H.C., Derks, M.F.L., Lopes, M.S., Madsen, O., Harlizius, B., van Son, M., Grindflek, E.H., Gòdia, M., Gjuvsland, A.B., Otto, P.I., Groenen, M.A.M., Guimaraes, S.E.F., 2022. Fine Mapping of a Major Backfat QTL Reveals a Causal Regulatory Variant Affecting the CCND2 Gene. Frontiers in genetics 13, 871516.

Palmer, B.F., Clegg, D.J., 2015. The sexual dimorphism of obesity. Molecular and cellular endocrinology 402, 113–119.

Pant, S.D., Karlskov-Mortensen, P., Jacobsen, M.J., Cirera, S., Kogelman, L.J.A., Bruun, C.S., Mark, T., Jørgensen, C.B., Grarup, N., Appel, E.V.R., Galjatovic, E.A.A., Hansen, T., Pedersen, O., Guerin, M., Huby, T., Lesnik, P., Meuwissen, T.H.E., Kadarmideen, H.N., Fredholm, M., 2015. Comparative Analyses of QTLs Influencing Obesity and Metabolic Phenotypes in Pigs and Humans. PLoS ONE 10, e0137356.

Pappenberger, E., 2014. Vergleich der Körperzusammensetzung konventioneller und alternativer Masthybriden mittels Dualenergieröntgenabsorptiometrie und Magnetresonanztomographie.

Pathak, P.K., Roychoudhury, R., Saharia, J., Borah, M.C., Dutta, D.J., Bhuyan, R., Kalita, D., 2018. Impact of seasonal thermal stress on physiological and blood biochemical parameters in pigs under different dietary energy levels. Tropical animal health and production 50, 1025–1032.

Patience, J.F., Rossoni-Serão, M.C., Gutiérrez, N.A., 2015. A review of feed efficiency in swine: biology and application. Journal of animal science and biotechnology 6, 33.

Pauly, C., Spring, P., O'Doherty, J.V., Ampuero Kragten, S., Bee, G., 2008. Performances, meat quality and boar taint of castrates and entire male pigs fed a standard and a raw potato starch-enriched diet. Animal 2, 1707–1715.

Pearce, S.C., Mani, V., Boddicker, R.L., Johnson, J.S., Weber, T.E., Ross, J.W., Rhoads, R.P., Baumgard, L.H., Gabler, N.K., 2013. Heat stress reduces intestinal barrier integrity and favors intestinal glucose transport in growing pigs. PLoS ONE 8, e70215.

Perna, S., Gasparri, C., Allehdan, S., Riva, A., Petrangolini, G., Ferraris, C., Guido, D., Alalwan, T.A., Rondanelli, M., 2023. Discovering the Physio-Pathological Mechanisms of Interaction between Bone Mineral Density, Muscle Mass, and Visceral Adipose Tissue in Female Older Adults through Structural Equation Modeling. Journal of clinical medicine 12, 2269.

Pietrobelli, A., Formica, C., Wang, Z., Heymsfield, S.B., 1996. Dual-energy X-ray absorptiometry body composition model: review of physical concepts. The American journal of physiology 271, E941-E951.

Pietrobelli, A., Wang, Z., Formica, C., Heymsfield, S.B., 1998. Dual-energy X-ray absorptiometry: fat estimation errors due to variation in soft tissue hydration. The American journal of physiology 274, E808-E816.

Pinna, A., Simoncini, N., Toscani, T., Virgili, R., 2012. Volatile organic compounds of Parma drycured ham as markers of ageing time and aged ham aroma. Italian Journal of Food Science: IJFS, 321–331.

Podder, M., Bera, S., Naskar, S., Sahu, D., Mukherjee, J., Patra, A.K., 2022. Physiological, blood-biochemical and behavioural changes of Ghoongroo pigs in seasonal heat stress of a hot-humid tropical environment. International journal of biometeorology 66, 1349–1364.

Pomar, C., Kipper, M., Marcoux, M., 2017. Use of dual-energy x-ray absorptiometry in non-ruminant nutrition research. Revista Brasileira de Zootecnia 46, 621–629.

Pope, W.F., Cárdenas, H., 2006. Androgens in female pig reproduction: actions mediated by the androgen receptor. Society of Reproduction and Fertility supplement 62, 55–67.

Positano, V., Christiansen, T., Santarelli, M.F., Ringgaard, S., Landini, L., Gastaldelli, A., 2009. Accurate segmentation of subcutaneous and intermuscular adipose tissue from MR images of the thigh. Journal of Magnetic Resonance Imaging 29, 677–684.

Poullet, N., Rauw, W.M., Renaudeau, D., Riquet, J., Giorgi, M., Billon, Y., Gilbert, H., Gourdine, J.-L., 2022. Plasticity of feeding behaviour traits in response to production environment (temperate vs. tropical) in group-housed growing pigs. Scientific Reports 12, 847.

Poulos, S.P., Hausman, D.B., Hausman, G.J., 2010. The development and endocrine functions of adipose tissue. Molecular and cellular endocrinology 323, 20–34.

Powell-Wiley, T.M., Poirier, P., Burke, L.E., Després, J.-P., Gordon-Larsen, P., Lavie, C.J., Lear, S.A., Ndumele, C.E., Neeland, I.J., Sanders, P., St-Onge, M.-P., 2021. Obesity and Cardiovascular Disease: A Scientific Statement From the American Heart Association. Circulation 143, e984-e1010.

Qu, H., Ajuwon, K.M., 2018. Adipose tissue-specific responses reveal an important role of lipogenesis during heat stress adaptation in pigs. Journal of animal science 96, 975–989.

Quiniou, N., Dubois, S., Noblet, J., 2000. Voluntary feed intake and feeding behaviour of group-housed growing pigs are affected by ambient temperature and body weight. Livestock Production Science 63, 245–253.

Raffan, E., Holden, S.L., Cullingham, F., Hackett, R.M., Rawlings, J.M., German, A.J., 2006. Standardized positioning is essential for precise determination of body composition using dual-energy x-ray absorptiometry in dogs. The Journal of nutrition 136, 1976S-1978S.

Ramirez, B.C., Hayes, M.D., Condotta, I.C.F.S., Leonard, S.M., 2022. Impact of housing environment and management on pre-/post-weaning piglet productivity. Journal of Animal Science 100, skac142.

Raschka, C., Ruda, L., Wenning, P., Stemm, C.-I. von, Pfarrer, C., Huber, K., Meyer, U., Dänicke, S., Rehage, J., 2016. In vivo determination of subcutaneous and abdominal adipose tissue depots in German Holstein dairy cattle. Journal of animal science 94, 2821–2834.

Rauw, W.M., La Mercado Peña, E. de, Gomez-Raya, L., García Cortés, L.A., Ciruelos, J.J., Gómez Izquierdo, E., 2020. Impact of environmental temperature on production traits in pigs. Scientific Reports 10, 2106.

Reckels, B., Hölscher, R., Schwennen, C., Lengling, A., Stegemann, U., Waldmann, K.-H., Visscher, C., 2020. Resource-Efficient Classification and Early Predictions of Carcass Composition in Fattening Pigs by Means of Ultrasound Examinations. Agriculture 10, 222.

Reinhardt, M., Piaggi, P., DeMers, B., Trinidad, C., Krakoff, J., 2017. Cross calibration of two dual-energy X-ray densitometers and comparison of visceral adipose tissue measurements by iDXA and MRI. Obesity 25, 332–337.

Renner, S., Blutke, A., Dobenecker, B., Dhom, G., Müller, T.D., Finan, B., Clemmensen, C., Bernau, M., Novak, I., Rathkolb, B., Senf, S., Zöls, S., Roth, M., Götz, A., Hofmann, S.M., Hrabě de Angelis, M., Wanke, R., Kienzle, E., Scholz, A.M., DiMarchi, R., Ritzmann, M., Tschöp, M.H., Wolf, E., 2018. Metabolic syndrome and extensive adipose tissue inflammation in morbidly obese Göttingen minipigs. Molecular metabolism 16, 180–190.

Ribeiro-Filho, F.F., Faria, A.N., Azjen, S., Zanella, M.-T., Ferreira, S.R.G., 2003. Methods of estimation of visceral fat: advantages of ultrasonography. Obesity research 11, 1488–1494.

Rickmann, A.-M., Senapati, J., Kovalenko, O., Peters, A., Bamberg, F., Wachinger, C., 2022. AbdomenNet: deep neural network for abdominal organ segmentation in epidemiologic imaging studies. BMC medical imaging 22, 168.

Rinaldo, D., Le Dividich, J., 1991. Assessment of optimal temperature for performance and chemical body composition of growing pigs. Livestock Production Science 29, 61–75.

Rosen, E.D., Spiegelman, B.M., 2014. What we talk about when we talk about fat. Cell 156, 20–44.

Ross, J.W., Hale, B.J., Seibert, J.T., Romoser, M.R., Adur, M.K., Keating, A.F., Baumgard, L.H., 2017. Physiological mechanisms through which heat stress compromises reproduction in pigs. Molecular reproduction and development 84, 934–945.

Rothammer, S., Bernau, M., Kremer-Rücker, P.V., Medugorac, I., Scholz, A.M., 2017. Genome-wide QTL mapping results for regional DXA body composition and bone mineral density traits in pigs. Archives Animal Breeding 60, 51–59.

Rothammer, S., Kremer, P.V., Bernau, M., Fernandez-Figares, I., Pfister-Schär, J., Medugorac, I., Scholz, A.M., 2014. Genome-wide QTL mapping of nine body composition and bone mineral density traits in pigs. Genetics Selection Evolution 46, 68.

Rothney, M.P., Xia, Y., Wacker, W.K., Martin, F.-P., Beaumont, M., Rezzi, S., Giusti, V., Ergun, D.L., 2013. Precision of a new tool to measure visceral adipose tissue (VAT) using dual-energy X-Ray absorptiometry (DXA). Obesity 21, E134-E136.

Schild, H.H., 1997. MRI. Made easy. 2nd edition. Schering, Berlin.

Schinckel, A.P., Mahan, D.C., Wiseman, T.G., Einstein, M.E., 2008. Growth of protein, moisture, lipid, and ash of two genetic lines of barrows and gilts from twenty to one hundred twenty-five kilograms of body weight. Journal of animal science 86, 460–471.

Schlegel, P., Gutzwiller, A., 2020. Dietary Calcium to Digestible Phosphorus Ratio for Optimal Growth Performance and Bone Mineralization in Growing and Finishing Pigs. Animals 10, 178.

Scholz, A., 2002. In-vivo-Methoden zur Analyse von Muskelstoffwechsel und Körperzusammensetzung beim Schwein unter besonderer Berücksichtigung genetischer Einflüsse.

Scholz, A.M., Bünger, L., Kongsro, J., Baulain, U., Mitchell, A.D., 2015. Non-invasive methods for the determination of body and carcass composition in livestock: dual-energy X-ray absorptiometry, computed tomography, magnetic resonance imaging and ultrasound: invited review. Animal 9, 1250–1264.

Scott, K.A., Melhorn, S.J., Sakai, R.R., 2012. Effects of Chronic Social Stress on Obesity. Current Obesity Reports 1, 16–25.

Sebo, Z.L., Rodeheffer, M.S., 2021. Testosterone metabolites differentially regulate obesogenesis and fat distribution. Molecular metabolism 44, 101141.

Seibert, J.A., Boone, J.M., 2005. X-ray imaging physics for nuclear medicine technologists. Part 2: X-ray interactions and image formation. Journal of Nuclear Medicine Technology 33, 3–18.

Seidell, J.C., Bakker, C.J., van der Kooy, K., 1990. Imaging techniques for measuring adipose-tissue distribution--a comparison between computed tomography and 1.5-T magnetic resonance. The American journal of clinical nutrition 51, 953–957.

Skoupá, K., Bátik, A., Šťastný, K., Sládek, Z., 2023. Structural Changes in the Skeletal Muscle of Pigs after Long-Term Administration of Testosterone, Nandrolone and a Combination of the Two. Animals 13, 2141.

Škrlep, M., Poklukar, K., Kress, K., Vrecl, M., Fazarinc, G., Batorek Lukač, N., Weiler, U., Stefanski, V., Čandek-Potokar, M., 2020a. Effect of immunocastration and housing conditions on pig carcass and meat quality traits. Translational animal science 4, 1224-1237.

Škrlep, M., Tomašević, I., Mörlein, D., Novaković, S., Egea, M., Garrido, M.D., Linares, M.B., Peñaranda, I., Aluwé, M., Font-i-Furnols, M., 2020b. The Use of Pork from Entire Male and Immunocastrated Pigs for Meat Products-An Overview with Recommendations. Animals 10, 1754.

Slart, Riemer H. J. A., Punda, M., Ali, D.S., Bazzocchi, A., Bock, O., Camacho, P., Carey, J.J., Colquhoun, A., Compston, J., Engelke, K., Erba, P.A., Harvey, N.C., Krueger, D., Lems, W.F., Lewiecki, E.M., Morgan, S., Moseley, K.F., O'Brien, C., Probyn, L., Rhee, Y., Richmond, B., Schousboe, J.T., Shuhart, C., Ward, K.A., van den Wyngaert, T., Zhang-Yin, J., Khan, A.A., 2025. Updated practice guideline for dual-energy X-ray absorptiometry (DXA). European Journal of Nuclear Medicine and Molecular Imaging 52, 539–563.

Soladoye, O.P., López Campos, Ó., Aalhus, J.L., Gariépy, C., Shand, P., Juárez, M., 2016. Accuracy of dual energy X-ray absorptiometry (DXA) in assessing carcass composition from different pig populations. Meat science 121, 310–316.

Soladoye, P.O., Shand, P.J., Aalhus, J.L., Gariépy, C., Juárez, M., 2015. Review: Pork belly quality, bacon properties and recent consumer trends. Canadian Journal of Animal Science 95, 325–340.

Sørensen, T.I.A., Martinez, A.R., Jørgensen, T.S.H., 2022. Epidemiology of Obesity. Handbook of experimental pharmacology 274, 3–27.

Speakman, J.R., Booles, D., Butterwick, R., 2001. Validation of dual energy X-ray absorptiometry (DXA) by comparison with chemical analysis of dogs and cats. International journal of obesity and related metabolic disorders 25, 439–447.

Spurlock, M.E., Gabler, N.K., 2008. The development of porcine models of obesity and the metabolic syndrome. The Journal of nutrition 138, 397–402.

Streicher, S.A., Lim, U., Park, S.L., Li, Y., Sheng, X., Hom, V., Xia, L., Pooler, L., Shepherd, J., Loo, L.W.M., Ernst, T., Buchthal, S., Franke, A.A., Tiirikainen, M., Wilkens, L.R., Haiman, C.A., Stram, D.O., Cheng, I., Le Marchand, L., 2023. Genome-wide association study of abdominal MRI-measured visceral fat: The multiethnic cohort adiposity phenotype study. PLoS ONE 18, e0279932.

Tchkonia, T., Thomou, T., Zhu, Y., Karagiannides, I., Pothoulakis, C., Jensen, M.D., Kirkland, J.L., 2013. Mechanisms and metabolic implications of regional differences among fat depots. Cell metabolism 17, 644–656.

Thibault, R., Genton, L., Pichard, C., 2012. Body composition: why, when and for who? Clinical Nutrition 31, 435–447.

Thrall, D.E., 2018. Textbook of veterinary diagnostic radiology. 7th edition. Elsevier, St. Louis.

Thurlow, S., Oldroyd, B., Hind, K., 2017. Scan Mode Selection on the GE-Lunar iDXA Densitometer. Journal of Clinical Densitometry 20, 533.

Toth, M.J., Tchernof, A., Sites, C.K., Poehlman, E.T., 2000. Menopause-related changes in body fat distribution. Annals of the New York Academy of Sciences 904, 502–506.

van den Broeke, A., Aluwé, M., Kress, K., Stefanski, V., Škrlep, M., Batorek, N., Ampe, B., Millet, S., 2022. Effect of dietary energy level in finishing phase on performance, carcass and meat quality in immunocastrates and barrows in comparison with gilts and entire male pigs. Animal 16, 100437.

Victoria Sanz Fernandez, M., Johnson, J.S., Abuajamieh, M., Stoakes, S.K., Seibert, J.T., Cox, L., Kahl, S., Elsasser, T.H., Ross, J.W., Isom, S.C., Rhoads, R.P., Baumgard, L.H., 2015. Effects of heat stress on carbohydrate and lipid metabolism in growing pigs. Physiological reports 3, e12315.

Wagner, D.R., 2013. Ultrasound as a tool to assess body fat. Journal of obesity 2013, 280713.

Wagner, D.R., Teramoto, M., Judd, T., Gordon, J., McPherson, C., Robison, A., 2020. Comparison of A-mode and B-mode Ultrasound for Measurement of Subcutaneous Fat. Ultrasound in medicine & biology 46, 944–951.

Wald, D., Teucher, B., Dinkel, J., Kaaks, R., Delorme, S., Boeing, H., Seidensaal, K., Meinzer, H.-P., Heimann, T., 2012. Automatic quantification of subcutaneous and visceral adipose tissue from whole-body magnetic resonance images suitable for large cohort studies. Journal of Magnetic Resonance Imaging 36, 1421–1434.

Walugembe, M., Swantek, P.M., Honeyman, M.S., Mabry, J.W., Stalder, K.J., Rothschild, M.F., 2016. Evaluation of growth, deposition of back fat, and loin muscle for purebred Berkshire pigs housed in bedded hoop buildings. Journal of animal science 94, 800–804.

Wang, H., Wang, X., Li, M., Wang, S., Chen, Q., Lu, S., 2022. Identification of key sex-specific pathways and genes in the subcutaneous adipose tissue from pigs using WGCNA method. BMC Genomic Data 23, 35.

Wang, J., Yan, D., Hou, X., Chen, P., Sun, Q., Bao, Y., Hu, C., Zhang, Z., Jia, W., 2017. Association of adiposity indices with bone density and bone turnover in the Chinese population. Osteoporosis international 28, 2645–2652.

Wang, Y., Zhang, H., Yan, E., He, L., Guo, J., Zhang, X., Yin, J., 2023. Carcass and meat quality traits and their relationships in Duroc × Landrace × Yorkshire barrows slaughtered at various seasons. Meat science 198, 109117.

Weigand, A.C., Schweizer, H., Knob, D.A., Scholz, A.M., 2020. Phenotyping of the Visceral Adipose Tissue Using Dual Energy X-Ray Absorptiometry (DXA) and Magnetic Resonance Imaging (MRI) in Pigs. Animals 10, 1165.

Wenczel, R., 2013. Untersuchungen zur Messung der Körperzusammensetzung und Knochenmineraldichte beim Schwein und beim Schaf mittels "Pencil-" und "Fan-Beam"-Dualenergie Röntgenabsorptiometrie. Tierärztliche Fakultät, Ludwig-Maximilians-Universität München.

Wood, J.D., Richardson, R.I., Nute, G.R., Fisher, A.V., Campo, M.M., Kasapidou, E., Sheard, P.R., Enser, M., 2004. Effects of fatty acids on meat quality: a review. Meat science 66, 21–32.

World Health Organization, 2024. Obesity and overweight, https://www.who.int/news-room/fact-sheets/detail/obesity-and-overweight. Accessed 22 September 2024.

Wu, J., Boström, P., Sparks, L.M., Ye, L., Choi, J.H., Giang, A.-H., Khandekar, M., Virtanen, K.A., Nuutila, P., Schaart, G., Huang, K., Tu, H., van Marken Lichtenbelt, W.D., Hoeks, J., Enerbäck, S., Schrauwen, P., Spiegelman, B.M., 2012. Beige adipocytes are a distinct type of thermogenic fat cell in mouse and human. Cell 150, 366–376.

Zaitsev, M., Maclaren, J., Herbst, M., 2015. Motion artifacts in MRI: A complex problem with many partial solutions. Journal of Magnetic Resonance Imaging 42, 887–901.

Zappaterra, M., Catillo, G., Lo Fiego, D.P., Belmonte, A.M., Padalino, B., Davoli, R., 2022. Describing backfat and Semimembranosus muscle fatty acid variability in heavy pigs: Analysis of non-genetic factors. Meat science 183, 108645.

Zhang, P., Peterson, M., Su, G.L., Wang, S.C., 2015. Visceral adiposity is negatively associated with bone density and muscle attenuation. The American journal of clinical nutrition 101, 337–343.

Zhao, J., Tao, C., Chen, C., Wang, Y., Liu, T., 2021. Formation of thermogenic adipocytes: What we have learned from pigs. Fundamental Research 1, 495–502.

Zhu, K., Hunter, M., James, A., Lim, E.M., Cooke, B.R., Walsh, J.P., 2020. Relationship between visceral adipose tissue and bone mineral density in Australian baby boomers. Osteoporosis international 31, 2439–2448.

Zomeño, C., Gispert, M., Brun, A., Carabús, A., Soler, J., Font-i-Furnols, M., 2022. Productive performance and in vivo body composition across the growing and finishing period and carcass traits in pigs of four sex types. Meat science 192, 108909.

Zomeño, C., Gispert, M., Čandek-Potokar, M., Mörlein, D., Font-i-Furnols, M., 2023. A matter of body weight and sex type: Pig carcass chemical composition and pork quality. Meat science 197, 109077.

IX. APPENDIX

1. Mineral pre mix composition

SALVANA MASTKRAFT - Amino-acid based mineral feed for pigs

Analytical components and concentrations: 8.00 % lysine, 1.00 % methionine, 1.50 % threonine, 21.00 % calcium, 3.00 % phosphorus, 5.00 % sodium, 2.50 % magnesium

Feed additives per kilogram: 200,000 IU vitamin A (3a672a), 50,000 IU vitamin D3 (E671), 3,000 mg vitamin E (all-rac-alpha-tocopheryl acetate (3a700)), 100 mg vitamin K, 50 mg vitamin B1 (3a831), 1,150 mg vitamin B2 (riboflavin), 100 mg vitamin B6 (pyridoxine hydrochloride 3a831), 1,000 µg vitamin B12 (cyanocobalamin), 700 mg niacinamide (3a315), 340 mg calcium D-pantothenate (3a841), 10 mg folic acid (3a316), 2,000 µg biotin (3a880), 10,000 mg choline chloride (3a890), 4,000 mg iron as iron-(II)-sulphate monohydrate (E1), 400 mg copper as copper-(II)-sulphate pentahydrate (E4), 2,500 mg zinc as zinc oxide (E6), 2,100 mg manganese as manganese-(II)-oxide (E5), 66 mg iodine as calcium iodine, water-free (3b202), 13 mg selenium as sodium selenite (E8), 16,666 FTU 3-phytase*** (4a1600), 680 mg butylated hydroxytoluene (BHT E321), 280 mg propyl gallate (E310)

2. Data overview of daily feed intake

Table 13: p-values, LSM and SEE of daily feed intake

daily feed intake

SEX	p-value	male	female
Fl_d [g/d]	<.0001	1814.21 ± 32.09 [a]	1647.64 ± 24.14 [b]

GENOTYPE	p-value	1	2	3	4	5	6
Fl_d [g/d]	<.0001	1681.41 ± 24.74 [b]	1706.03 ± 53.75 [b]	1621.17 ± 26.08 [b]	1648.62 ± 44.09 [b]	1950.68 ± 41.47 [a]	1777.64 ± 114.73 [ab]

SEASON	p-value	1	2	3	4	5
Fl_d [g/d]	<.0001	2071.03 ± 42.38 [a]	2027.62 ± 34.19 [a]	1636.40 ± 38.86 [b]	1704.41 ± 42.48 [b]	1215.16 ± 38.25 [c]

FEEDING WEEK	p-value	1	2	3	4	5	6	7	8	9	10
Fl_d [g/d]	<.0001	1088.18 ± 49.14 [g]	1314.79 ± 43.69 [f]	1360.73 ± 43.86 [f]	1487.57 ± 43.55 [e]	1690.53 ± 46.09 [d]	1873.42 ± 47.33 [c]	1900.04 ± 45.10 [c]	2112.32 ± 43.96 [b]	2282.74 ± 44.32 [a]	2198.93 ± 47.24 [ab]

Significance levels (p-value), least squares means and standard errors of estimation (LSM ± SEE) of daily feed intake, different superscripts within rows describe significant differences, with p < 0.05
Genotype groups 1 = PiDuDLDE_DEDLDuPi, 2 = _DEDLPiDu, 3 = _DLDEPiDu, 4 = _DuPiDEDL, 5 = _DuPiDLDE, 6 = _PiDuDLDE
Feeding weeks 1 = starts at age of approx. 70 days (admission to outside-climate stable), 10 = week until examination day

3. Further analyses for the larger cohort

3.1. Sample distribution of the larger cohort

Table 14: Sample distribution of the larger cohort

sex		genotype		season x year	
male	n = 46	PiDuDLDE_DEDLDuPi	n = 50	3 / 2021	n = 20
female	n = 92	PiDuDLDE_DEDLPiDu	n = 8	4 / 2021	n = 10
all	n = 138	PiDuDLDE_DLDEPiDu	n = 44	5 / 2021	n = 24
		PiDuDLDE_DuPiDEDL	n = 20	1 / 2022	n = 19
		PiDuDLDE_DuPiDLDE	n = 11	2 / 2022	n = 27
		PiDuDLDE_PiDuDLDE	n = 5	3 / 2022	n = 22
				4 / 2022	n = 16

3.2. Relationship between volume and mass of VAT (DXA)

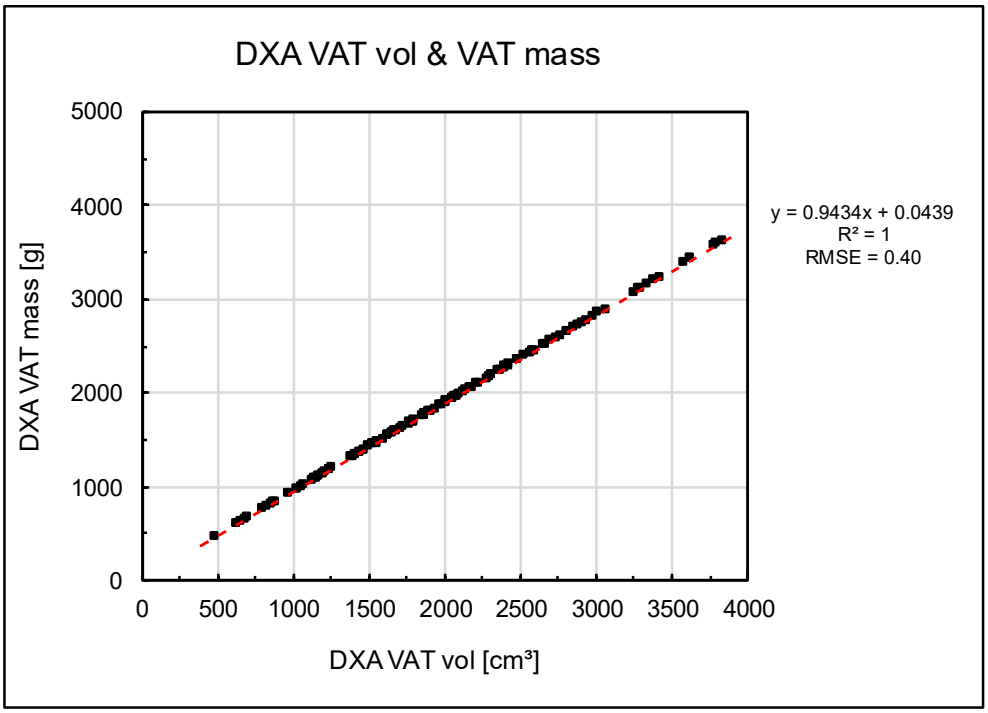

Figure 62: Relationship between volume and mass of VAT (DXA)

3.3. Relationships between abdominal adipose tissues for the larger cohort

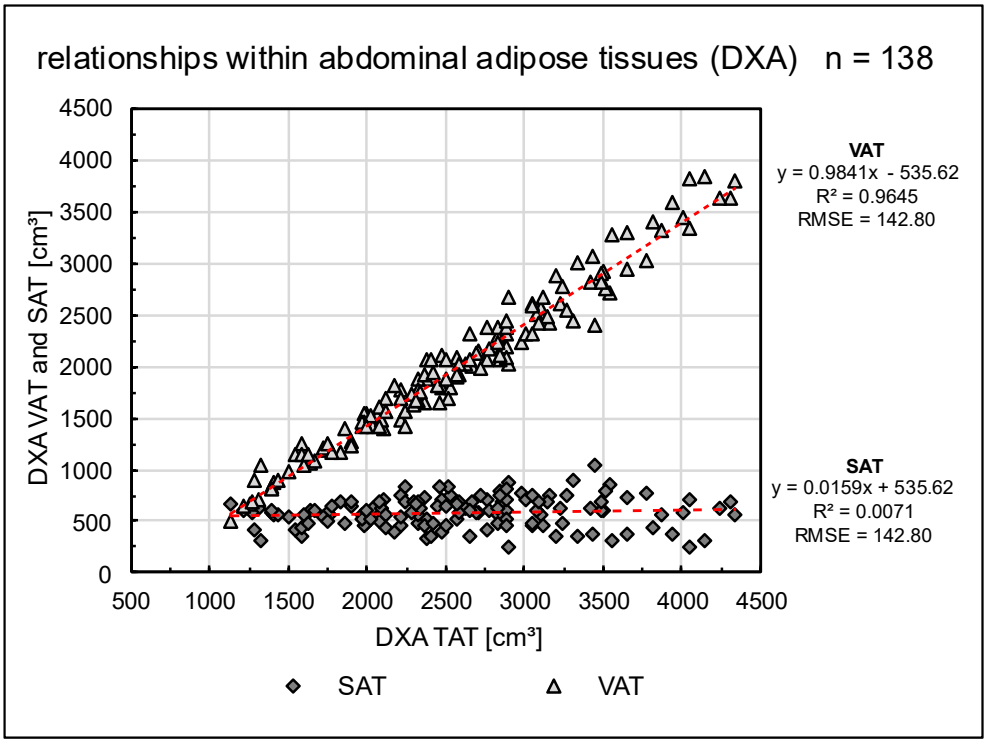

Figure 63: Relationships within abdominal adipose tissues (DXA) for the larger cohort

3.4. Data overview of the larger cohort

Table 15: p-values, LSM and SEE of sample characteristics and body composition parameters between sexes in the larger cohort

sample characteristics and body composition parameters n = 138

	SEX	p-value	male	female
	weight [kg]	0.1634	99.23 ± 1.45	97.31 ± 1.13
	age [d]	0.3956	147.31 ± 0.25	147.11 ± 0.20
	stable days [d]	0.8785	72.46 ± 0.20	72.49 ± 0.15
DXA	VAT [cm³]	<.0001	2158.15 ± 86.73 [a]	1794.16 ± 66.52 [b]
DXA	SAT [cm³]	<.0001	425.79 ± 20.52 [b]	625.29 ± 15.74 [a]
DXA	TAT [cm³]	0.0451	2583.94 ± 86.82 [a]	2419.46 ± 66.59 [b]
DXA	android fat [%]	0.0390	14.96 ± 0.47 [a]	14.05 ± 0.36 [b]
DXA	fat [g]	0.0137	15152 ± 379.30 [a]	14264 ± 290.90 [b]
DXA	lean [g]	0.0962	78514 ± 436.64	79199 ± 334.88
DXA	BMC [g]	0.9519	1948.64 ± 20.85	1949.82 ± 15.99
DXA	BMD [g/cm^2]	0.7856	1.0574 ± 0.01	1.0599 ± 0.01

Significance levels (p-value), least squares means and standard errors of estimation (LSM ± SEE) for abdominal adipose tissues and body composition variables assessed with DXA, different superscripts within rows describe significant differences, with p < 0.05

Abdominal adipose tissues VAT visceral adipose tissue, SAT: subcutaneous adipose tissue, TAT: total abdominal adipose tissue, android fat percentage: fat mass percentage of the total soft tissue in the android region

Body composition variables fat total body fat mass, lean: total soft tissue lean mass, BMC: bone mineral content, BMD: bone mineral density

Table 16: p-values, LSM and SEE of sample characteristics and body composition parameters between genotypes in the larger cohort

	GENOTYPE	p-value	1	2	3	4	5	6
sample characteristics and body composition parameters n = 138	weight [kg]	0.0001	96.29 ± 1.57 ^{bc}	89.75 ± 3.13 ^{c}	95.18 ± 1.62 ^{c}	100.36 ± 2.13 ^{b}	96.60 ± 2.88 ^{bc}	111.42 ± 3.95 ^{a}
	age [d]	<.0001	147.83 ± 0.27 ^{b}	144.31 ± 0.54 ^{d}	145.47 ± 0.28 ^{c}	147.97 ± 0.37 ^{b}	147.66 ± 0.50 ^{b}	150.02 ± 0.69 ^{a}
	stable days [d]	0.0001	73.22 ± 0.22 ^{a}	72.15 ± 0.43 ^{ab}	72.28 ± 0.22 ^{b}	72.61 ± 0.29 ^{ab}	71.63 ± 0.40 ^{b}	72.94 ± 0.54 ^{ab}
DXA	VAT [cm³]	0.0010	2069.25 ± 91.99 ^{ab}	1996.49 ± 186.86 ^{ab}	2347.72 ± 95.12 ^{a}	1780.57 ± 127.07 ^{b}	1780.09 ± 168.96 ^{b}	1882.82 ± 245.98 ^{ab}
	SAT [cm³]	0.0273	590.19 ± 21.77 ^{a}	550.11 ± 44.22 ^{ab}	535.49 ± 22.51 ^{ab}	474.72 ± 30.07 ^{b}	514.98 ± 39.98 ^{b}	487.76 ± 58.21 ^{ab}
	TAT [cm³]	0.0001	2659.44 ± 92.08 ^{ab}	2546.60 ± 187.05 ^{abc}	2883.21 ± 95.22 ^{a}	2255.29 ± 127.20 ^{c}	2295.06 ± 169.13 ^{c}	2370.58 ± 246.24 ^{bc}
	android fat [%]	0.0002	15.82 ± 0.49 ^{a}	14.56 ± 1.00 ^{ab}	16.50 ± 0.51 ^{a}	13.13 ± 0.68 ^{b}	14.40 ± 0.91 ^{ab}	12.64 ± 1.32 ^{b}
BIA	fat [g]	0.0003	15673 ± 402.28 ^{ab}	14803 ± 817.19 ^{abc}	15959 ± 415.99 ^{a}	13141 ± 555.72 ^{c}	14914 ± 738.91 ^{abc}	13759 ± 1075.76 ^{bc}
	lean [g]	0.0017	77588 ± 463.10 ^{b}	78720 ± 940.74 ^{ab}	77782 ± 478.89 ^{b}	80535 ± 639.73 ^{a}	78707 ± 850.62 ^{ab}	79807 ± 1238.40 ^{ab}
	BMC [g]	0.2051	1967.70 ± 22.11	1969.08 ± 44.92	1949.26 ± 22.86	1943.42 ± 30.54	2029.09 ± 40.61	1836.81 ± 59.13
	BMD [g/cm²]	0.4134	1.0682 ± 0.01	1.0522 ± 0.02	1.0563 ± 0.01	1.0477 ± 0.01	1.0998 ± 0.02	1.0277 ± 0.03

Significance levels (p-value), least squares means and standard errors of estimation (LSM ± SEE) for abdominal adipose tissues and body composition variables assessed with DXA, different superscripts within rows describe significant differences, with $p < 0.05$

Genotype groups 1 = PiDuDLDE_DEDLDuPi, 2 = _DEDLPiDu, 3 = _DLDEPiDu, 4 = _DuPiDEDL, 5 = _DuPiDLDE, 6 = _PiDuDLDE

Abdominal adipose tissues VAT: visceral adipose tissue, SAT: subcutaneous adipose tissue, TAT: total abdominal adipose tissue, android fat percentage: fat mass percentage of the total soft tissue in the android region

Body composition variables fat: total body fat mass, lean: total soft tissue lean mass, BMC: bone mineral content, BMD: bone mineral density

Table 17: p-values, LSM and SEE of sample characteristics and body composition parameters in season-year categories in the larger cohort

sample characteristics and body composition parameters n = 138

	SEASON x YEAR	p-value	3 / 2021	4 / 2021	5 / 2021	1 / 2022	2 / 2022	3 / 2022	4 / 2022
	weight [kg]	<.0001	97.34 ± 2.05 ^{bcd}	104.73 ± 2.89 ^{a}	101.04 ± 1.82 ^{abc}	104.40 ± 2.64 ^{ab}	94.59 ± 1.76 ^{de}	94.57 ± 2.57 ^{cde}	91.20 ± 2.49 ^{e}
	age [d]	<.0001	146.44 ± 0.36 ^{cd}	145.81 ± 0.50 ^{de}	149.41 ± 0.32 ^{b}	150.88 ± 0.46 ^{a}	145.63 ± 0.31 ^{de}	145.02 ± 0.45 ^{e}	147.28 ± 0.43 ^{c}
	stable days [d]	<.0001	78.10 ± 0.28 ^{a}	69.43 ± 0.40 ^{e}	76.53 ± 0.25 ^{b}	72.59 ± 0.36 ^{d}	69.13 ± 0.24 ^{e}	66.33 ± 0.35 ^{f}	75.19 ± 0.34 ^{c}
D	VAT [cm³]	0.0059	1893.70 ± 120.83 ^{bc}	2413.61 ± 175.68 ^{a}	1996.59 ± 110.08 ^{abc}	2217.42 ± 161.15 ^{ab}	1789.37 ± 103.50 ^{c}	1840.18 ± 151.32 ^{c}	1682.23 ± 148.54 ^{c}
X	SAT [cm³]	0.0057	542.27 ± 28.59 ^{ab}	549.26 ± 41.58 ^{ab}	527.32 ± 26.05 ^{abc}	468.22 ± 38.14 ^{bc}	582.83 ± 24.49 ^{a}	439.80 ± 35.81 ^{c}	569.11 ± 35.15 ^{ab}
A	TAT [cm³]	0.0048	2435.97 ± 120.95 ^{bc}	2962.87 ± 175.87 ^{a}	2523.91 ± 110.19 ^{bc}	2685.64 ± 161.32 ^{ab}	2372.19 ± 103.61 ^{bc}	2279.98 ± 151.48 ^{c}	2251.33 ± 148.69 ^{bc}
	android fat [%]	0.0175	14.52 ± 0.65 ^{abc}	16.56 ± 0.94 ^{a}	15.15 ± 0.59 ^{abc}	14.87 ± 0.87 ^{ab}	13.74 ± 0.56 ^{bc}	13.22 ± 0.81 ^{c}	13.48 ± 0.80 ^{bc}
	fat [g]	0.0204	14967 ± 528.42 ^{abc}	16196 ± 768.33 ^{a}	15130 ± 481.40 ^{ab}	14609 ± 704.78 ^{b}	14479 ± 452.63 ^{bc}	13175 ± 661.79 ^{c}	14399 ± 649.61 ^{abc}
D	lean [g]	0.0474	78784 ± 608.31 ^{ab}	77821 ± 884.49 ^{bc}	78591 ± 554.18 ^{ab}	79653 ± 811.33 ^{a}	79595 ± 521.06 ^{ac}	77891 ± 761.84 ^{b}	79660 ± 747.82 ^{ab}
X	BMC [g]	0.0008	1939.30 ± 29.04 ^{bc}	2046.43 ± 42.23 ^{a}	1924.45 ± 26.46 ^{bc}	1968.29 ± 38.74 ^{ab}	1966.69 ± 24.88 ^{ab}	1856.61 ± 36.38 ^{c}	1942.82 ± 35.71 ^{abc}
A	BMD [g/cm²]	0.0037	1.0567 ± 0.01 ^{abc}	1.1004 ± 0.02 ^{a}	1.0435 ± 0.01 ^{bc}	1.0741 ± 0.02 ^{ab}	1.0690 ± 0.01 ^{ab}	1.0262 ± 0.02 ^{c}	1.0406 ± 0.02 ^{bc}

Significance levels (p-value), least squares means and standard errors of estimation (LSM ± SEE) for abdominal adipose tissues and body composition variables assessed with DXA, different superscripts within rows describe significant differences, with p < 0.05

Seasons 1 = January + February, 2 = March + April, 3 = May + June, 4 = July + August, 5 = September + October

Abdominal adipose tissues VAT: visceral adipose tissue, SAT: subcutaneous adipose tissue, TAT: total abdominal adipose tissue, android fat percentage: fat mass percentage of the total soft tissue in the android region

Body composition variables fat: total body fat mass, lean: total soft tissue lean mass, BMC: bone mineral content, BMD: bone mineral density

Table 18: Significance of covariate weight in the larger cohort

Covariate WEIGHT

		p-value
DXA	VAT [cm³]	<.0001
	SAT [cm³]	0.0171
	TAT [g]	<.0001
	android fat [%]	<.0001
DXA	fat [g]	<.0001
	lean [g]	<.0001
	BMC [g]	<.0001
	BMD [g/cm²]	<.0001

Significance levels (p-value) of covariate weight on abdominal adipose tissues and body composition variables assessed with DXA
Abdominal adipose tissues VAT: visceral adipose tissue, SAT: subcutaneous adipose tissue, TAT: total abdominal adipose tissue, android fat percentage: fat mass percentage of the total soft tissue in the android region
Body composition variables fat: total body fat mass, lean: total soft tissue lean mass, BMC: bone mineral content, BMD: bone mineral density

4. Bland-Altman plots of differences against MRI

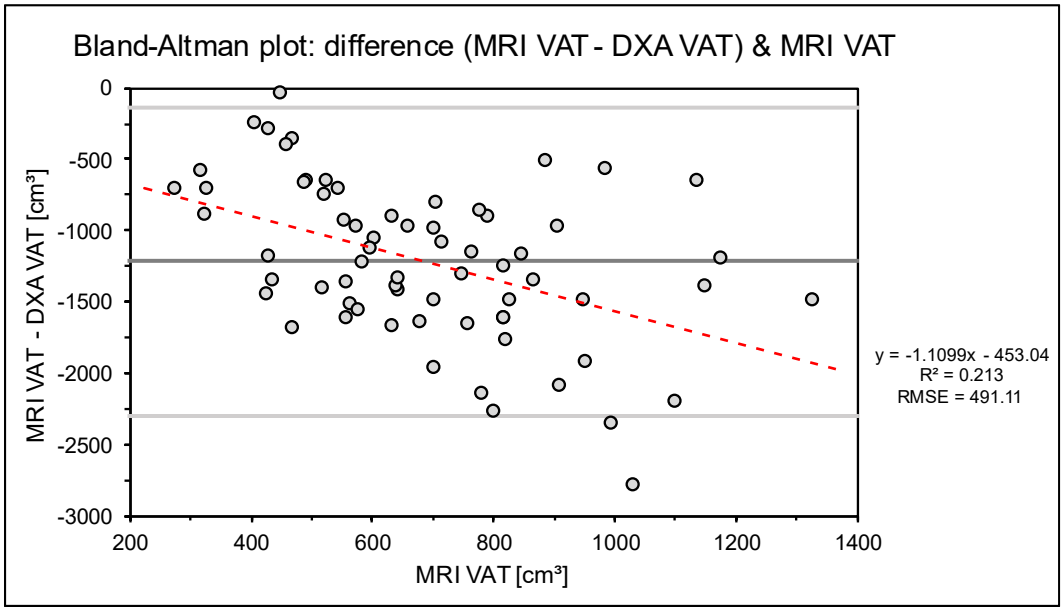

Figure 64: Bland-Altman plot with differences of MRI and DXA against MRI for VAT

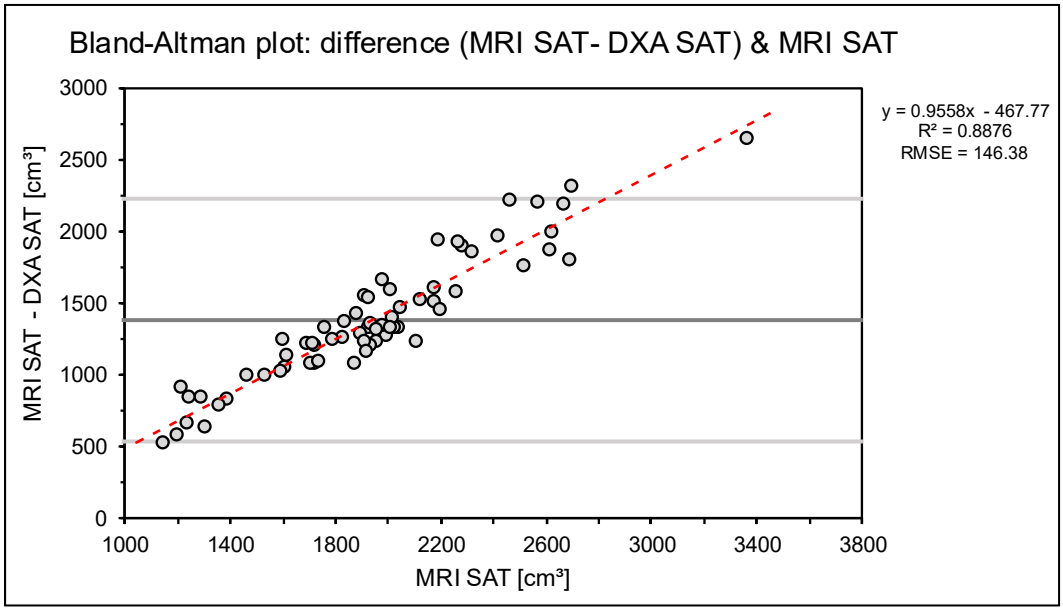

Figure 65: Bland-Altman plot with differences of MRI and DXA against MRI for SAT

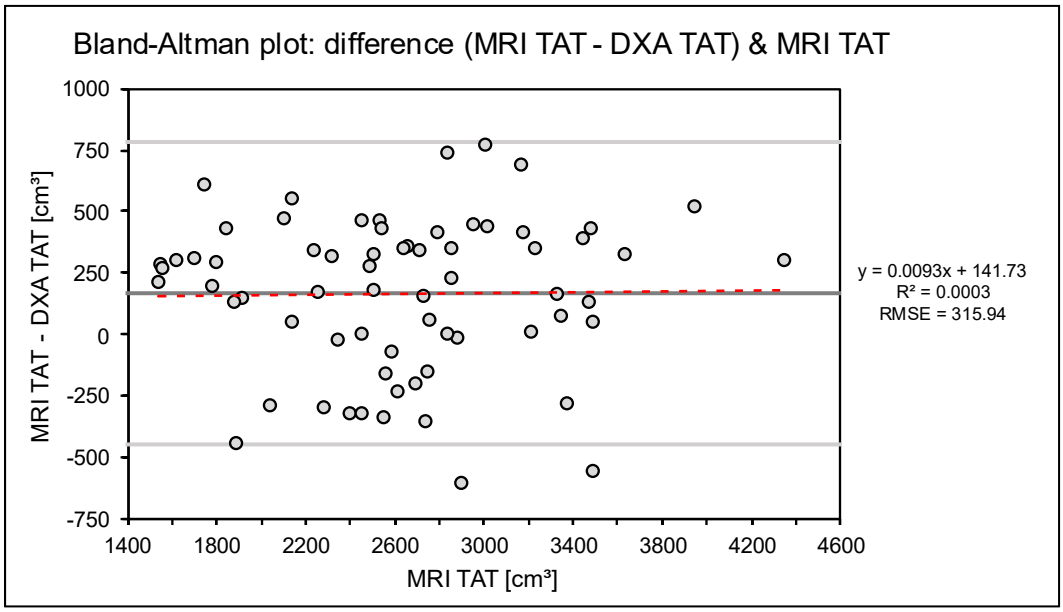

Figure 66: Bland-Altman plot with differences of MRI and DXA against MRI for TAT

X. ACKNOWLEDGMENT

First of all, I would like to thank Prof. Dr. Armin M. Scholz for giving me the opportunity to pursue my doctoral thesis at the Lehr- und Versuchsgut of the Veterinary Faculty, and for offering me this interesting and practical research topic. Thanks for the assistance with all research-related questions, the interesting discussions, and the prompt help whenever there were technical issues with the moody MRI scanner.

I would like to thank all my colleagues at the LVG, especially Dr. Helen Schweizer and Dr. Stefan Nüske, as well as Dr. Lina Fonteyne, Dr. Sebastian Schwanitz, and Dr. Anne Reus, for the professional exchange and for always providing support when there were questions. The collegial interactions made my start in this job smoother and further strengthened my passion for this profession. A big thank you to everyone who helped make the long scanning days with heavy pigs possible. Many thanks to Dr. Roberto Kappes for the fantastic teamwork. It was a pleasure showing you around Munich and having someone to share the literal pain (and ibuprofen) of evaluating all the images made it easier. Thanks to all my colleagues in the cattle and pig departments for their great cooperation, and to Richard Bätz and Lea Benninger for their help in providing additional data for my project. Thanks to Christa, who always looked after the well-being of both humans and dogs during busy times. Because of you all, I had a great time at the LVG.

I dedicate this work to the people I love. My deepest gratitude goes to my mother, Andrea. Thank you for everything you have done for me and for always believing in me. Your endless support and the freedom you have given me to choose my own path means everything to me. I am also incredibly grateful for my sisters Ann-Kathrin and Teresa, for always standing together as a family – forever.

My special thanks go to Paul, my partner in life and laughter. Thank you for always being by my side, for your encouragement to achieve my dreams and complete this work and for always putting a smile on my face. You are the best.

A big thank you goes out to all my friends for their constant support and motivation – both near and far. And especially to Janina, who has always been there for me and pushed me to keep going.

I am very grateful to have you all in my life.